ULTIMATE LIMIT STATE ANALYSIS IN GEOTECHNICAL ENGINEERING USING DISCRETE ELEMENT METHOD, PLASTICITY AND EXTREMUM PRINCIPLE

LI NA

Ph.D

The Hong Kong Polytechnic University

2018

THE HONG KONG POLYTECHNIC UNIVERSITY

DEPARTMENT OF CIVIL AND ENVIRONMENTAL ENGINEERING

Ultimate Limit State Analysis in Geotechnical Engineering using Discrete Element Method, Plasticity and Extremum Principle

LI NA

A Thesis Submitted in Partial Fulfillment of the Requirements

for the Degree of Doctor of Philosophy

AUGUST 2017

CERTIFICATE OF ORIGINALITY

I hereby declare that this thesis is my own work and that, to the best of my knowledge and belief, it reproduces no material previously published or written, nor material that has been accepted for the award of any other degree or diploma, except where due acknowledgement has been made in the text.

Signed_____

Name Li Na

Abstract of thesis entitled

ULTIMATE LIMIT STATE ANALYSIS IN GEOTECHNICAL ENGINEERING USING DISCRETE ELEMENT METHOD, PLASTICITY AND EXTREMUM PRINCIPLE

submitted by Na Li

for the degree of Doctor of Philosophy

at The Hong Kong Polytechnic University in August 2017

Lateral earth pressure, ultimate bearing capacity and slope stability problems are three important and classical geotechnical problems which are well considered by the use of the limit equilibrium method, limit analysis method and method of characteristics in the past. These three classical problems are considered separately in the past, though they are all related to the ultimate limit state of a system. The author views that these problems are governed by similar ultimate requirements, and they can be considered as different views of the ultimate limit state of the system. Therefore, this research focuses on the theoretical analysis of the ultimate limit state in geotechnical engineering using a continuum plasticity as well as discrete element approach.

Firstly, classical bearing capacity problem is re-considered using slip-line method, adaptive finite element limit analysis and discrete element analysis. It is considered from the elastic stage, plastic stage to the rupture stage under the ultimate condition. The large scale failure mechanism and movement of soil for a strip footing are studied, and the influences of the micro-parameters on the bearing capacity of soil are also investigated. This work helps to identify the failure mechanism in bearing capacity problem and the assessment of the classical Limit Equilibrium and plasticity

Methods for which the constitutive model and initial conditions are neglected. The differences between different methods of analyses are then investigated and discussed. It is found that there are noticeable differences between the continuum and discontinuum analyses, and the well-known log-spiral transition zone is also not apparent in both the discrete element approach as well as the laboratory tests, which is one useful new contribution in this study.

Next, discrete element method and slip line method are adopted to analyze the lateral pressure behavior of soil under different boundary conditions and friction angles. The large displacement failure mechanism and movement of soil with the lateral earth pressure of a backfill is further investigated, and the ultimate limit state and the influence of the micro-parameters on the lateral pressure of soil are also observed and compared with the classical plasticity based methods.

Moreover, in order to develop the lower bound solution and extremum principle with internal and external variables in limit equilibrium analysis, the well-known slip line solutions is then applied on a bearing capacity problem to determine the interslice force function f(x) and the thrust line for a ‘‘horizontal slope’’. It is found that it is not important that which variables are used in the stability formulation, either external boundary forces or internal forces, if the ultimate state is considered. Furthermore, it is demonstrated that the maximum extremum from the limit equilibrium analysis is equivalent to the slip line solution of the classical bearing capacity problem.

Lastly, the author demonstrates the equivalence between the classical lateral earth pressure and bearing capacity problem by the slip line method. The equivalence between the lateral earth pressure problem and slope stability problem is then illustrated by the use of the extremum principle. The three classical geotechnical problems can then be unified by varying f(x) until the maximum resistance of the system is fully mobilized, and the corresponding solution is practically equivalent to the plasticity slip line solution. Such unification is not surprising because the fundamental principles behind the three problems are exactly the same: equilibrium and yield. By using an extremum limit equilibrium slope stability program, the author has also determined the bearing capacity factors and lateral earth

pressure coefficients which are exactly the same as those classical plasticity slip line solutions. The classification of a problem is hence just a matter of convenience instead of the difference in the nature of the problem. Through the present works, the three classical geotechnical problems are unified which is an innovative and interesting result in geotechnical engineering and also another new contribution in this study.

In conclusion, the innovations in this thesis include the unification of the three classical geotechnical problems by slip line method and extremum principle; the equivalence of external or internal variables formulations of limit equilibrium method and the equivalence of the limit equilibrium method with the plasticity analysis under the ultimate condition and the consideration of the failure mechanism under very soil movement and the corresponding comparisons with the distinct element analysis.

Key words: ultimate limit state, lateral earth pressure, bearing capacity, slope stability, distinct element, plasticity

ACKNOWLEDGEMENTS

My deepest gratitude goes first and foremost to my supervisor Dr. Y.M. Cheng, for his professional guidance, his teaching, his constant encouragement, his patience in supervisions and massive help during the past three years. Without his consistent and illuminating instructions, I would not have come so far in my education, and this thesis would not have reached its present form.

Secondly, I would like to express my sincere gratitude to my co supervisor Prof. Henry Wong and other professors and lecturers at the Department of Civil and Environmental Engineering, who have instructed and helped me a lot during my study.

Moreover, I also own my heartfelt gratitude to my friends, my roommates, and my fellow classmates, Xu Ying, Jiao Yang, Tina Wang, Li Dazhong, Liu Wenfei, Liu Leilei, Li Kaihui et al. who offer me their helps and times with their encouragement and great support and make my day in Hong Kong.

Lastly, my thanks would go to my beloved family, my parents, Peng Hua and Zhang Jingzhi for their endless love and selfless support. Without them, there would be not who I am today.

LIST OF PUBLICATIONS

Journal Articles:

1. Cheng Y.M. and **Li N.** (2017), Equivalence between Bearing Capacity, Lateral Earth Pressure and Slope Stability by the Slip-line and Extremum Methods, International Journal of Geomechanics, ASCE, 17(12), 04017113.

2. **Li N.** and Cheng Y.M. (2016), Discrete Element Modeling on Bearing Capacity Problems, International Journal of Environmental, Chemical, Ecological, Geological and Geophysical Engineering, Vol:10, No:6, 560-567.

3. **Li N.** and Cheng Y.M. (2015), Laboratory and 3D-Distinct Element Analysis of Failure Mechanism of Slope under External Surcharge, Natural Hazards and Earth System Sciences, 15, 35–43.

4. Cheng Y.M., **Li N.** and Yang X.Q. (2015), Three Dimensional Slope Stability Problem with a Surcharge Load, Natural Hazards and Earth System Sciences, 15, 2227–2240.

5. Yi Yang, **Na Li**, Peng Yin and Y.M. Cheng (2013), Flow pattern for multi-size silos, Int. J. of GEOMATE, Dec, 2013, Vol. 5, No. 2 (Sl. No. 10), pp. 712-716.

6. Cheng Y.M., Lansivaara T., Baker R. and **Li N.** (2013), The use of internal and external variables and extremum principle in limit equilibrium formulations with application to bearing capacity and slope stability problems, Soils and Foundations, 53(1), 130–143.

7. Cheng Y. M., Au S.K., Pearson A. M. and **Li N.** (2013), An innovative Geonail System for soft ground stabilization, Soils and Foundations, 53(2), 282–298.

8. Cheng Y. M., Li D.Z., **Li N.**, Lee Y. Y., Au S. K. (2013), Solution of some engineering partial differential equations governed by the minimal of a functional by global optimization method, Journal of Mechanics, 29(03), 507-516.

9. Li D.Z, Cheng Y.M., Wang J.A., Yang Y., **Li N.** (2013), Finite element based limit analysis with mesh adaptation and applications in geotechnical engineering, Chinese Journal of Geotechnical Engineering, 35(5), 922-929.

10. Cheng Y.M., Chau K.T., Xiao L.J. and **Li N.** (2010), Flow pattern for silo with two layers of materials with single and double openings, Journal of Geotechnical and Geoenvironmental Engineering, ASCE, 136(9), 1278-1286.

11. **Li N.** and Cheng Y.M. (2017), Bearing Capacity Problem by Discrete Element Method and Comparisons with classical methods and Laboratory tests, International Journal of Geomechanics, ASCE (under review)

12. **Li N.** and Cheng Y.M. (2017), Lateral Earth Pressure Problem by Discrete Element Method and Comparisons with Classical Methods and Slip-line method, Journal of Geotechnical and Geoenvironmental Engineering, ASCE (under review)

13. Cheng Y.M. and **Li N.** (2017), Laboratory Test and Optimized DEM Analysis of Debris Flow (under preparation)

14. Cheng Y.M. and **Li N.** (2017), Particle flow pattern for silos with single and twin openings for homogeneous and nohomogeneous grains (under preparation)

TABLE OF CONTENTS

LIST OF TABLES

LIST OF FIGURES

CHAPTER 1 INTRODUCTION, OBJECTIVE AND SCOPE

1.1 Introduction

For most of the geotechnical problems, it is not easy to define the initial stresses, constitutive model as well as the load path precisely. In this respect, most of the engineers and researchers still adopt the ultimate limit state of the system for the assessment of a typical geotechnical system. There are several classical geotechnical problems which are commonly encountered in practice: lateral earth pressure, bearing capacity and slope stability problems. These three topics are covered separately in practically every textbook in soil mechanics and foundation engineering, and there are still significant amount of active research works in these areas at present. The treatments of these problems are generally different with separate methods developed for these problems. In literature, various methods of analysis and experiments have been developed for the three classical geotechnical problems, and there are great differences in the methods of analysis and conceptual assessment of these problems.

For the ultimate limit state of bearing capacity and slope stability problems, the use of the finite element/finite difference is sometimes adopted by the engineers, but not on a routine basis. On the other hand, the use of finite element method is not commonly adopted in actual practice for lateral earth pressure problem. For simple engineering problems, the use of bearing capacity factors and lateral earth pressure coefficients are commonly adopted, which is very different from slope stability analysis for which numerical method is commonly adopted. It appears that there are great differences between slope stability problem with bearing capacity/lateral earth pressure problems. It should also be noted that there are three bearing capacity factors as well as lateral earth coefficients in general, and such similarity is not simply by chance. On the other hand, the use of trial wedge method for lateral earth pressure and method of slices for slope stability analysis also looks similar to each other in some aspects. Despite such similarity, these three problems have been considered to be independent

problems in the past, and they are treated separately in virtually all the classical textbooks as well as research works. Visually, it is true that the three problems do not look similar to each other. For the methods of analysis, similarities between these methods are however found which are mentioned above. Such similarities should be considered, and this is one of the main objective of the present research work.

For slope stability problem, Cheng (2007e) and Wei and Cheng (2009b, 2009c, 2010b) have found that for normal problem, the results from the finite element method may be close to the classical limit equilibrium method. On the other hand, the finite element method has the disadvantages: (1) nonlinear solution problem with a soft band of frictional soil; (2) difficult to assess the local minima; (3) difficult to define the factor of safety and a precise 3D failure mechanism for slope with soil nails; (4) results can be sensitive to the mesh design or dilation angle. The close results between the use of finite element method and limit equilibrium in slope stability should be considered, as there may be underlying factors behind such similarities.

There are two major principles in geotechnical engineering: lower bound method and upper bound method. Based on these two principles, the upper and lower limits of the ultimate limit state of a geotechnical problem can be determined. Lower-bound method considers only equilibrium and yield, and classical limit equilibrium method is shown to be an approximate lower bound with a simplified internal force assumption (Cheng 2013a). In slope stability problem which is statically indeterminate in nature, assumptions on the interslice shear force function f(x) is required to determine the factor of safety. Though the choice of f(x) has only minor effect in most cases, there are also many cases where f(x) may have major impact on the analysis (Abramson et al. 2002, Cheng 2008e, Cheng 2010a), but there is no way to determine f(x) based on the classical approach. In general, lower bound analysis is much more difficult to be applied than the upper bound analysis.

If the geometry of the problem is simple, the plasticity based slip line method which is a typical lower bound method can be adopted for bearing capacity and lateral earth pressure problem. The results from slip line analysis are also usually taken to be the rigorous solutions which are used to calibrate the finite element analysis. In bearing capacity problem where a buried foundation is located away from the edge of a slope, Graham (1988), Booker (2002) and Cheng (2005c) have considered this problem using an approximate slip line method. The approximate method may be sufficient for design purpose, but conceptually this approach is not rigorous. Since the classical method by the method of characteristics has assumed the yield criterion in its basic formulation, the approximate method cannot be further improved under the context of classical method of characteristics. A refined and improved method using the analogy between global optimization method and variational principle towards this problem is achieved by Cheng (2013a) based on the extension of the previous works by Cheng (2008e, 2010a, 2011b). Under the new concept in this study, the extension of slip line method to partially yielded zone is approximately considered by limit equilibrium method with the internal force function being considered as the control variables. Through this approach, the equivalence between bearing capacity/slope stability problem as well as the slip line method/optimized limit equilibrium method are basically established. Actually, the same approach can also be applied to lateral earth pressure problem which will be shown in this thesis.

At present, the bearing capacity factors are commonly based on those obtained by the slip method, which is a typical lower bound solution of the governing equilibrium equation. For lateral earth pressure problem, the use of the Rankine solution, Coulomb solution or those based on the slip line method are commonly used. On the other hand, for slope stability problems, the use of the "simplified" or "rigorous" limit equilibrium methods are the most popular methods while the finite element or limit analysis are not commonly adopted. Although all the three classical geotechnical problems are controlled by the same equilibrium and yield conditions, there are great differences

between the slope stability problem and the other two geotechnical problems. Such difference are considered and investigated in the present work.

1.2 Objectives and scope

The present study focuses on the ultimate limit state analysis in geotechnical engineering using discrete element method, plasticity and extremum principle in limit equilibrium formulation. The present work is complicated and highly theoretical in nature, but the techniques developed can be used for general complicated problems without the use of assumptions which are required in the classical approaches. The four main objectives of this research are as follows:

1. To investigate the large scale failure mechanism and movement of soil on the bearing capacity of a strip footing by distinct element based particle flow analysis, and to observe the influence of micro-parameters on the bearing capacity of soil. This work will help to identify the failure mechanism of bearing capacity problems and identify the differences between DEM with classical Limit Equilibrium / plasticity solutions.

2. To analyze the lateral pressure behavior of soil under different boundary conditions and friction angles between a wall and particles using DEM and slip line method. To investigate the large displacement failure mechanism and movement of soil with the lateral earth pressure of a backfill, and the influence of the micro-parameters on the lateral pressure of soil is also observed. Through objectives 1 and 2, the limitations of the classical plasticity based method are investigated.

3. To develop the lower bound solution and extremum principle with internal and external variables in limit equilibrium slope stability analysis. Using the well-known bearing capacity solutions (slip-line method) to determine f(x), the thrust line and the base normal forces for a ‘‘horizontal slope’’ are determined. The equivalence between slope stability and bearing capacity problems by slip-line

and extremum limit equilibrium method is then demonstrated.

4. To demonstrate the equivalence between bearing capacity, lateral earth pressure and slope stability problems by slip-line and extremum principle in limit equilibrium methods in terms of the failure mechanism and ultimate loads.

This report is organized as follows:

Chapter 2 introduces Limit Equilibrium Method, Slip-line Method, Limit analysis and Discrete Element Method.

In **Chapter 3**, discrete element analysis (DEM) is carried out to study the bearing capacity problem of a shallow foundation, and to investigate the large scale failure mechanism and movement of soil as well as the influence of micro-parameters on the bearing capacity of soil. The numerical results obtained are then compared with the classical plasticity results by the Slip-line Method, Limit Equilibrium Method and laboratory tests.

Chapter 4 adopts DEM and Slip-line Method to analyze the lateral pressure behavior of soil under different boundary conditions and friction angles between a wall and soil. The large displacement failure mechanism and movement of soil with the lateral earth pressure of a backfill is further investigated, and the influence of the micro-parameters on the lateral pressure of soil is also observed. The numerical results obtained are then compared with the classical plasticity, slip-line method, and laboratory tests.

Chapter 5 firstly considers using slip line solutions for a bearing capacity problem. f(x) and thrust line for a ‘‘horizontal slope’’ are determined. It is proved that it is not important which

forces/variables are used in the stability formulation, either the external boundary forces or internal forces, if only the ultimate state is considered. Furthermore, it is demonstrated that the slip line solution is equivalent to the maximum extremum from the limit equilibrium analysis using a classical bearing capacity problem.

Chapter 6 demonstrates the equivalence between the classical lateral earth pressure and bearing capacity problem by the slip line method. The equivalence between the lateral earth pressure problem and slope stability problem will then be illustrated by the use of extremum principle. Based on these results, it can be concluded that the three classical problems are equivalent in the basic principles, and each problem can be viewed as the inverse of the other problems.

Chapter 7 presents the conclusions and summarizes the findings. The suggested further works are also proposed and discussed, which is to develop the lower bound/extremum principle for two and three-dimensional analysis by global optimization method, and Limit Analysis (DLO & FELA)**.**

CHAPTER 2 LITERATURE REVIEW

2.1 Introduction

In terms of stability analysis in geotechnical engineering, lower bound and upper bound theorems offer powerful tools, because they provide rigorous bounds that bracket the exact solutions which so far no other widely used methods could achieve, such as limit equilibrium method, slip line method or finite element method.

Limit equilibrium method is most widely used technique in geotechnical engineering, especially for slope stability analysis. The so-called limit equilibrium method has traditionally been used to obtain approximate solution to the problems in soil mechanics. Examples of this approach are the solutions presented in the book by Terzaghi (1943). The method can probably best be described as an approximate approach to the construction of slip-line field and generally entails an assumed failure surface of various simple shapes-planes, circular or log-spiral. With this assumption, each of the stability problems is now reduced to finding the most critical position for the failure or slip surface of the shape chosen which may not be particularly well-founded, but quite often gives acceptable results. In this method, it is also necessary to make sufficient assumption regarding the stress distribution along the failure surface such that an overall equation of equilibrium, in terms of stress resultants, may be written for a given problem. Therefore, this simplified approach makes it possible to solve various problems by simply statics. Various solutions obtained by this method are summarized in graphical or tabular form in the texts by Terzaghi (1943) and by Taylor (1948). The popularity of limit equilibrium resides in (1) its simple application to problems that include various loading condition, complex geometries, and soil profile; (2) ease to code into versatile software, and this method has been implemented into many commercial codes, making the technique even more attractive to practitioners.

However, it is worth mentioning here that none of the equations of solid mechanics is explicitly satisfied everywhere inside or outside the slip surface, and the equilibrium condition is satisfied only in a limited sense. Therefore, it is difficult to qualify the accuracy of this method.

Another important method adopted in the geotechnical engineering, primarily for soil mechanics, is the method of characteristics, also called the slip-line method. This method combines the Coulomb yield condition with the equilibrium to give a set of differential equations of plastic equilibrium. Together with the stress boundary condition, this set of differential equations can be used to investigate the stress at the ultimate condition. For instance, the bearing capacity of footing or the lateral earth pressure behind a retaining structure can be determined by slip line method. In order to solve specific problems, it is convenient to transform this set of equations to curvilinear coordinates whose direction at every point in this yielded region coincide with the direction of failure or slip plane. These slip directions are known as slip lines and network is called the slip-line field.

Kötter (1903) was believed to be the first to derive these slip-line equation for the case of plane deformation. The first analytical closed form solution to these was derived by Prandtl (1920), who developed the solution with a singular point with a pencil of straight slip-lines passing through it. These results were later applied by Reissner (1924) and Novotortsev (1938) to certain problems on the bearing capacity of footings on a weightless soil, when the slip-lines family were straight with close form solutions. Ponderable soil was treated later by iterative finite difference method by Sokolovskii (1960, 1965), who obtained a number of interesting problems on the bearing capacity of footings or slopes as well as the pressure of a fill on the retaining walls, for which closed form solution is impossible to find. De Jong (1957) on the other hand adopted a different approach and developed a graphical procedure for the solutions. Other forms of approximate solution include the application of perturbation methods (by Spencer, 1961) and series expansion methods. More recent results considering seismic effects, axisymmetric, etc. using slip line method were given by Cheng (2003, 2005, 2007) for bearing capacity and lateral earth pressure problems.

In general, in a slip-line solution, only a part of the soil mass beneath a footing or behind a retaining wall is assumed to be in a stage of plastic equilibrium. The solution consist of constructing a slip field in the region, which satisfies all the stress boundary conditions that directly concern the region, as well as the equilibrium and yield condition at every point inside the region. The stress field so defined is call partial stress field. The difficulties appear when attempting to extend the plastic stress field outside the slip network and stisfying equilibrium, yield condition, and boundary condition at the same time. When the velocity characteristics cannot be determined, which is often the case for many real problem, the corresponding stress characteristics do not repersent a complete solution by themselves. The detailed discuss on the above mentioned traditional method was presented in Chen (1975). Nevertheless, the solutions as obtained from the slip line method are usually taken as rigorous, and are commonly used to calibrate other numerical methods.

Finite element/finite difference methods have been widely used for many geotechnical stability problems over the past years. The most attractive aspect of these methods is the ability to simulate the material non-linearity and loading process by incremental analysis and in addition, it gives deformation which could be used as an alternative indicator rather than conventional factor of safety. Solutions given by Frydman (1997) and Griffiths (1982) are based on this method. FEM has played a dominant role in many engineering disciplines, however, a main drawback of this method is the requirement of the complex stress–strain relationship and the initial stress condition in the calculation. Cheng (2007, 2008) has carried out detailed study on the application of finite element method in slope stability methods, and many important limitations of the finite element methods are found.

Thanks to the bounds theorems by Drucker *et al*., though similar theorems are deducible from other work principle (Gvozdev 1960 and Hill 1950), lower and upper bound solutions can be calculated on a sound theoretical basis. The lower bound states that any load calculated from a statically admissible stress field, i.e. satisfying the equilibrium condition and boundary condition, nowhere violate the yield condition, would be less than the true collaspe load. On the other hand,

upper bound theorem states that any load calculated by equating the work done by the external force to power dissipation by a kinematically admissible velocity field must be greater than the true collpse load. A kinematically admissible velocity field must satisfy compatibility, velocity boundary conditions, and an associated flow rule.

The objective of the limit analysis is finding the most critical bounds, i.e. highest lower bound solution and lowest upper bound solution from possible statically admissible stress field and kinematically admissible velocity field respectively. The resulting mathematical optimization problem is solved luckily by the method of calculus for some simple cases, and more often, for modern limit analysis, would always be cast into standard mathematical programming, linear programming (LP) or non-linear programming(NLP) , with the stress field or velocity field constructed by the finite element metohd.

2.2 Limit equilibrium method

Up to the present, Limit Equilibrium Method (LEM) has been playing a dominant role in the stability analysis of real geotechnical problems, mainly due to its simplicity and the capability in obtaining approximate but realistic solutions for many complicated problems. The LEM is well known to be a statically indeterminate problem, and method of slices based on the LEM is commonly used by engineers for assessing the factor of safety of slopes. To determine the factor of safety, assumptions on the distributions of internal forces (or thrust line) are required for the solution of the factor of safety. Morgenstern and Price (1965) adopted an assumption that the relation between the interslice normal and shear forces could be specified to make the stability problem statically determinate. In this method, the relation between the interslice normal and shear forces can be described as

$$X=\lambda f(x)E \tag{2.1}$$

in which $\lambda f(x)$ is the inclination of interslice force, X and E are the interslice shear and normal forces, and λ can be determined by the equilibrium conditions when a given f(x) is prescribed by the engineers. In practice, f(x) is unknown, and several simple relations have been adopted in practice. Luckily, for most of the problems, the results of analysis are not sensitive to the choice f(x), hence most of the engineers have not paid sufficient attention to the definition of f(x). Cheng has asked many engineers about the definition of f(x) in several engineer technical seminars, and it appears that virtually no engineer is aware the meaning of f(x). It should also be noted that there are also many counter-examples where the choice of f(x) is important for the analysis, but the choice of f(x) cannot be determined simply from the simple limit equilibrium approach.

Spencer (1967) assumed that all the interslice forces could be assumed to be parallel to obtain the FOS. $f(x)$is hence actually specified to be 1, and $f(x)$ is constant in the Spencer's method. Some researchers have made different efforts on the investigation of interslice force function. Chen and Morgenstern (1983) have proposed that the interslice force relations for the first and last slices should be based on the Mohr-circle consideration. Fan, Fredlund and Wilson (1986) have proposed a function similar to the error function which is derived from an elastic finite element stress analysis. The validity of this function should actually be questioned as the stress state for slope stability analysis should be the ultimate limit state instead of the elastic stress state. Liang, Zhao and Vitton (1997) adopted the hypothesis of least resistance which stated that among all the forces satisfying the geometrical boundary conditions of a system, the smallest interslice force derived from local moment equilibrium of a slice will be the required force. This method will eliminate the requirement for $f(x)$ at the expense that the hypothesis is not necessarily the true phenomenon. The moment equilibrium of the last slice is also not considered in this formulation, and this formulation is very similar to the original Janbu's rigorous method (1973) and can be modified from the Janbu's rigorous method (1973) by varying the thrust line until the smallest interslice force is obtained.

For “rigorous” methods, “failure to converge” is well known among many engineers, in particular, for complicated problems with heavy external loads or soil reinforcement. Cheng et al. (2008b) have carried out a detailed study on the convergence problem in stability analysis and have concluded that there are two reasons for failure to converge with the rigorous methods. Firstly, the iteration method that is commonly used to determine the factor of safety may fail to converge because the interslice shear force is assumed to be zero in the first step of the iterative analysis. Cheng (2003) has developed the double QR method, which can evaluate the factor of safety and internal forces directly from a Hessenberg matrix. Based on this method, failure to converge in stability calculations due to the first reason can be eliminated. There are however many cases for which the double QR method determines that a physically acceptable answer does not exist for a given f(x), which means that no meaningful factor of safety will be available unless f(x) can be varied. Actually, some engineers have questioned the meaning of “no factor of safety available” for a given failure surface, as such concept does not appear in structural engineering. So far, there is little previous study on this type of failure to converge, and no “rigorous” stability method can guarantee convergence for the general case. Since the critical failure surface may not necessarily converge according to the existing “rigorous” methods of analysis (Cheng et al. 2008b, 2010), there is always a chance that the critical failure surface may be missed during optimization analysis. It is also interesting to note that it has never been proved that a slip surface that fails to converge in stability analysis is not a critical slip surface, but all commercial programs will simply neglect those slip surfaces which fail to converge. Although this problem may not be critical in general, a failure surface with no FOS is still physically surprising. A system without factor of safety is not real and this is just the human deficiency in making the wrong assumption, and this situation never appears in structural engineering or other similar disciplines. Factor of safety always exists for a problem, but it is possible that we are not able to determine it simply because of the use of wrong assumption, and this is supported by the study by

Cheng et al. (2008b) that many smooth slip surfaces can also fail to converge using the popular Spencer's analysis.

The popularity of LEM resides in: (1) simple to be used for problems which include various loading conditions, complex geometries, and soil profiles; (2) ease to code into general engineering software, and this method has been implemented into many commercial codes, making the technique attractive to practitioners. Despite the wide acceptance and the accumulated experience in the applications of LEM, there remain several weaknesses inherited in this approach: (1) none of the equations of solid mechanics is explicitly satisfied everywhere inside or outside the slip surface; (2) equilibrium condition is satisfied only in a limited sense.

2.3 Slip line method

Slip line method (SLM), also known as the characteristics method, provides an alternative to assess the ultimate limit state of soil mass. This method was developed in the beginning of 20th century under the theory of plasticity for metal. SLM combines the yield condition with the equilibrium conditions to give a set of differential equations of plastic equilibrium. Given the stress boundary condition, this set of differential equations can be used to investigate the stresses at the ultimate limit state. To solve specific problem, it is convenient to transform the plastic equilibrium equations to curvilinear coordinates where the direction at every point in the yielded region coincide with the direction of the failure or slip plane, which is why it is known as the slip line method (Hill 1950). The slip directions are called the slip lines, and the network of slip lines is called the slip-line field.

The solution of the slip line methods consists of constructing a slip-line field in a limited region that satisfies all the stress boundary conditions at the boundary points of the concerned region, as well as the equilibrium and yield condition at every point inside the region. As a result, the slip line method

could be considered as an incomplete “lower bound” technique, as only part of the soil mass beneath a footing or behind a retaining wall is assumed to be in the stage of plastic equilibrium. The stress field so defined is called the partial stress field. There is however difficulty in extending the plastic stress field outside the slip network and satisfying equilibrium, yield condition, and boundary condition at the same time. When the velocity characteristics cannot be determined, which is often the case for many real problems, the corresponding stress characteristic do not represent a complete solution. More detailed discussion on the above mentioned traditional methods is presented in Chen (1975, 1990).

2.4 Limit analysis

The underlying idea in limit analysis is to estimate the actual collapse load from two extremes by seeking the highest lower bound and lowest upper bound solutions under the framework of the bound theorems in the theory of plasticity (Drucker 1953; Drucker et al. 1952; Gvozdev 1960; Hill 1950). With the limit analysis, the lengthy elasto-plastic incremental analysis in the full numerical analysis is avoided. In comparison to other simplified methods, solutions by limit analysis are rigorous under the assumptions of (1) perfect plasticity, (2) associated flow rule and (3) small deformation. Similar to LEM, this method is not suitable to assess the deformation as well as the effect of progressive failure as the constitutive relation is not required in the analysis.

The theorem of lower bound (also known as the static principle of the limit analysis) states that any load calculated from a stress field that satisfies the equilibrium condition, boundary condition, and nowhere violates the yield condition would be less than or at most equal to the true collapse load. The stress field so defined is called the statically admissible stress field. On the other hand, the upper bound theorem (also known as the kinematic principle of the limit analysis) states that any load determined by equating the work done by external forces to the internal power dissipation

corresponding to a particular kinematically admissible velocity field must be greater than or at least equal to the true collapse load. The kinematically admissible velocity field refers to the velocity field that satisfies the compatibility condition and the velocity boundary condition. With the two principles, the exact collapse load could be bounded from the top and bottom, and the quality of the estimates of the true collapse load is automatically obtained by evaluating the gap between the two bounds. As limit analysis views the problem at the moment of the collapse, the only required inputs are the strength parameters (e.g. cohesion and friction angle for MC material) which are similar to the LEM. This method is therefore easier and simpler to use in practice in comparison to the full numerical methods.

The upper bound approach with simplified failure mechanism has received much attention from many researchers. Works following this line of research include: Chen (1975), Chen and Liu (1990), Michalowski (1989), Donald and Chen (1997), Chen et al. (2001a, 2001b), Wang et al. (2001a, 2001b, 2004), Wang and Yin (2002) and many others. Unlike the upper bound analysis, the rigorous lower bound analysis has been lagging behind due to the difficulties in the manual construction of the statically admissible stress field even for a simple problem, particularly when extending the stress field to a semi-infinite domain, which is usually the case in the geotechnical problems.

2.5 Discrete element method

The Discrete Element Method (DEM) was initially developed by Cundall (1971, 1974) for the study of Rock Mechanics problems. The method was later enhanced to various applications (Cundall and Strack 1979). The DEM has been used extensively to study physical and geotechnical phenomena such as stability of rock masses, constitutive relations for soil, mechanisms of deformation, flow of granular media, ground collapse and other types of geotechnical phenomena.

The distinct-element approach describes the mechanical behavior of both the discontinuities and the solid material. This method is based on a force-displacement law which is specifying the interaction between the deformable rock blocks and a law of motion which is determining displacements caused in the blocks by out-of-balance forces. Joints are treated as boundary conditions. Deformable blocks are discretized into internal constant-strain elements (Eberhardt, 2003).

In the DEM, the studied medium is divided into discrete elements with arbitrary shapes. Cundall and Strack (1979) demonstrate that the interaction of these elements is viewed as a transient problem with the states of equilibrium developing whenever the internal forces are balanced. The Newton's law is used to find the incremental displacements, velocities, and accelerations of the element, and the calculation cycle alternates between the sum of forces acting on an element resulting from a force-displacement law at the contacts. The time step is selected to be small enough so that disturbances do not propagate to more than the adjacent particles during each time step, and the accelerations can be assumed to be constant during that time step (Cundall and Strack 1979).

There are a series of computer program codes available in the literature for the application of the DEM. Most of these codes follow the pioneering work by Cundall (1974, 1978) with variations either in the modeling of the contact forces or in the solution algorithm. The first DEM code was developed for the study of rock mass behavior by Cundall (1971, 1974). Cundall also developed the Universal Discrete Element Code (UDEC) to model jointed rock mass and BALL and TRUEBALL for the study of granular media. UDEC is suitable for highly jointed rock slopes subjected to static or dynamic external loading. Two-dimensional analysis of the translational failure mechanism allows to simulating large displacements, modeling deformation or material yielding (Itasca, 2000). Three-dimensional DEMs have been developed in the early 1990s. Three-dimensional discontinuum code 3DEC contains modeling of multiple intersecting discontinuities and therefore it is suitable for the analysis of wedge instabilities or the influence of rock support (e.g. rockbolts, cables) (Eberhardt, 2003).

Discontinuous rock mass can be modeled with the help of distinct-element method in the form of particle flow code, e.g. program PFC2D/3D (Itasca, 1999) or other codes. Spherical particles interact through frictional sliding contacts. Simulation of joint bounded blocks may be realized through the specified bond strengths. The law of motion is repeatedly applied to each particle and the force-displacement law is imposed to each contact. Particle flow method enables modeling of granular flow, deformation between particles caused by shear or tensile forces, fracture of intact rock, transitional block movements, dynamic response to blasting or seismicity. These codes also allow to model subsequent failure processes of rock slope, e.g. simulation of rock fracture (Eberhardt, 2003). The method of particle flow code employs a time-stepping, explicit-calculation scheme (Cundall and Strack, 1979), which has advantages over traditional implicit calculation schemes in that it can handle a large number of particles with modest memory requirements because there are no matrices to be inverted, as the solution scheme solves the full dynamic equations of motion by dynamic propagation of waves through the material, and the velocities of the waves are dependent on the stiffness, density and packing of particles (Hazzard et al., 1998). This also allows physical instabilities such as shear-band formation to be modeled without numerical difficulty because kinetic energy that accompanies shear-band formation is released and dissipated in a physically realistic way (Itasca, 1999a). On the other hand, the use of dynamic relaxation to solve the system equation in DEM requires extensive cycle time to reach the equilibrium state. If the time-step chosen is excessive, the results obtained from the analysis can be meaningless. In practical application, greater care, knowledge and judgment is required for DEM as compared with FEM, and a large problem using DEM may require days or even weeks for the solution.

While distinct element methods are powerful tools for numerical analysis of discontinuous material in geotechnical problems and geological mechanics, there are also various limitations which should be pointed out here. The granular materials are considered to be packed assemblies of particles in DEM simulation, and the mechanical interaction between particles is assumed to be simple.

However, in reality, the contact between particles is highly complex and it is hard to be detected explicitly. Also it is difficult to generate complicated model geometry. In addition, Thornton and Lanier (1997) mentioned that the development of accurate contact constitutive models for use in discrete element analysis is non-trivial. The effective stress in a soil will govern its response and including pore water pressures in a discrete element framework is also non-trivial.

A central limitation of discrete element modeling is the difficulty associated with modeling the large number of particles that exist within soil volumes large enough to be of practical interest to the engineers. A real soil specimen, with a distribution of particle sizes would contain many more particles than simulated model. Also, the computational power will limit the maximum number of particles in the numerical models, not to say the duration of a virtual simulation. Moreover, it is difficult to provide the detailed information about the distribution and evolution of the contact forces and internal stresses available in a DEM analysis. In general, DEM is more suitable for qualitative than quantitative study, and its applications for real problems are not promising.

CHAPTER 3 BEARING CAPACITY PROBLEM BY DISCRETE ELEMENT METHOD, CLASSICAL METHODS AND LABORATORY TESTS

3.1 Introduction

Bearing capacity problem is always a main concern to the geotechnical engineers, and a shallow foundation needs to satisfy both the settlement and bearing capacity criteria. The ultimate bearing capacity for shallow foundations with simple geometry has been solved by many investigators. The methods of analysis can be classified into the following four major categories: (1) the limit equilibrium method (Terzaghi 1943; Meyerhof 1951); (2) the method of characteristics (Prandtl 1920; Reissner 1924; Sokolovskii 1960; Hansen 1961; Bolton and Lau 1993; Booker and Zheng 2000; Cheng and Au 2005, Martin 2005, Han et al. 2016); (3) the upper/lower-bound plastic limit analysis (Shield 1954a,b; Chen 1975; Sarma 1979; Sarama and Iossifelis 1990; Drescher and Detournay 1993; Michalowski 1995, 1997, 2001; Soubra 1999; Hjiaj et al. 2005; Krabbenhoft et al. 2005; Kammoun et al. 2010; Kumar and Khatri 2011; Ukritchon et al. 2003); and (4) numerical methods based on either the finite-element technique (FEM) or finite-difference method (Griffiths 1982; Manoharan and Dasgupta 1995; Frydman and Burd 1997; Yin et al. 2001; LimitState 2015). For the first three groups of methods, only the ultimate condition is considered, and a simple perfectly plastic soil model is implicitly assumed. The results from the first three groups of methods are also usually the same or very close to each other, and these results have been used for geotechnical design for many years. For the finite element method which can consider both the elastic and plastic stage, usually a simple constitutive model is assumed. With the same soil strength parameters, the ultimate bearing capacity from FEM are usually close to those from the first three groups of methods. In particular, the dilation angle is usually assumed to be either zero or the friction angle for soil in many FEM analyses and

sometimes in limit analyses. For the first two groups of method, dilation angle is however not required.

The failure mechanism and post-failure development are also important after the determination of the collapse load of foundations for some problems. While the finite element based methods can be used for the modelling of the pre-failure state and failure mechanism, the extension of FEM to very large displacement with separation of soil mass condition is difficult to be adopted. The particle-based distinct element method provides an alternative to the aforementioned issue. The distinct element method (DEM) initiated from Cundall and Strack (1979) has the advantage in modeling the development and propagation of failure after the initiation of the failure. For problem where the displacement is very significant, the use of DEM will be more appropriate than the classical continuum based method. It should also be noted that there are very limited applications of the DEM for bearing capacity problem up to the present, especially about the progressive failure mechanism of shallow foundations.

The objective of this chapter is to evaluate the bearing capacity problem by DEM, with comparisons to elasticity and plasticity theory, from the elastic condition to plastic condition with very large displacement condition. The large scale failure mechanism and movement of soil for the bearing capacity of a strip footing is further investigated, and the influence of the micro-parameters on the bearing capacity of soil is also observed. The numerical solution is established using a distinct-element-based procedure of the software PFC2D (particle flow code in two dimension). The numerical results obtained are then compared with the classical plasticity results by the slip-line method and laboratory tests.

3.2 Bearing capacity theory

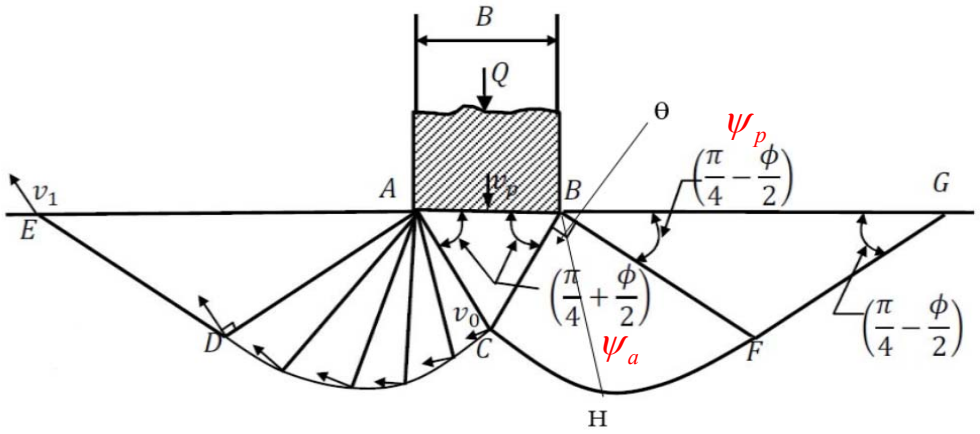

Figure 3.1 Prandtl's Mechanism

Bearing capacity problem is a classical problem which has been studied by Prandtl (1920), Hill (1950), Sokolovskii (1965), Chen (1975), Cheng and Au (2005) and many others using plasticity theory, limit analysis and slip line method. Prandtl (1920) has solved the slip line equation and obtained the failure mechanism as shown in Figure 3.1, assuming the weight of soil to be negligible. The two-dimensional strip footing's ultimate bearing capacity q_u for a frictional-cohesive material loaded by a uniformly distributed surcharge pressure q can be expressed as:

$$q_u = cN_c + qN_q \qquad (3.1)$$

where c and q are the cohesive strength and surcharge term respectively. N_c and N_q are actually exactly the same as those by Vesic (1973), Hansen (1970) and Meyerhof (1963). For the effect of the self weight γ of soil N_γ, different values have been obtained by different researchers based on different methods of analysis, and Sokolovskii (1965), Cheng and Au (2005) and others have demonstrated the finite difference solution of the slip line problem which are useful for more complicated cases. Typical slip line fields for the case of N_c (same as N_q) and N_γ as obtained by Cheng and Au (2005) are shown in Figure 3.2. It should be noted that in Figure 3.2a, the typical wedge-log-spiral-wedge is different

from that in Figure 3.2b, where the zone directly underneath the footing is not really a wedge while the transition zone is also not a true log-spiral zone. A wedge is however still found outside the transition zone in Figure 3.2b. It should be mentioned that some authors adopt the failure mechanism as shown in Figure 3.2a for the N_γ analysis by using the limit analysis method, and the author has found that the results using this approach are still close to that by the method of characteristics in most cases. Anyway, it is generally accepted that the transition zone takes a log-spiral shape (or close to log-spiral) which are obtained from the analytical and finite element solutions, and are further supported by limited experimental tests in the past (Yamamoto et al. 2009).

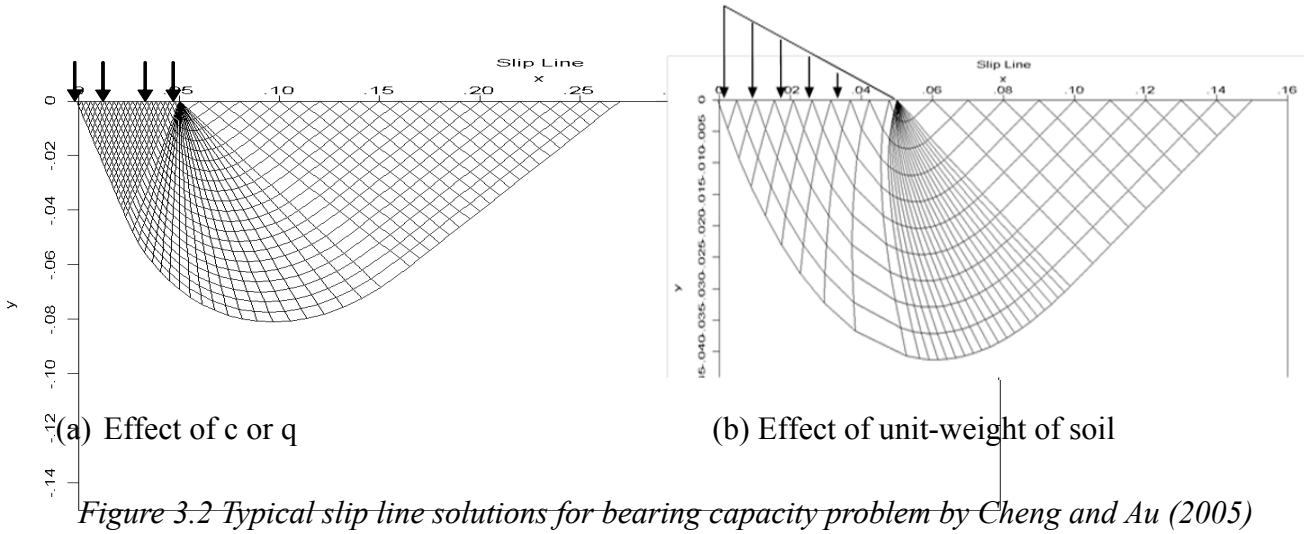

(a) Effect of c or q (b) Effect of unit-weight of soil

Figure 3.2 Typical slip line solutions for bearing capacity problem by Cheng and Au (2005)

3.3 Distinct element modelling of bearing capacity problem (elastic stage)

The author has tried to study this classical problem using the distinct element approach and laboratory tests. The reasons for using the DEM approach are: the complicated soil behavior (particularly the post-failure condition) is difficult to be modelled by simple elastic-perfectly plastic model or other simple constitutive models; (2) the higher order effect due to the geometric distortion at the collapse stage.

In the DEM analysis, the width B of the rigid footing on ground surface is set as 400mm as shown in Figure 3.3. Since the problem is symmetric, only half of the problem domain is considered, so that the footing width in the numerical model is 200mm. The half-domain has a depth of 3000mm and extends 5800mm beyond the edge of the footing, which is relatively large enough to eliminate the "boundary influence" on the estimation of the collapse load as well as for the prediction of the failure mechanism (shown in Figure 3.3). Two different loading patterns on the shallow foundation have been carried out in the numerical simulation: a prescribed velocity or a force on a horizontal footing, representing strain controlled test and stress controlled test respectively. Since there are no major difference in the results between the two loading patterns (similar to the results on the analysis of a loaded slope by Li and Cheng 2015), the loading pattern of the strain control/velocity control will be presented in the following sections. The uniform loading was simulated by applying a vertical velocity of 0.01mm/s on the footing.

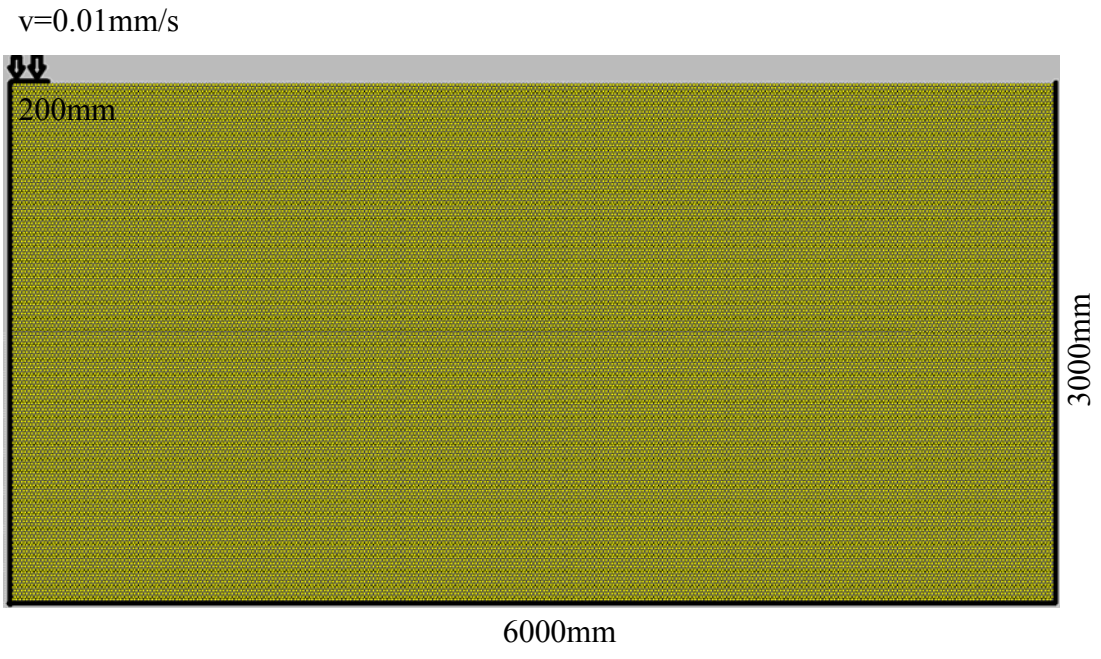

Figure 3.3 PFC Model for the simulation

The micro-properties of the sandy soil as shown in Table 3.1 are determined by varying the micro-properties until the macro-properties obtained numerically match with the experimental results (angle of repose and stress-strain relation), which is the approach as adopted by Cheng et al. (2009) and Cheng et al. (2010).

Table 3.1 Microscopic Parameters of the Sands for Particle Flow Analysis

Microscopic Parameters	Value (units)
Density (kg/m^3)	2650
Normal and shear stiffness (N/m^2)	1 x 10^7
Frictional coefficient of particle	0, 0.577; 0.700 ; 0.839
Diameter of particle (mm)	0.02; 0.06; 0.1
Contact Bond - Normal Strength (N)	0; 1000; 5000; 10000
Contact Bond - Shear Strength (N)	0; 1000; 5000; 10000

The values of the vertical stress σ_{yy} for first 60mm settlement are recorded in the DEM simulation in order to investigate the elastic stage of loading. If the stress is small with no yielding, the load/settlement relation should be a linear relation which is also predicted by the use of distinct element analysis as shown in Figure 3.4. The frictional coefficient of the particle has no practically effect on the result until a settlement of about 20mm, after which the effect of the frictional coefficient will affect the stress/settlement relation. The results in Figure 3.4 are in general compliance with the load-displacement relations from laboratory and field tests. It is also noticed from Figure 3.4 that soil with higher friction coefficient will have higher elastic limit. From the slope of the initial linear portion, Young's modulus of the dense soil can be estimated to be 10600 kPa from elasticity theory, which is similar to the Young's modulus of the typical compacted fill in Hong Kong.

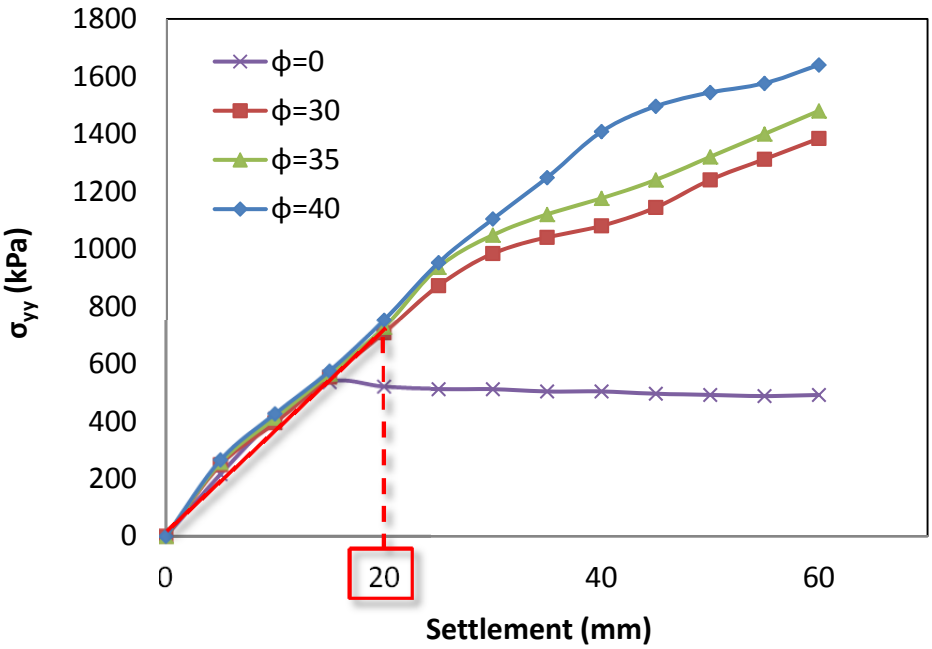

Figure 3.4 Variation of vertical stress with different settlement for dense sand (for initial 60mm vertical deformation)

3.4 Slip line method for the ultimate bearing capacity

When the deformation of soil is large enough to reach the plastic state, nonlinear stress/deformation behavior will be obtained which is clearly indicated in Figure 3.5. The bearing capacity or the ultimate limit state of a simple footing is governed by the plasticity slip line equations (2) and (3) under the Mohr-Coulomb yield criterion, and analytical and numerical solutions to these equations have been developed by Sokolovskii (1965), Booker and Zheng (2000), Cheng and Au (2005), Cheng et al. (2007) and many others. The classical slip line equations are governed by the following two α and β characteristics equations as follows:

$$\alpha \ characteristics: -\frac{\partial p}{\partial S_\alpha}\sin 2\mu + 2R\frac{\partial \theta}{\partial S_\alpha} + \gamma(\sin(\varepsilon + 2\mu)\frac{\partial y}{\partial S_\alpha} + \cos(\varepsilon + 2\mu)\frac{\partial x}{\partial S_\alpha}) = 0 \quad (3.2)$$

$$\beta \ characteristics: \frac{\partial p}{\partial S_\beta}\sin 2\mu + 2R\frac{\partial \theta}{\partial S_\beta} + \gamma(\sin(\varepsilon - 2\mu)\frac{\partial y}{\partial S_\beta} + \cos(\varepsilon - 2\mu)\frac{\partial x}{\partial S_\beta}) = 0 \quad (3.3)$$

where μ= (π/4-ϕ/2), γ is the unit weight of soil, θ is the direction of the major principal stress to y axis and ε is the angle between the body force and y-axis; and

$$p = \frac{\sigma_1 + \sigma_3}{2} \quad , \quad R = \frac{\sigma_1 - \sigma_3}{2} = p\sin\phi + c\cos\phi \quad (3.4)$$

where σ_1 and σ_3 are the major and minor principal stresses respectively, c and ϕ are the cohesive strength and friction angle of soil. The angle ε is generally 0 for this problem, as no earthquake is considered in this section.

From the results of program **SLIP** developed by Cheng and Au (2005), the slip line fields for N_γ (weight of soil is considered) are shown in Figure 3.5 with ϕ=10°, 20°, 30°, 40° and c=0, where the pressure on the ground surface at the left-hand side is determined from a slip line analysis. Similar results are also given by Davis and Selvadurai (2002). It is noticed that the active zones are actually curved, while the intermediate radial shear zone deviates from the classical log-spiral zone (still curved) with an inscribed angle less than 90°, following by the passive wedge zone at the right-hand sides of the problem domain, where the principal stresses are the vertical and horizontal stresses in the passive wedge. In Figure 3.5a where ϕ=10°, the radial shear zone is very small and the active zone will dominate the problem. When ϕ is further increased to 20°, 30° and 40°, the radial transition zone as well as the passive zone grow longer and larger and the slip line field widely spreads to a larger disturbed area. The extent of the failure zone in Figures 3.5a to 3.5d is smaller than the classical Prandtl's mechanism for all cases. There are two major factors affecting the slip line profile: unit weight of soil γ and friction angle ϕ, among which ϕ is the most influential factor as shown in Figures 3.5a to 3.5d. The corresponding results from Li (2014) using adaptive finite element limit analysis as

shown in Figures 3.5e and 3.5f are however basically similar to the classical failure mechanism as shown in Figure 3.1.

The active and passive Rankine zone angles ψ_a and ψ_p are calculated from the slip line analysis and compared with classical theory. The results are listed in Table 3.2, and the angles obtained from these two theories are very close to each other. These angles as obtained from slip-line method can be expressed as ψ_a =45.9°+0.5ϕ and ψ_p =45.9°-0.5ϕ, which will tends to the classical solutions of ψ_a =45°+0.5ϕ and ψ_p =45°-0.5ϕ if the mesh is fine enough in the calculation. The small differences between the results from SLIP and the classical theory is possibly due to the mesh size and the number of iteration adopted in the analysis (see Cheng 2003). It should also be pointed that the angle ψ_a from slip line analysis is the initial angle along the ground surface only, as this angle will be changing at different locations below the ground surface while it will be constant in the classical failure mechanism. Using the adaptive finite element limit analysis for the same problem, Li (2014) has obtained the failure mechanisms as shown in Figures 3.5e and 3.5f which are close to the classical failure mechanism as shown in Figure 3.1. For the wedge underneath the footing, there is a minor curvature to the inclined side of the wedge which is basically similar to that by the slip line method. The amount of the curvature of the wedge side from adaptive finite element limit analysis is however much less than that by the slip line method. Even though there are great differences between the failure mechanism as shown in Figures 3.5f and 3.5a to 3.5b, the bearing capacity N_γ from the two analyses are however similar with a maximum difference of about 2% only. The differences between slip line method and the adaptive finite element limit analysis is possibly due to the difference in the distribution of the vertical pressure underneath the foundation. A uniform pressure underneath the

footing is applied in the finite element limit analysis while a triangular pressure underneath the footing is back-computed from the slip line analysis.

From Figure 3.5, it is noticed that the transition zone from slip line/plasticity formulation does not look like the classical log-spiral zone, and the shape is actually close to that of a triangular zone for the effect of N_γ. However, the transition zone is a nice log-spiral curve for all cases (Figure 3.2a), as long as the unit weight of soil is zero. The actual failure profile will be one of the main area of study in this chapter, and both the plasticity method as well as laboratory and distinct element analysis will also be employed to study this problem.

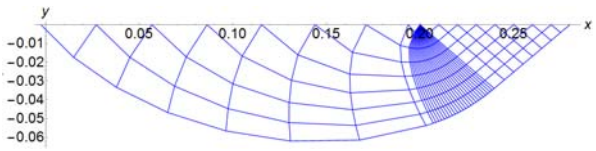

(a) Slip line field for ϕ=10°

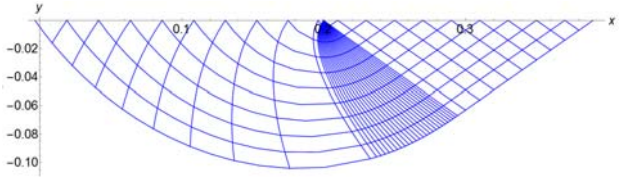

(b) Slip line field for ϕ=20°

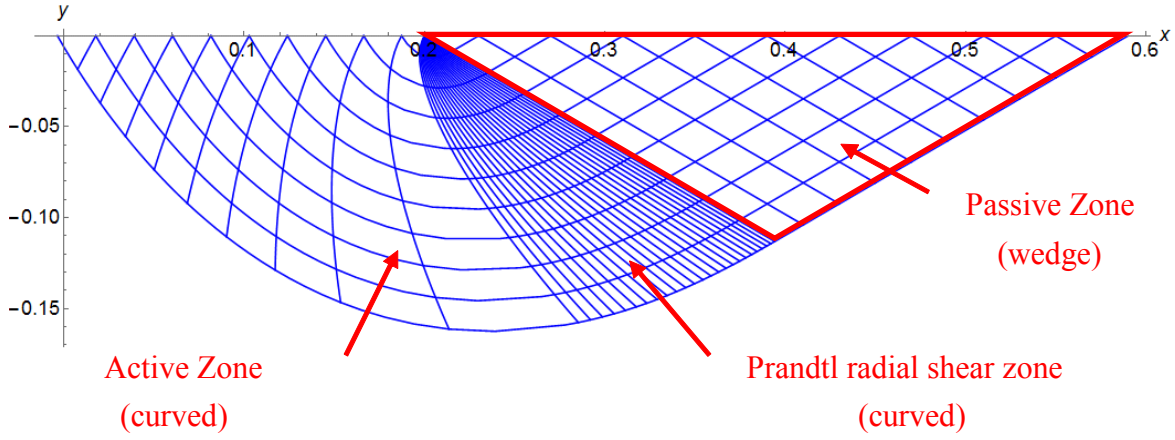

(c) Slip line field for ϕ=30°

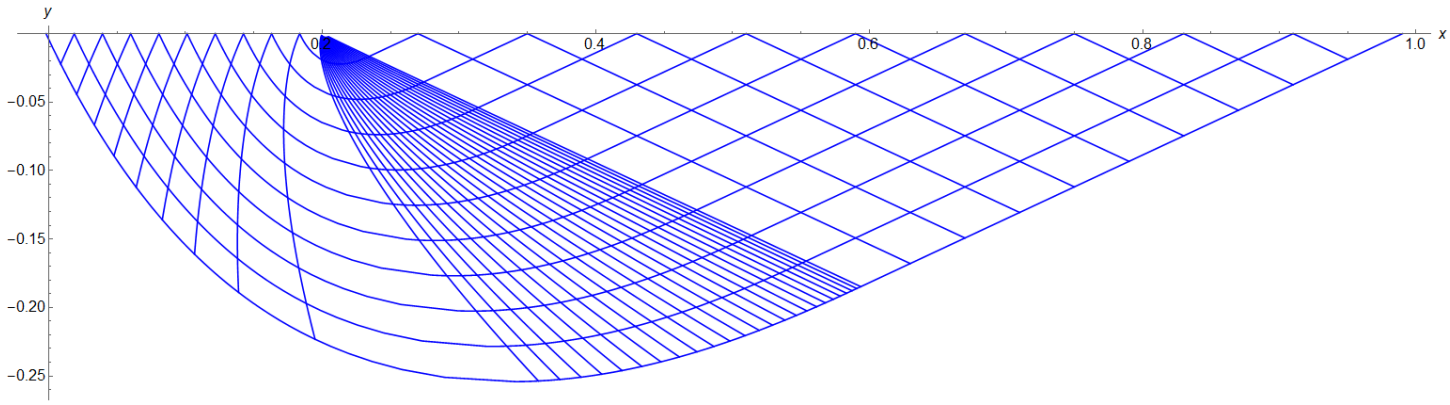

(d) Slip line field for ϕ=40°

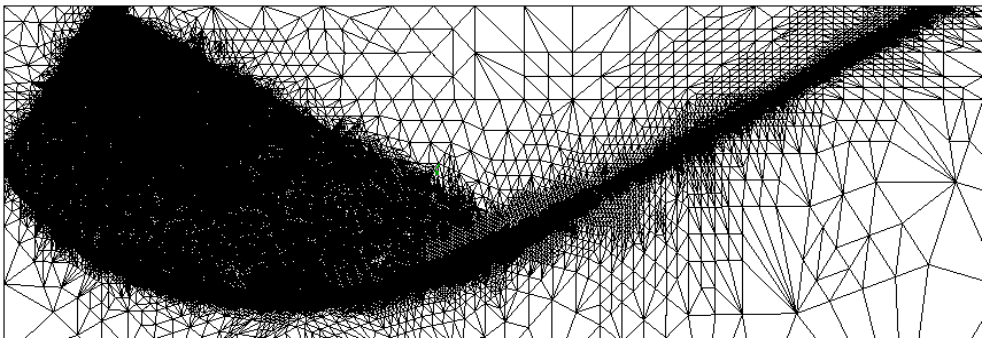

(e) Effect of c (ϕ=40°)

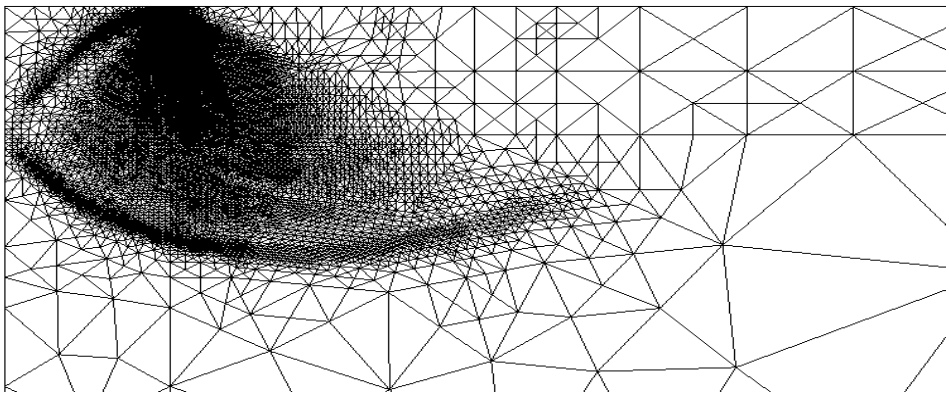

(f) Effect of unit-weight of soil (ϕ=35°)

Figure 3.5 Failure mechanism for case of N_γ when ϕ=10°, 20°, 30° and 40° by slip line analysis and adaptive finite element limit analysis (5a to 5d are results from slip line analysis and 5e and 5f are results from adaptive finite element limit analysis)

Table 3.2 Comparison of Active and Passive Rankine Zone Angles between SLIP and Prandtl Theory

ϕ	SLIP		Prandtl (1920)	
	ψ_a	ψ_p	ψ_a	ψ_p
10°	50.88°	40.88°	50°	40°
20°	55.89°	35.89°	55°	35°
30°	60.87°	30.88°	60°	30°
35°	63.39°	28.38°	62.5°	27.5°
40°	65.9°	25.89°	65°	25°

3.5 DEM analysis of general shear failure mechanism in densely packed soil

If the soil is densely packed, the failure mechanism from DEM will be similar to the classical general shear failure. The densely packed model is considered in a DEM analysis, and the progressive failure mechanism is illustrated in Figures 3.6 and 3.7. Two typical types of contact bond strength 0 and 5kN with $\phi = 35^o$ are considered to assess the general failure mode of densely compacted soil with no cohesive strength and with cohesive strength. It should be pointed out that the contact bond strength in distinct element analysis is not exactly equal to the cohesive strength in classical soil mechanics, but it can reflect the influence of the cohesive strength qualitatively.

For the soil with zero contact bond strength, the corresponding classical mechanism is the N_γ case, and the progressive failure is illustrated in Figure 3.6. Firstly, there is a small disturbed area

underneath the footing, then the affected area is extended. Two zones can be clearly seen in this process. The formation of a clear boundary for Zone I: Active Rankine Zone is noticed in Figure 3.6b. Soil particles underneath the foundation move further to the bottom right and develop Zone II: Transition Zone, and upheaval at ground surface further develops away from the edge of the footing. When settlement has achieved 70mm, Plastic Zone II is formed, and it gradually becomes clear under 200mm movement of the footing. Soil particles move further to the upper right, but unit weight of soils and bonding force chain between soil particles resist the shear slipping, and Zone III is then developed: Passive Rankine Zone which is noticed in Figure 3.6c. Traditionally, three zones are generated during the settlement of footing. However, there are additional shear band appearing in Figure 3.6c when the settlement is large enough, which may be due to the lack of soil contact bonding strength in this case (contact bond=0), and the slipping resistance is not sufficient to avoid development of shear cracking inside the soil mass. This phenomenon differs from the other cases with contact bond strength (> 0) which is shown in Figure 3.7. It is noticed in Figures 3.6c-3.6e that plastic zone I becomes smaller and smaller while its height grows shorter and shorter. Furthermore, a secondary shear failure surface is formed in Figure 3.6d and further upheaval occurs on soil particles above it due to the excessive settlement of the footing. Multiple failure zones similar to water ripples appear in Figure 3.6d, which represents the transformation of plastic zones from the disturbance area to the surroundings. Eventually, the displacement vectors form an anti-clockwise circular loop at the edge of footing resulting with mutiple shear failure surfaces in the disturbance area in Figure 3.6e. It should also be noted that the precise failure shapes can be slightly affected by the DEM computation, which is the typical problem for DEM analysis.

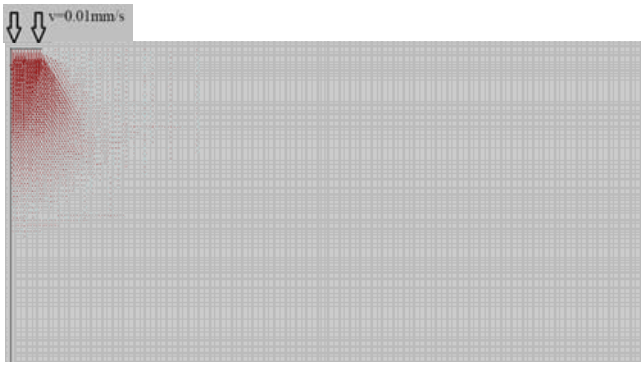

(a) Settlement=5mm

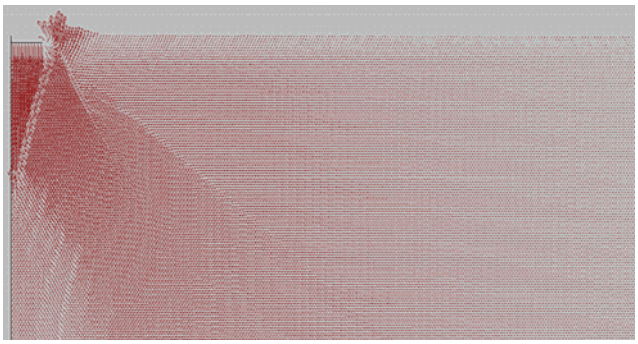

(b) Settlement=70mm
(Formation of Zone I & II)

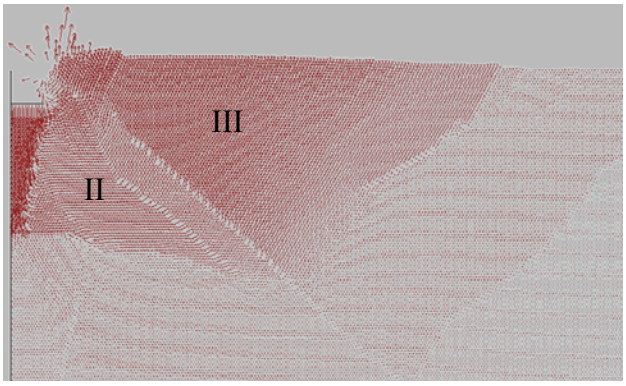

(c) Settlement=200mm
(Formation of Zone III-Rankine's Passive Zone)

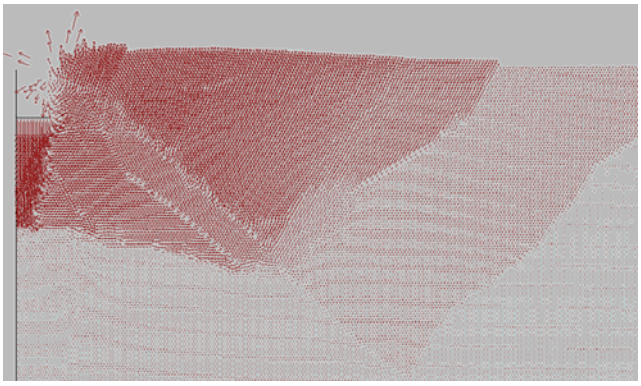

(d) Settlement=300mm
(Formation of Secondary Plastic Failure Zones)

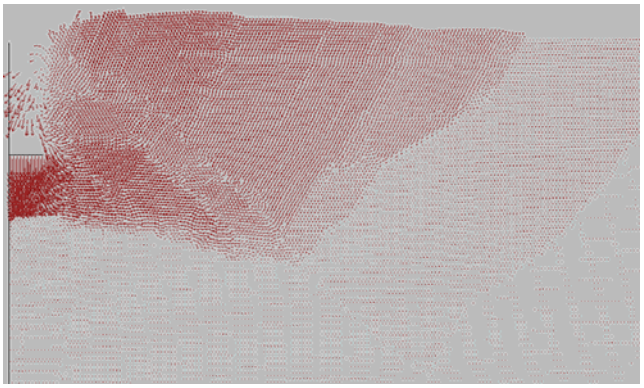

(e) Settlement=650mm (Eventual failure)

Figure 3.6 Failure progress of densely packed soil foundation (contact bond=0, ϕ =35^o)

For the soil with contact bond strength of 5kN, the soil particles go further downward with an increasing influenced area in Figure 3.7a. A clear boundary for Zone I: Active Rankine Zone is generated in Figure 3.7b, and soil particles underneath move further to the bottom right and Zone II: Prandtl Zone is developed. Upheaval further develops away from the edge of footing. Soil particles move further to the upper right but the unit weight of soils resists the shear slipping. Next, Plasctic Zone III: Rankine's Passive Zone is formed in Figure 3.7c. Soil within the Passive Rankine Zone is pushed by the soil from Zone II and starts to move upward causing upheaval. The shear band boundary of Zone II is then produced, and the primary shear failure surface penetrated through the plastic zone when the settlement reaches 100mm as shown in Figure 3.7d. Soil particles far away from the footing are affected by the shear slipping, and the primary plastic faulure zones further develop. Gradually, a secondary shear failure surface is formed and upheaval continues to grow, and a typical view of the failure zones with shear failure surface is given in Figure 3.7e. Further upheaval and deeper disturbance to the soil are induced from the excessive settlement of the footing. At this stage, the foundation is no longer a shallow foundation problem, as the depth of footing is equal to the width of footing, and the problem approaches that of a deep foundation problem. Furthermore, the displacement vectors form an anti-clockwise circular loop, and eventually 650mm settlement is generated after 65000 time-steps have been executed with a secondary plastic failure zones formed in Figure 3.7f.

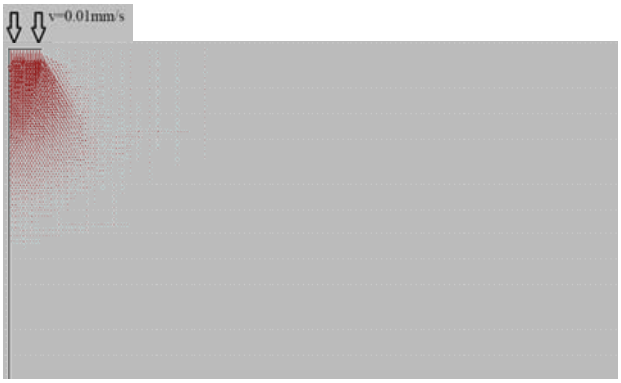

(a) Settlement=5mm

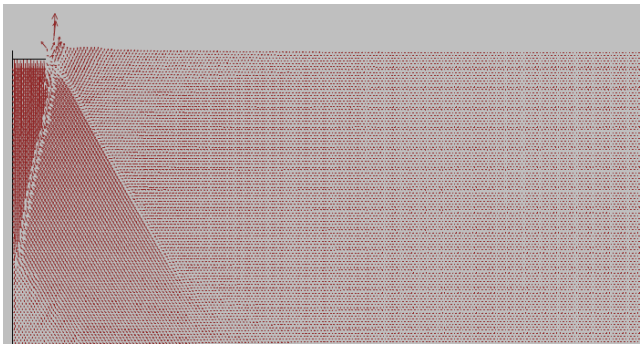

(b) Settlement=10mm
(Formation of Zone I-Active Rankine Zone)

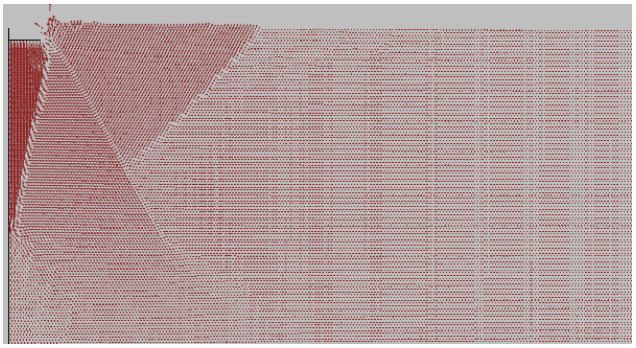

(c) Settlement=70mm
(Formation of Zone III-Rankine's Passive Zone)

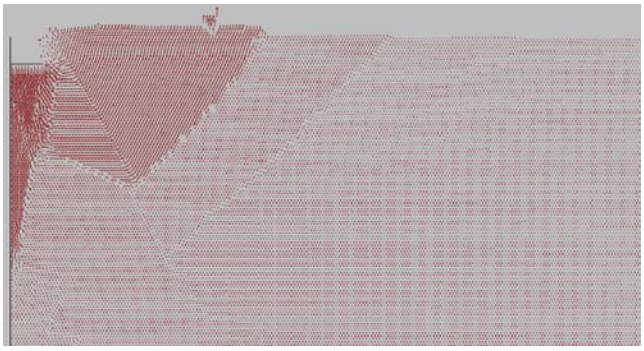

(d) Settlement=100mm
(Formation of Zone II: Prandtl Zone)

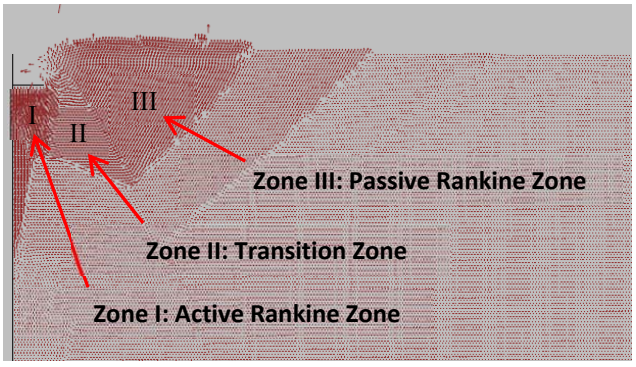

(e) Settlement=200mm
(Formation of Secondary Plastic Failure Zones)

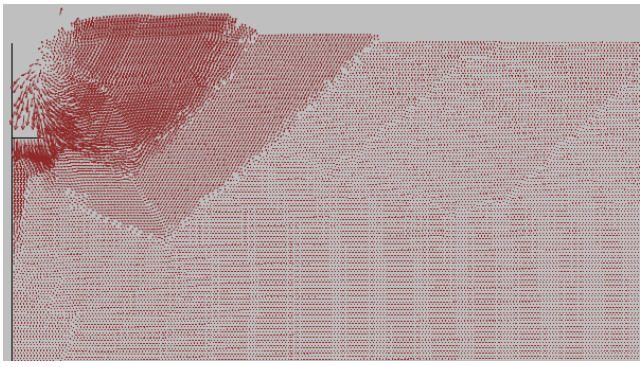

(f) Settlement=650mm
(Eventual failure)

Figure 3.7 Failure progress of densely packed soil foundation for a 0.2m width foundation (contact bond=5kN, ϕ =35^o)

From the results as shown, the failure mechanisms from DEM basically match with that by Prandtl (1920) in Figure 3.1. Among all, the failure pattern of the active and transition zones are similar to that by plasticity theory, and soil particles with higher friction angle has larger passive zone. The major difference between the present result and that by the classical plasticity theory is the transition zone.

Failure occurs when shear stress exceeds the shear strength, shear failure surface will then appear and a shear band will be formed. The mass of soil above the shear band is sliding uphill in relation to the stationary mass of soil below. In dense sands, there is a considerable degree of interlocking between particles. When interlocking is progressively overcome by the action of the external loading, the stresses acting on the soil particles decreases with increasing strain. The reduction in the degree of interlocking produces an increase in the volume of the specimen (dilatancy) during shearing, so that there will be volume change resulting with shear cracking as well as upheaval in soil mass.

Consider the soil underneath the footing in a microscopic view. The shear band has a thickness of h which is equal to the sum of several particle diameters in size, and the localized deformation occurs within the shear band. As shown in Figure 3.8, particles are in loose arrangement with visible void within the shear band if we view the particles carefully in microscopic scale as in Figure 3.8b. The average values of the shear and normal stress required for equilibrium can be found by the particles within the shear band with an extremely complex system of inter-particle contact forces. It is apparent that large shearing deformation will occur within the shear band, and some particles must either fracture on the surfaces parallel to the direction of slip, or else move out of the way so that other particles may slide past. Some fracturing will occur as the average shear stress grows, but it will most probably involve the breaking off of asperities from the particle surfaces rather than a major fracture along the slip direction. In this DEM simulation, circular particle is used to simplify the soil mass model, and crushable soil or so called fracture/breakage mechanism which is a more complicated phenomenon which is not studied here.

The soil mass above the shear surface moves with a displacement which has components both parallel and normal to the shear surface. The direction of the motion will lie at an angle ψ, called the angle of dilatancy, above the shear surface. In general, the angle of dilatancy will be smaller than the angle of internal friction ϕ as shown in Figure 3.8. If we recall that the soil shear strength is given by the product of the angle of internal friction and the normal effective stress on the slip surface, we can see that the friction angle actually represents two sources of strength. One is the frictional resistance caused by particles grinding past one another and the second is interlocking. Interlocking of particles causes dilation and may contribute significantly to the overall soil strength.

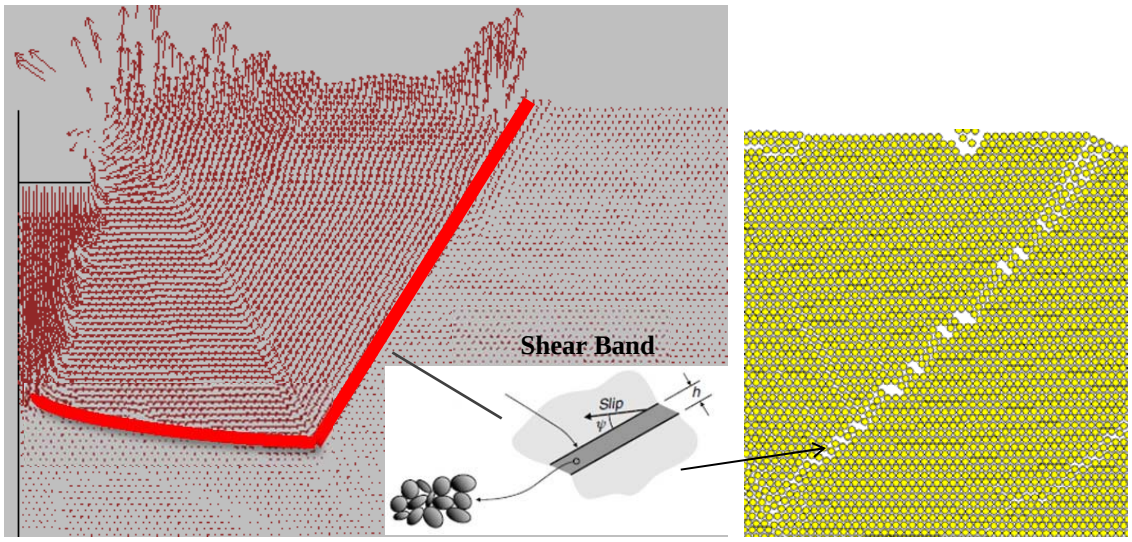

(a) Displacement vector (b) Enlarged soil particle model

Figure 3.8 Shear band within a typical shear failure surface

3.6 Influence of friction angle

Four values of friction angles, 0^o, 30^o, 35^o, 40^o are considered for soil with contact bond strength = 5 kN, for the study on the influence of friction angle on the failure mechanism. The shear failure modes for each friction angle under the same settlement are represented in displacement vector figures

in Figure 3.9. It is found that the shape of the failure depends mostly on the friction angle. The angle of Zone I ψ_a differs from that in Figures 3.9a to 3.9d, and the area of Zone I grow larger with steeper triangle following with increasing disturbance area (plastic failure zone), so that failure patterns among these four cases are different. Thus, friction angle influences the shear failure mechanism more than the bond strength. Meanwhile, the disturbed area is enlarged with the increasing soil friction angle from Figure 3.9 which is also consistent with the classical theory.

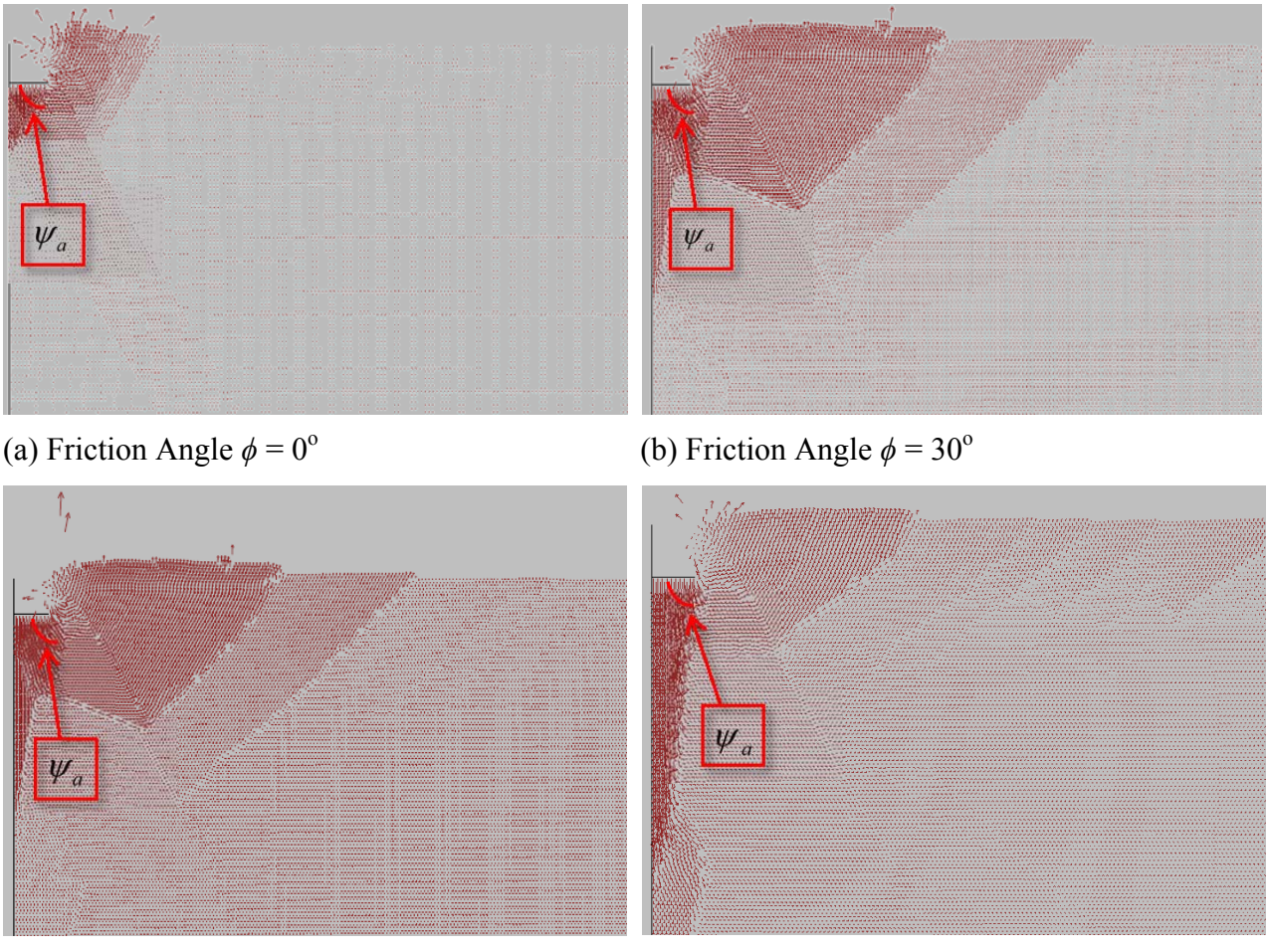

(a) Friction Angle $\phi = 0^o$ (b) Friction Angle $\phi = 30^o$

(c) Friction Angle $\phi = 35^o$ (d) Friction Angle $\phi = 40^o$

Figure 3.9 Shear failure mode of a strip foundation under ultimate bearing capacity with different friction angles of sandy soil (unit weight of soil≠0, contact bond strength = 5 kN)

3.7 Influence of unit weight of soil

To assess the equivalent N_c analysis, the unit weight of soil is set to be negligible in this section. Classically, many researchers still adopt the log-spiral zone in the failure mechanism even though the results from plasticity analysis in Figure 3.5 do not support the log-spiral failure zone. From our DEM analysis in Figure 3.10, such a distinct log-spiral transition zone is not obtained even when the unit weight of soil is negligible, which is different from the classical solutions. If the unit weight of soil is considered which is shown in Figure 3.11, it appears that the failure zone will be reduced with the self-weight of soil. The local failure beneath the footing is also less prominent in Figure 3.11, as compared with that in Figure 3.10 (bearing in mind that the ultimate settlement of the footing is extremely large).

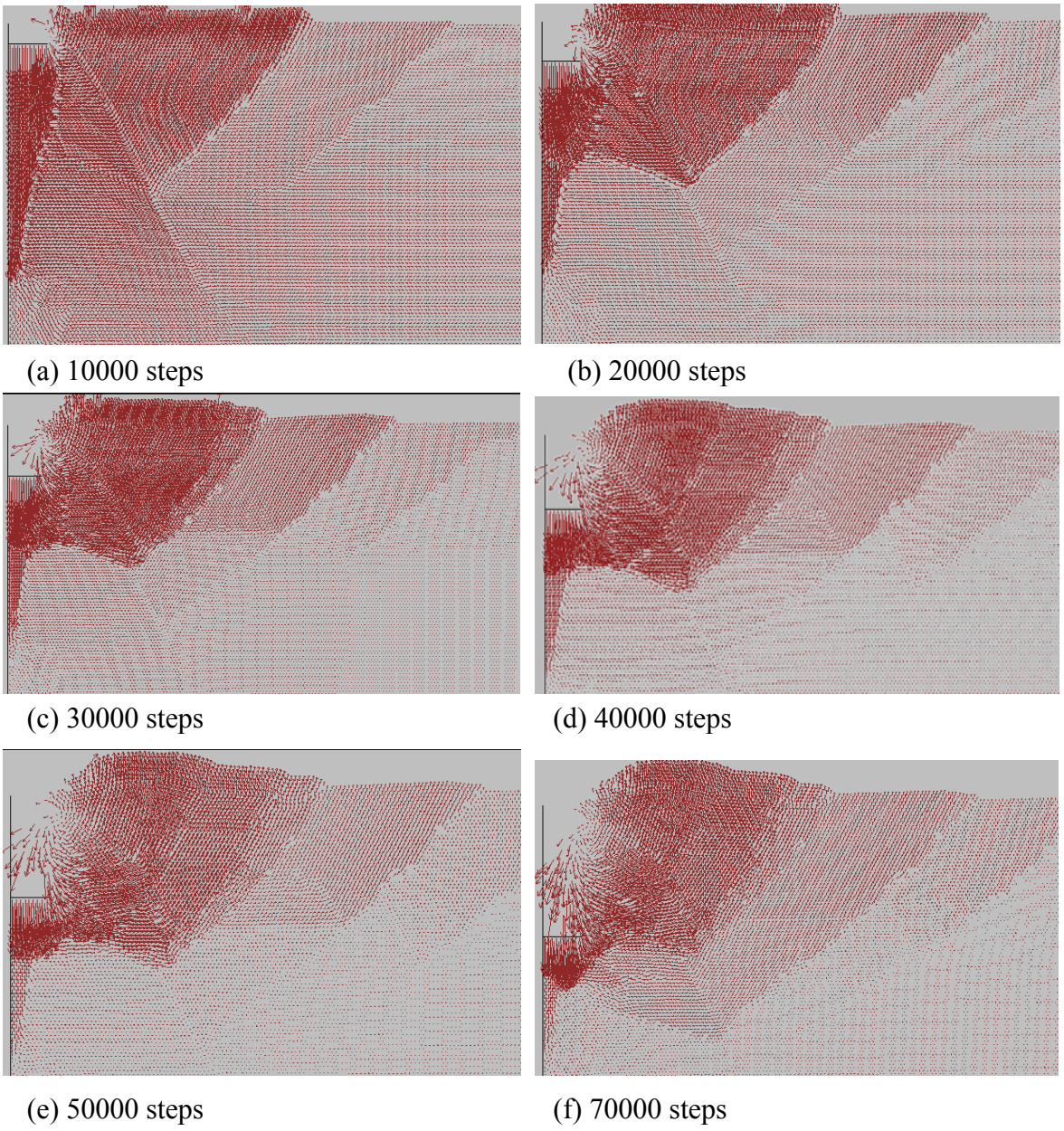

Figure 3.10 Shear failure mode of a strip foundation under ultimate bearing capacity with unit weight of soil $\gamma = 0$ (contact bond strength = 5 kN, $\phi = 35^o$)

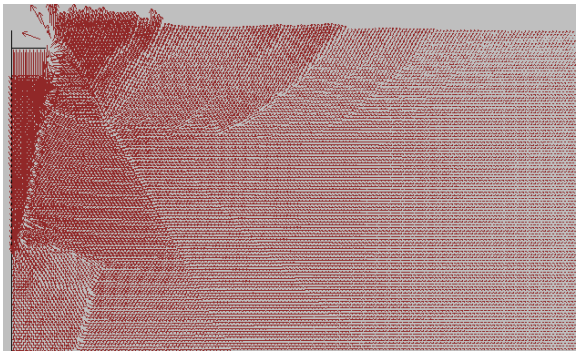

(a) 10000 steps

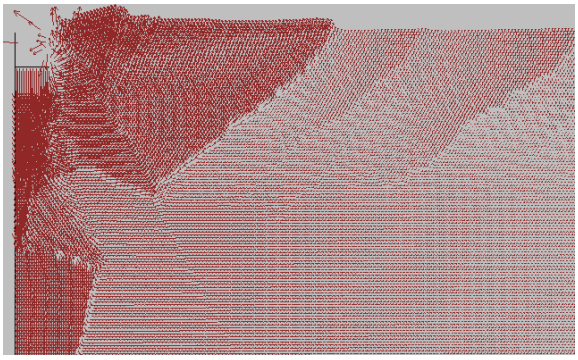

(b) 20000 steps

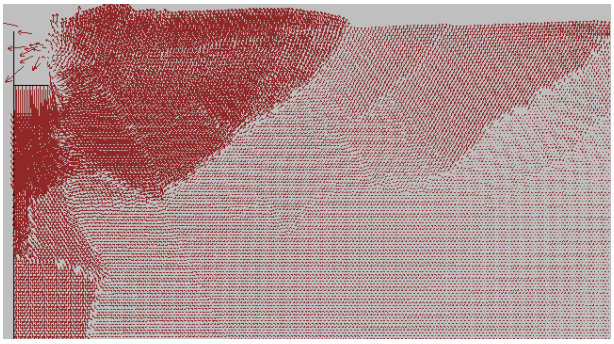

(c) 30000 steps

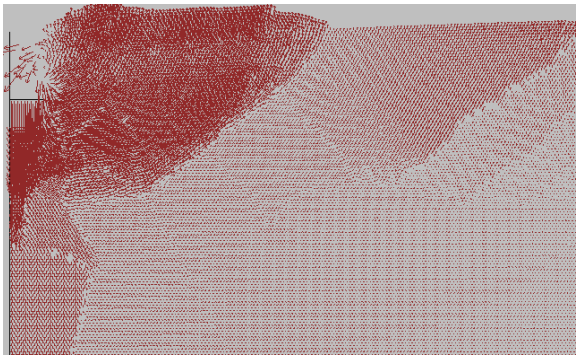

(d) 40000 steps

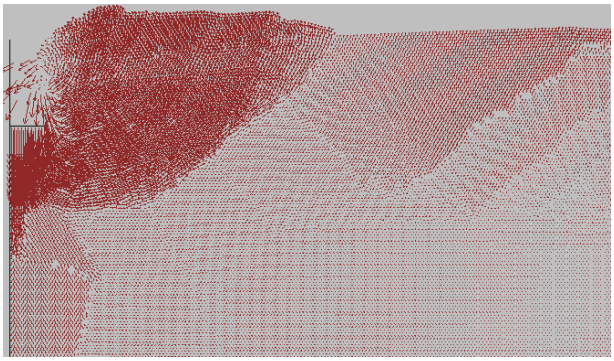

(e) 50000 steps

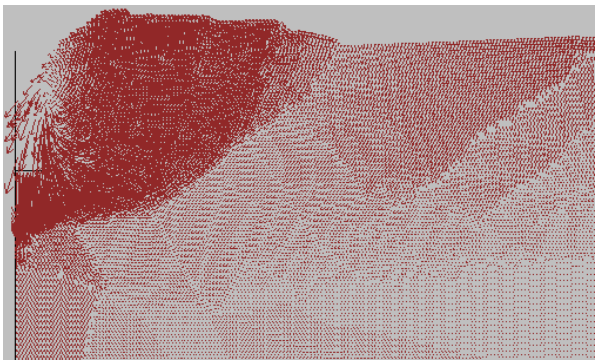

(f) 70000 steps

Figure 3.11 Shear failure mode of a strip foundation under ultimate bearing capacity with self weight of soil γ (contact bond strength = 5 kN, $\phi = 35^o$)

3.8 Discussion on the load-settlement relation from DEM

The load-settlement relations with the variation of soil friction angles obtained from DEM simulation are plotted in Figure 3.12. When ϕ = 35°, the ultimate bearing capacity (vertical stress σ_{yy}) is around 2400 kPa, and is equal to 3200 kPa when the friction angle=40°. The ultimate bearing capacity is highly dependent on the friction angle of soil, but not for the initial slope of the load settlement relation. Inner-particle bonds are mobilized in the first stage of load settlement relation until the peak resistance, beyond that some inter-particle bonds are broken with a drop of the bearing stress, but the microstructure is still randomly oriented where most of the frictional resistance still work. The increasing deformation gradually produces an aligned microstructure along the failure surface, and eventually a residual strength of about 1000 kPa is obtained. The precise load deformation relation as shown in Figure 3.12 is highly affected by various factors such as void ratio and angularity of particles, but qualitatively, the numerical result can describe the behaviour of real soil. The initial interlocking effect between dense sand particles has been progressively overcome during the compression, and the shear dilatancy effect for dense sand occurs followed by increase in volume and porosity which are illustrated in Figure 3.13. It can be concluded that with increasing footing settlement, compression to soil particle has overcome the interlocking effect, resulting in volume and porosity increase, followed by slipping (shear failure), further volume expansion and upheaval on the ground surface.

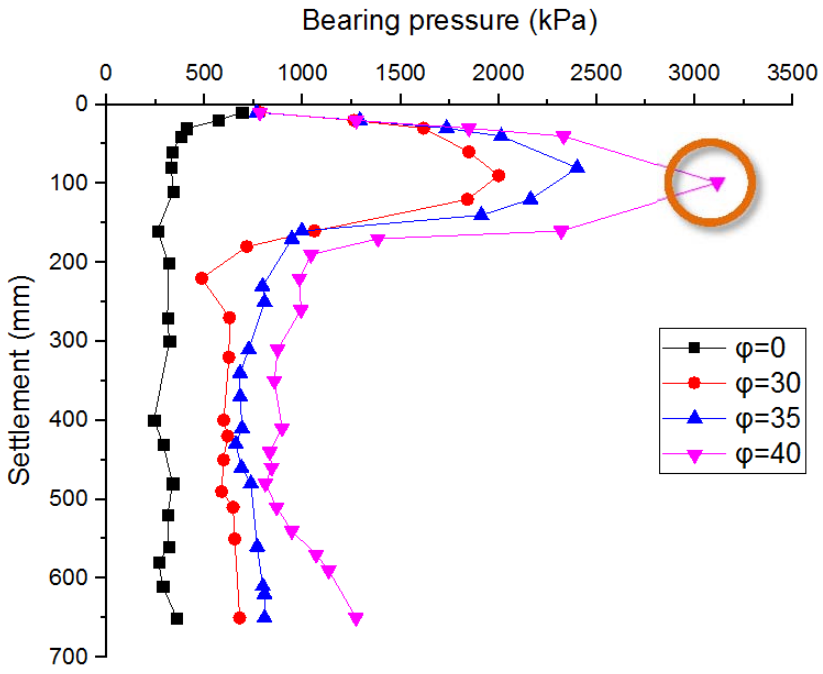

Figure 3.12 Load-settlement curves with different friction angles for bond strength = 10kN

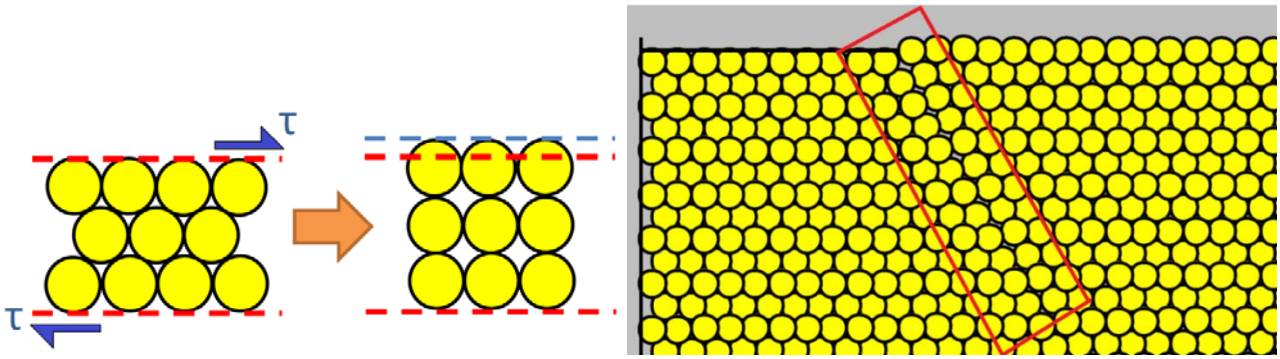

(a) Dilatancy for dense sand (b) Volume expansion causes upheaving

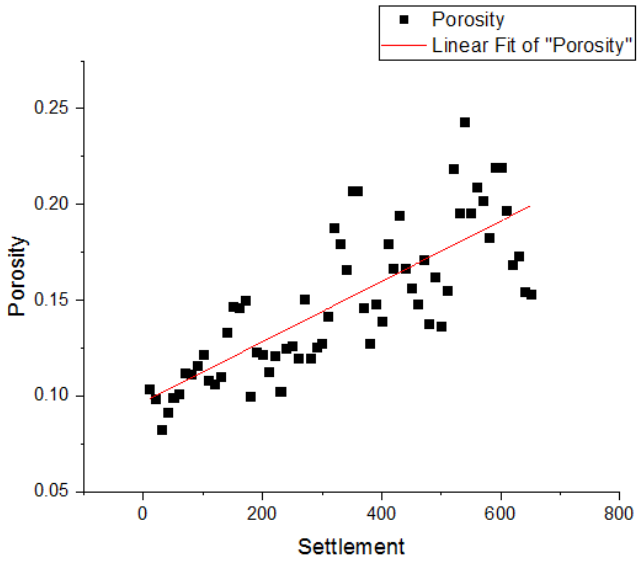

(c) Porosity increase during footing settlement

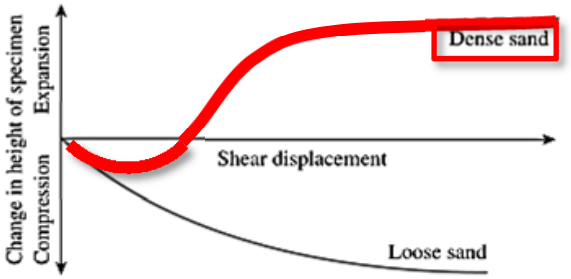

(d) Variation of volume with settlement of shear box test

Figure 3.13 Volume dilation for shallow foundation on dense sands

3.9 Discussion on the ultimate bearing capacity between various methods

Figure 3.14 shows the variation of ultimate bearing capacity with friction angle under N_γ case, obtained by DEM analysis and compared with the classical Vesic Equation and slip-line method. Cohesive/bond strength and surcharge for soils are hence not considered here. The results by Vesic equation is higher than those by slip line method, and this has been discussed by Cheng and Au (2005). It is observed that the results by DEM are always greater than those by the slip line method or Vesic equation, and this phenomenon is not surprising as DEM is well known to be more appropriate to qualitatively than quantitative analysis. In general, the results from DEM are not bad. N_γ is well known to increase rapidly with the friction angle, and this phenomenon is also captured by DEM in the analysis. In this respect, we can safely accept the qualitatively study on the failure mechanism of shallow foundation as given in previous sections.

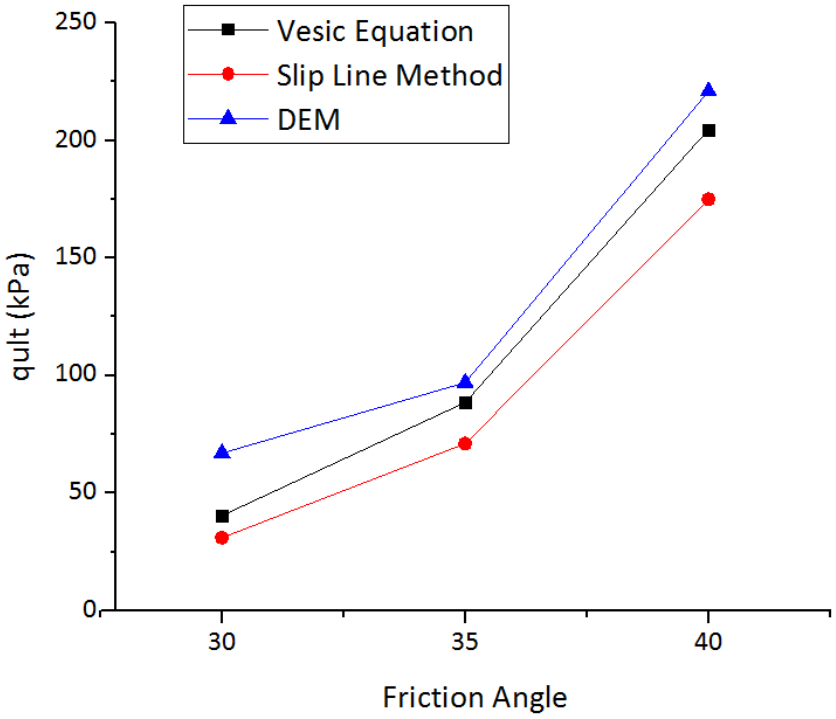

Figure 3.14 Variation of q_{ult} with friction angle using DEM & Prandtl Mechanism (Vesic Equation) & Slip-line Method under Nr case (width of foundation=0.2m) (results from adaptive finite element limit analysis are close to those by slip line method and are not shown for clarity)

3.10 Discussion and comparisons with laboratory test

In the previous studies using DEM, it is found that the classical log-spiral zone is not found from the analysis. Actually, the author has tried to vary the micro-parameters over a wide range, but the log-spiral zone is still not obtained. With the use of finite element analysis, log-spiral zones are obtained by some researchers (Conte et al. 2013), but not for all. Manoharan and Dasgupta (1995) have found the radial shear zone and Yamamoto and Otani (2002) have obtained circular surface zone by finite element analysis, while Yamamoto and Kusuda (2001) applied upper bound analysis and get circular surface transition zone. The author has also tried several finite element programs, and log-spiral failure zone as shown in Figure 3.15 is obtained for the case of N_c by Plaxis. From the

author's trials, it appears that not every finite element program (actually very few) will give the log-spiral transition zone even for the case of N_c, not to say for the case of N_γ. The sensitivity of the N_γ failure mechanism has been noticed by Griffith (1982), Manoharan and Dasgupta (1995), Frydman and Burd (1997) and many others, and the author has noticed that not every researcher can obtain the log-spiral (or close to log-spiral zone) in the numerical analysis. Based on the X-ray CT imaging of 3-D bearing capacity test by Takano et al. (2012), it appears that the log-spiral transition may not necessarily be formed. The author has also carried out series of three-dimensional bearing capacity laboratory tests, and the three test results with no reinforcement are given in this section. The author has noticed that it is not easy to capture precisely the failure mechanism for many cases, and the log-spiral transitions are also not clearly reported in many previous experimental or numerical studies.

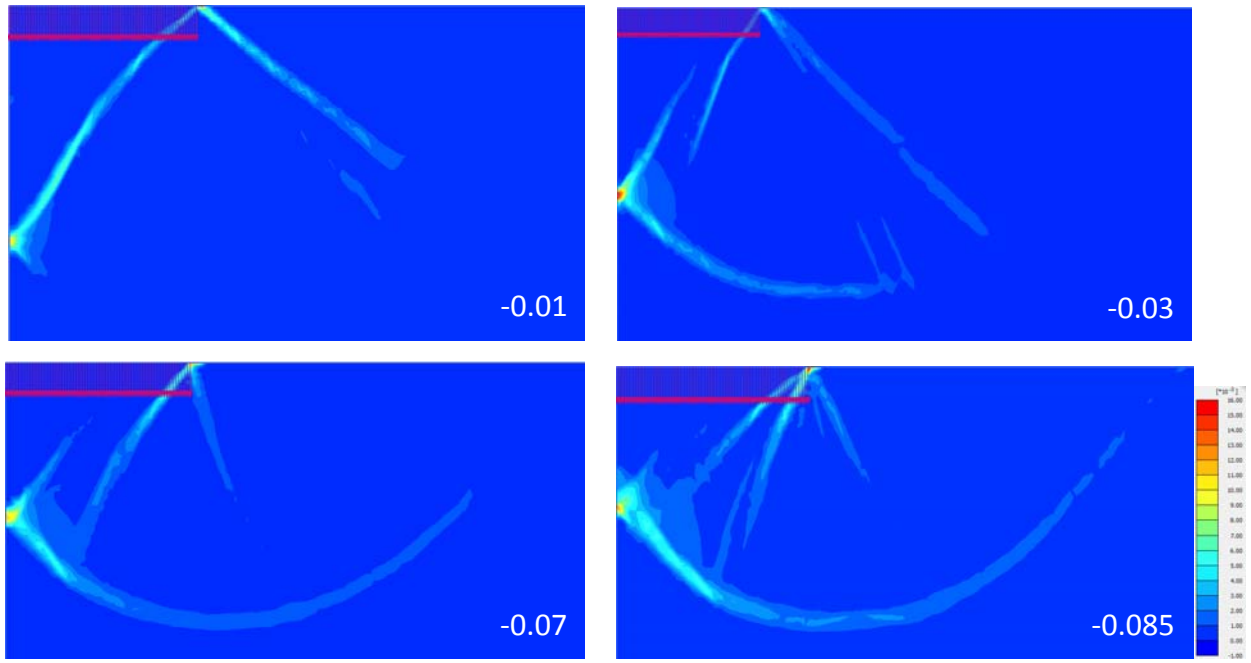

Figure 3.15 Accumulated shear strain increment under the indicated uniform prescribed displacement (m) in the vertical direction during the whole failure progress using finite element analysis by Plaxis

To gain a better understanding about the failure mechanism, the author has constructed series of model tests with a slope in front of the footing, and the failed mass are removed for examination of the actual failure surfaces. In Figure 3.16, the hydraulic jack applies a local load on top of a 0.8 m high 65° inclined slope for which the soil is highly permeable, poorly graded river sand. The unit weight and the relative density of the river sand which is obtained in Hong Kong are γ = 15.75 kN/m^3 and 0.55. The soil parameters are c' = 7 kPa and ϕ' = 35°. The depth, breadth and height of the tank are 1.5 m, 1.85 m and 1.2 m respectively. Five Linear Variable Differential Transducers (LVDT) are set up to measure the displacement of soil at different locations, and the displacements at different vertical loads are monitored up to failure. The 10mm thick steel bearing plate has a size B = 0.3 m and L = 0.644 m at 0.13 m away from the crest of the model, and an ultimate load of 35 kN is attained at a displacement of about 6 mm as shown in Figure 3.17. As a result, the ultimate bearing capacity of the slope under the current soil properties, geometrical conditions and boundary conditions is 181.2 kPa which gives a factor safety 1.021 by the present method, and this value is very close to 1.0 which demonstrates that the result is reasonable. For the slope surface, the corresponding displacement at the maximum pressure is about 2 mm and 1 mm at top and bottom of the slope respectively. Beyond the peak load, the applied load decreases with the increasing jack displacement. It is observed that the displacements of the slope are basically symmetrical. The failure surface of the present test is shown in Figures 3.16a and 3.16b, and the sectional view at the middle of the failure mass is shown in Figure 3.16c. In Figure 3.16a, after the maximum load is achieved, the load will decrease with increasing displacement. At this stage, the local triangular failure zone is fully developed while the failure zones at the two ends of the plate are not clearly formed. When the applied load has decreased down to about 25 kN (the settlement develops to approximately 8mm), the load maintained constant for a while and the failure zones at the two ends are becoming visually clear. When the displacements are further increased, the applied load decreases further and the failure zone propagates towards the slope surface until the failure surface as shown in Figure 3.16b is obtained. For this test, there are several

interesting phenomena worth discussing. The failure profile and cracks are firstly initiated beneath the footing as shown in Figure 3.16b, which is a typical bearing capacity/slope stability failure with a triangular failure zone noted clearly in Figure 3.16c. As the load increased, the failure zone extended and propagated towards the toe of the slope and the final failure surface is shown in Figure 3.16b. It is observed that the failure mechanism of the physical model test is hence a local triangular failure beneath the bearing plate, and the failure surface propagates towards the slope surface until a failure mechanism is formed. The classical failure mechanism for bearing capacity with an inclined slope based on that by Cheng and Au (2005) or Sokolovskii (1965) where a transition log-spiral will appear after the triangular wedge underneath the footing is however not clearly developed. Instead of that, the transition zone appears to be another wedge which is followed by another wedge adjacent to the transition zone. The actual failure mode in Figure 3.16c appears to match better with the results by DEM than by FEM or plasticity theory. If the position of the loading plate is varied as shown in Figure 3.18, then failure mechanisms from experiments still appears to be composed of three or more wedges instead of the classical failure mechanism. Yamamoto and Kusuda (2001) have obtained transition zone which is closer to a circular arc than a log-spiral zone from the laboratory tests. In the experimental tests by Mwebesa et al. (2012), it is also found that the log-spiral zone is not found in the bearing capacity test in Philippi Dune sand which has a soil parameter of ϕ'=34°and c'=6.7 kPa. Actually, it appears there are only limited test results where the log-spiral transition is actually obtained in tests. Apparently, many researchers have jumped into the adoption of the log-spiral mechanism and have overlooked that there are also many counter-examples in literature.

(a) Bearing failure beneath bearing plate

(b) Global three-dimensional failure beneath bearing plate

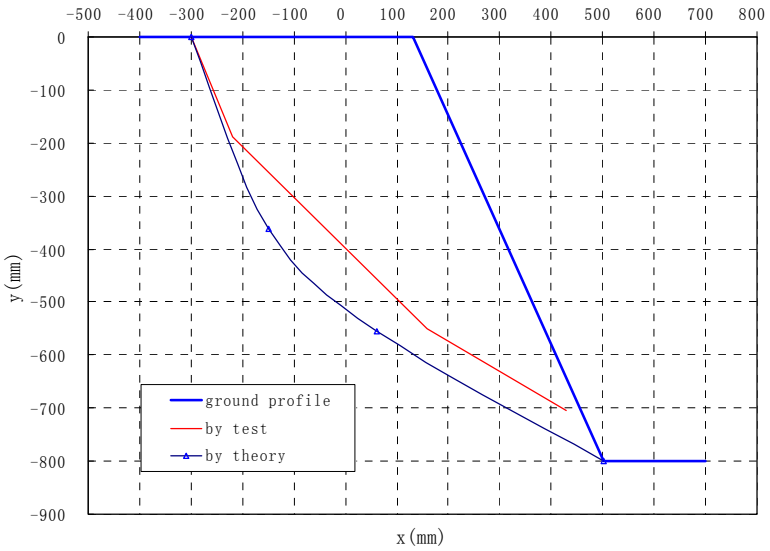

(c) Comparisons between the measure and the predicted failure surface profile at mid-section of failure

Figure 3.16 Laboratory bearing capacity test and investigation of failure surface

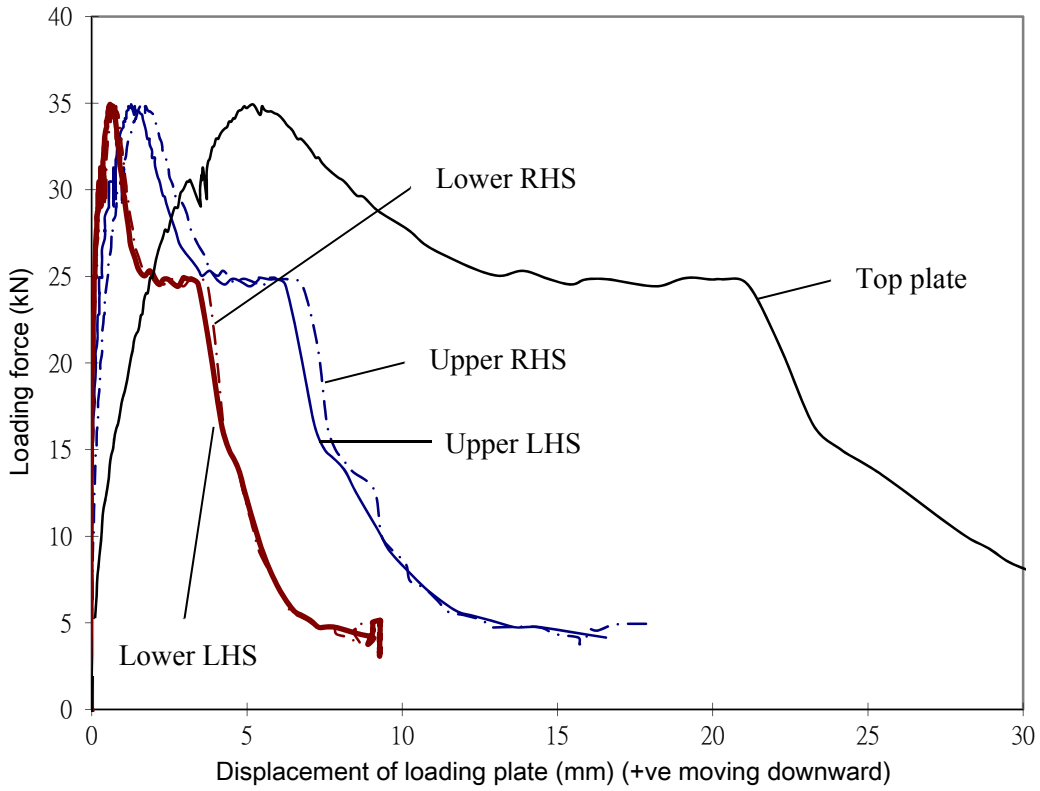

Figure 3.17 Loading force against the displacement of slope surface

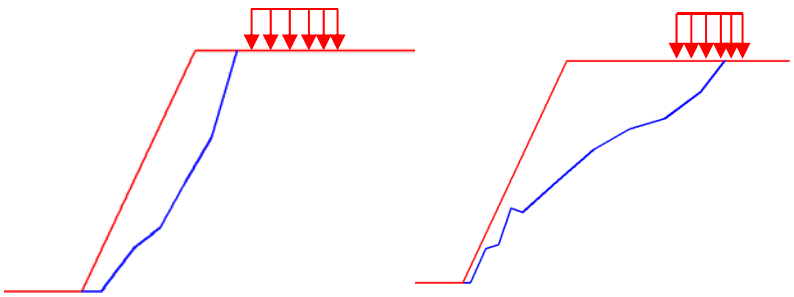

(a) Loading closer to crest (b) Loading further away from crest

Figure 3.18 Failure mechanism with change of loading plate position for the laboratory test in Figure 3.16

3.11 Discussion

In this study, slip-line method, adaptive finite element limit analysis and discrete element analysis are used to study the bearing capacity problem of a shallow foundation and to investigate the shear failure development from elastic condition to plastic condition, then extend to large displacement condition. The large scale failure mechanism and movement of soil on the bearing capacity of a strip footing are also studied. The numerical results obtained by the Discrete Element Method based particle flow analysis are then compared with the plasticity solution by Prandtl (1920), the slip-line method as well as the laboratory tests.

For the elasticity analysis, the general behaviors of soil particles analyzed by Discrete Element Method coincide well with that derived by the theoretical elasticity method. For the plastic condition, the slip-line method differ from the adaptive finite element limit analysis if the unit weight of soil is considered. The failure mode of bearing capacity problem under large displacement simulation is hence studied by the use of DEM. Densely packed soil foundation is considered to investigate the general shear failure mechanism. The progressive failure progress is studied and concluded as follows: as the uniform loading is applied to footing acting on soil, firstly there is a small disturbed area under the footing, then plastic area is extended showing clearer view of Plastic Zone I and Zone II, and finally Zone III appears. Next, shear failure surface becomes continuous, followed by upheaval on ground surface. As the settlement keep increasing, plastic zones extend to the surrounding area, so that secondary failure surface occurs and multiple failure zones show up, and the plastic failure transfers to a larger disturbed area followed by further upheaval.

It is found that punching shear failure will occur in fairly loose sand or soft clay (not shown in this thesis). This failure mode also occurs in soil of low compressibility. From the DEM studies using different micro-parameters, it is found that the friction angle influences more than the bond strength on the shear failure mode of foundation. For the case of uniform loading on shallow foundation for dense sands, elastic footing settlement takes place in the very beginning, inducing compression to soil

particle to overcome the interlocking effect and resulting in soil mass volume increase as well as increase in the porosity (shear dilatancy effect). As the loading increases, that will be followed by slipping (shear failure), volume expansion and upheaval on the ground surface. Above all, DEM gives a very good visualized results, and basically coincides well with the classical understanding. It is however unable to reproduce the well-known log-spiral transition zones in all the cases over different micro-parameters (including many other results not shown in this chapter) in this study.

Fu et al. (2016) has obtained a near log-spiral transition zone from DEM which is not able to be reproduced in the present study (despite various trials of micro-parameters). To assess the acceptability of a proper failure mechanism, particularly for the case of the self-weight of soil, several laboratory tests have been carried out. From the test results by the author, it is found that the classical log-spiral mechanism as given by the classical plasticity based approach (for zero unit weight) is not obtained which is also consistent with some of the previous test results. On the other hand, the failure mechanism which is comprised of three wedges from DEM or plasticity theory as given by Figure 3.5a to 3.5d can match better with the experimental results. In this respect, the validity of the log-spiral transition zone can only be viewed as an approximate solution which may be good enough for engineering use only.

3.12 Conclusion

While the concept of log-spiral transition zone has been widely accepted and used for analysis, design and stabilization, the validity of this failure mechanism should be further verified. In the present study, different numerical methods have been used, and it is found that the classical log-spiral transition zone concept is possibly an approximation only, and the suitability may decrease with increasing friction angle. So far, there is only very limited application of the discrete element method in the bearing capacity problem. The author has demonstrated the suitability of using DEM for both

the elastic and plastic stage bearing capacity problem, and the failure modes as obtained are in form of wedges which are similar to the present and some previous laboratory tests. It is true that the present DEM results cannot reproduce all the previous laboratory based failure modes, but neither can the classical plasticity based method or the finite element method can reproduce all the observed failure modes.

The author suspects that unless an advanced soil constitutive model considering the micro-behaviour of soil is adopted, together with the anisotropy or other possible factors, different methods can only reproduce some of the observed failure modes. Up to the present, there is very few application of DEM in the study of the bearing capacity problem, but the author views that there are some potential advantages in using DEM for qualitative study of the bearing capacity problem. In the Discrete Element Method, the micro-parameters such as the normal and shear stiffness, granular size, particle size distribution, porosity, interlocking effect can affect the bearing capacity which is not included in the classical Prandtl and Vesic Equation, not to say the shear dilatancy effect. From the present study, the author has observed that DEM seems to be an appropriate method for the bearing capacity problems. It can provide additional insights into many geotechnical problems which are not possible with other methods. With the rapid development in computer technologies, it is believed that DEM can be widely used and can supplement the continuum method such as FEM to solve some geotechnical engineering problem in the near future.

CHAPTER 4 LATERAL EARTH PRESSURE PROBLEM BY DISCRETE ELEMENT METHOD AND COMPARISONS WITH CLASSICAL METHODS AND LABORATORY TESTS

4.1 Introduction

Lateral earth pressure is usually considered in the design of earth retaining structures such as retaining wall, lateral support excavation system and bridge abutments. To determine the magnitude and distribution of the lateral soil pressure, the stress-strain behavior of soil should be considered. Similar to many geotechnical problems, the complete analysis is usually hindered by insufficient information on the insitu stresses, constitutive behavior of soil and other uncertainties. Virtually, all practical analyses on lateral earth pressure are still based on the ultimate limit state analysis. There are many existing theories in predicting the lateral pressure in an empirical or analytical way. Rankine earth pressure theory based on the basic yield criterion (Rankine, 1857) is the lower bound solution which is commonly used for the lateral active and passive lateral earth pressure determination. On the other hand, Coulomb theory (Coulomb, 1776) provides the upper bound solution based on the assumption of an assumed failure mechanism which will be varied in the solution until the critical result is obtained. Besides theoretical approach, Terzaghi (1932, 1934a, 1934b), Schofield (1961), Matteotti (1970), Bros (1972), Sherif and Mackey (1977), Matsuo and Kenmochi (1978) and Fang et al. (1986, 1994, 2002) have carried out the experimental tests on the development of lateral earth pressure.

In addition, the plasticity solution (slip line method), limit analysis, finite element and other methods have also been proposed for this problem. In general, there are no major differences between the results from these methods. Many other researchers and professionals (e.g. Bang 1985; Mei et al.

2009) have also studies this topic in order to accurately determine the lateral earth pressure. The estimation of the movement of a real retaining wall is complicated which involves several factors such as wall rigidity, construction method, wall movement and support conditions, and an extensive study on the rotation of a retaining wall conditions was studied by Fang et al. (1994), Osman (1990), Ouria and Sepehr (2015) and others. The studies indicated that if the centre of rotation was further away from the wall, the effect of the rotational wall movement on the passive earth pressure became less significant, and vice versa. As the centre is far enough from the wall, the wall movement becomes translational. Fang et al. (2002) conducted a series of experiments to figure out the effect of soil density on the passive earth pressure for dense, medium dense and loose soils. Both dense and medium dense soils exhibit a peak value in K_p after small wall movement, but the K_p coefficients of soils with different initial densities finally converge to the same magnitude after a relatively large passive wall displacement is mobilized.

In reality, for the sake of simplicity and convenience, the pressure by Rankine's and Coulomb's theories with the use of suitable factor of safety is commonly adopted in engineering design. However, the overestimation of the passive earth pressure in Coulomb's theory is well known, and diverse results of the passive earth pressure with high wall friction (Cheng, 2003) exist in different earth pressure theories. Additionally, the earth pressures from these classical theories only give a general picture without the effects from the modes of the wall movement.

Rankine and Coulomb earth pressure represent two limits of the ultimate earth pressure. For lower bound approach, the conditions of equilibrium and yield are satisfied without the consideration of the mode of deformation. The Mohr-Coulomb failure criterion is also used to be the yield criterion. In the upper bound approach, a mechanism of plastic collapse is formed by choosing a slip surface (usually a combination of surfaces with log-spiral curve) and the work done by the external forces is equated to the loss of energy by the stresses acting along the slip surface, without consideration of the equilibrium. The chosen collapse mechanism is not necessarily the true mechanism, but it must be

kinematically admissible and the motion of the sliding soil mass must be compatible with its continuity and with any boundary restrictions. Lower and upper bound plasticity solutions have been given by Atkinson (1981) and Parry (1995).

In general, the four methods as outlined in chapter 3 for bearing capacity problem are also applicable to the lateral earth pressure problems. For plasticity based method, the ultimate lateral pressure can be obtained by the partial differential equations (PDE) approach which can be solved by the method of characteristics proposed by Sokolovskii (1960). The results are usually considered as the rigorous solutions for the ultimate lateral pressure, and further improvements or simplifications have been proposed by Kumar (2001), Kumar and Chitikela (2002), Cheng (2003), Absi and Kerisel (1990), Subra and Choudhury (2006), Shukla et al. (2009), Liu et al. (2009a, 2009b), Salman et al. (2010), AbdelAziz (2013), Peng and Chen (2013), Liu (2014), Vo and Russell (2014), Hamidi et al. (2017) and many others. Cheng et al. (2007) have also obtained the three lateral earth pressure coefficients for axi-symmetric problem based on the method of characteristics.

For seismic lateral earth pressure, method of characteristics has been used by many scholars. Kumar (2001), Kumar and Chitikela (2002) have studied the seismic passive earth pressure coefficients using the method of characteristics, while Pathmanathan (2006) has applied numerical method to the evaluation of seismic lateral earth pressure. Cheng (2003) has proposed a rotation of axes for the solution of the slip line equations for determining the lateral earth pressure with the presence of seismic loading under general conditions.

However, the theoretical solutions cannot represent the realistic constitutive behavior of soil, and numerical approach like Finite Difference Method (FDM), Finite Element Method (FEM) and Distinct Element Method (DEM) are now also adopted to investigate the earth pressure distribution with higher flexibility. Such approaches can consider the initial states of soil (stress, density, porosity and other parameters) which are totally neglected in the classical plasticity or limit analysis methods. Clough and Duncan (1971) have carried out finite element analysis to study the retaining wall

behavior. Ozawa and Duncan (1976) have adopted elasto-plastic finite element model to consider sand deformation on the earth pressure problems. Potts and Fourie (1986) have analyzed the effects of wall deformation on earth pressure by means of the finite element method, and also studied a propped cantilever wall in clay, incorporating an elastic–perfectly plastic stress–strain relationship. Bhatia and Bakeer (1989) have used the finite element method in modeling a static earth pressure problem. Osman (1990) has conducted experimental tests and finite element analysis on the lateral earth pressure problems. Matsuzawa and Hazarika (1996) have also employed FEM to determine the variation of earth pressure in relation to the wall movement. Griffiths et al. (2008), Hamidi et al. (2017), Elchiti et al. (2017) have also carried out detailed finite element analyses on the present problem, and Pathmanathan (2006) has obtained the seismic lateral earth pressure through the use of finite element method.

There are many others who have applied the finite element or finite difference method for the study of lateral earth pressure, but the use of distinct element method for lateral earth pressure problem is still limited up to the present. Maynar and Rodríguez (2005), Jiang et al. (2014), Weng et al. (2014) have carried out some works on the application of DEM on lateral earth development. In general, the results are close to that by the finite element method, but DEM can study the lateral earth pressure under a very large lateral displacement which is not possible for the finite element method.

In this chapter, DEM and slip line method are adopted to analyze the lateral pressure behavior of soil under different boundary conditions and friction angles between a wall and particles. The large displacement failure mechanism and movement of soil with the lateral earth pressure of a backfill is further investigated, and the influence of the micro-parameters on the lateral pressure of soil is also observed. A numerical solution is established using a distinct-element-based procedure of the software PFC2D (particle flow code in two dimensions). The numerical results obtained are then compared with the classical methods as well as the slip-line method and laboratory tests.

4.2 Slip line method for the ultimate earth pressure

Rankine and Coulomb solutions are the two bounds to the rigorous solution. "Rigorous" formulation of Ka and Kp are governed by combining the yield criterion and the equilibrium and formulate the governing plasticity equations along the failure surface as the slip line equations by

$$\alpha \ characteristics: -\frac{\partial p}{\partial S_\alpha}\sin 2\mu + 2R\frac{\partial \theta}{\partial S_\alpha} + \gamma(\sin(\varepsilon + 2\mu)\frac{\partial y}{\partial S_\alpha} + \cos(\varepsilon + 2\mu)\frac{\partial x}{\partial S_\alpha}) = 0 \quad (4.1)$$

$$\beta \ characteristics: \frac{\partial p}{\partial S_\beta}\sin 2\mu + 2R\frac{\partial \theta}{\partial S_\beta} + \gamma(\sin(\varepsilon - 2\mu)\frac{\partial y}{\partial S_\beta} + \cos(\varepsilon - 2\mu)\frac{\partial x}{\partial S_\beta}) = 0 \quad (4.2)$$

where μ= (π/4-ϕ/2), γ is the unit weight of soil, θ is the direction of the major principal stress to y axis and ε is the angle between the body force and y-axis; and

$$p = \frac{\sigma_1 + \sigma_3}{2} \quad , \quad R = \frac{\sigma_1 - \sigma_3}{2} = p\sin\phi + c\cos\phi \quad (4.3)$$

where σ_1 and σ_3 are the major and minor principal stresses respectively, c and ϕ are the cohesive strength and friction angle of soil. The angle ε is generally 0 for static geotechnical problems, as gravity acts downward.

These two partial differential equations can only be solved by iterative finite difference method. Rigorous solution has indicated that log-spiral curve is a close approximation of the actual failure surface. Design figures are given in Hong Kong GEO Guide 1 and detailed solutions are provided by the earth pressure tables by Kerisel and Absi (1990). It should be noted that Equations (4.1) and (4.2) have not considered the soil deformation as well as the construction process, and the whole solution domain is assumed to be in a plastic state which is also different from the other numerical methods.

4.3 DEM analysis of general shear failure mechanism in densely packed backfill

In this chapter, DEM will be used to carry out a study on the development of lateral earth pressure under different wall movement types: translation, rotation about wall top and bottom. The analysis is carried out to a very large lateral displacement which is not possible for all the other numerical methods. To begin with the analysis, some of the basic parameters for the sand are given in Table 4.1. The DEM model is generated by the explode repulsive method, which is a typical model generation method suitable for lateral earth study, and the model is shown in Figure 4.1.

Table 4.1 Microscopic Parameters of the Sands for Particle Flow Analysis

Microscopic Parameters (units)	Value (1)	Value (2)
Total particle number	88419	57500
Density (kg/m^3)	2650	2650
Normal and shear stiffness (N/m^2)	1 x 10^7	1 x 10^7
Frictional coefficient of particle	0.577	0.577
Diameter of particle (mm)	6	40
Contact Bond – Normal / Shear Strength (N)	0	0
Velocity of the wall in active cases (m/s or rad/s)	5×10^{-7}	1×10^{-5} *
Velocity of the wall in passive cases (m/s or rad/s)	1×10^{-6}	1×10^{-5}

Remark: (1) the model for limited wall movements; (2) the model for progressive failure process; (*) except for RT mode, the velocity=1×10^{-6} m/s

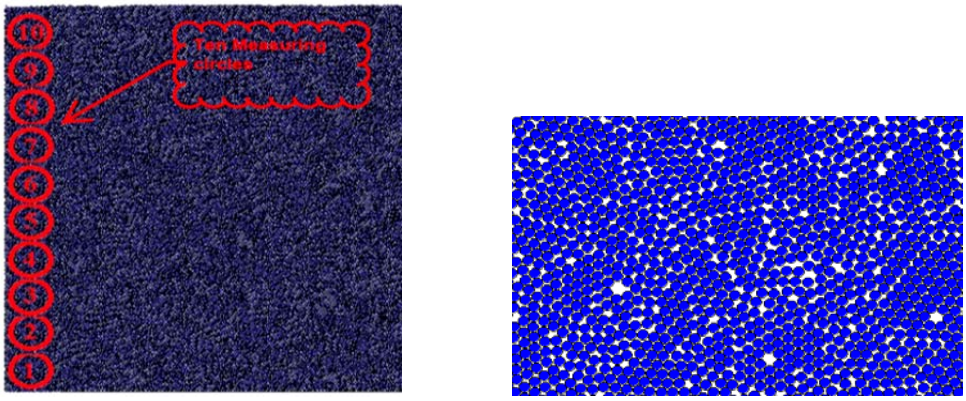

(1) Measure circles behind retaining wall (2) Irregular dense packing particles

Figure 4.1 Model simulation by using explode repulsive method

The model under limited wall movement is generated with irregular packing soil particles (See Figure 4.1). The width and height of the model was set to be 1m and 3m respectively. The particles were generated by the explosive repulsion method. As many particles were created, some large overlaps might occur to cause large contact forces so that removal of the kinetic energy was executed to achieve the state of equilibrium (Itasca, 2004). Gravity was then added to the soil particles on both models, and the mean unbalanced force was measured and checked to ensure the models reach their static gravitational equilibrium. The right hand side and the bottom of the wall were considered as rigid boundaries, and the top of the wall was removed after particle generation to act as an unconstrained boundary for the soil particles to upheave. The left hand side of the wall was a movable boundary to control different wall displacement patterns. There are translational wall movement (T mode), rotation at the base of the wall (RB mode) and rotation at the top of the wall (RT mode) for both active and passive conditions, as shown in Figures 4.2 & 4.3. Bridge abutments or strutted retaining walls were simulated by RT mode.

Ten measuring circles along the wall were used to collect the stresses after certain movement of the retaining wall, and each circle contains about 220 particles. The circles can record the

corresponding stresses when the retaining wall experiences certain movement. Meanwhile, the position of total earth force resultant exerting on the wall was calculated by dividing the pressure profile into small segments and then determining the distance of each centroid of the segment from the reference line. The coefficient of lateral earth pressure is regarded as the ratio of total horizontal thrust to $\gamma h^2/2$.

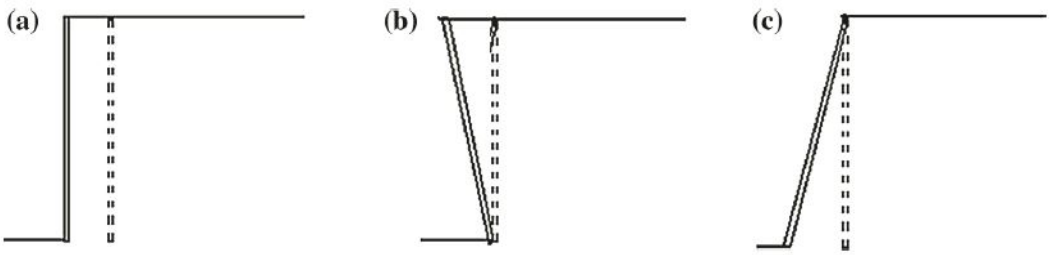

Figure 4.2 Three types of active wall movements: (a) T mode (b) RB mode (c) RT mode

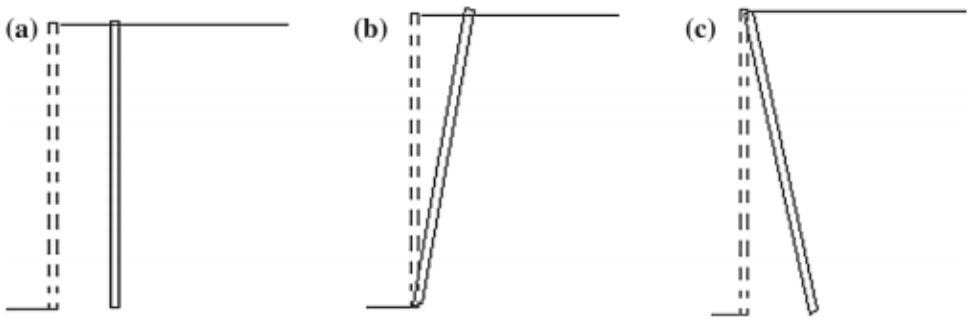

Figure 4.3 Three types of passive wall movements: (a) T mode (b) RB mode (c) RT mode

4.4 Failure patterns of large displacement on different wall movements

The failure planes of different model cases are observed to be similar in displacement vector figures, as active T mode is illustrated in Figure 4.4. The angle to the horizontal is converged in a range between 65° to 70°. This result agrees well with the classical result that the failure plane in

active zone should be 45°+ϕ/2 (i.e. 60°) to the horizontal without the presence of wall friction and inclined backfill. The region of shear failure zones in all the three active wall movements as shown in Figures 4.5a to 4.5c enlarges with the increase of the wall displacement. Among these three active modes, active T was the largest and active RB was the smallest with regard to the area of shear failure zone. As the mobilization of shear strength in soils is proportional to the area of failure zone, the shear strength of soils in active T utilizes to the highest extent.

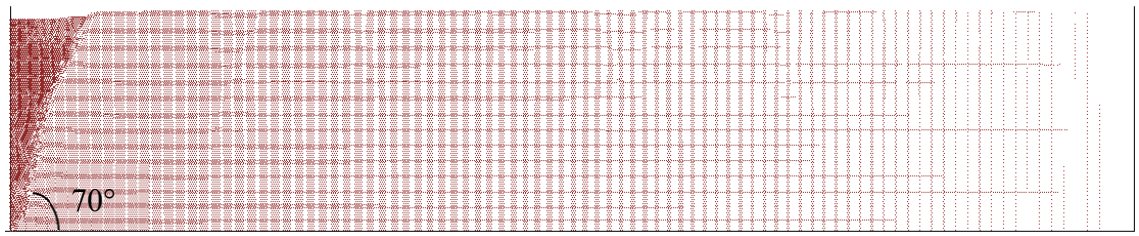

(a) S_{max}/H= 0.03

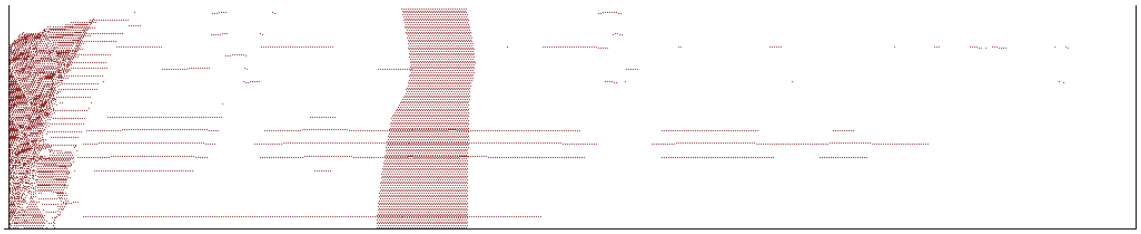

(b) S_{max}/H= 0.07

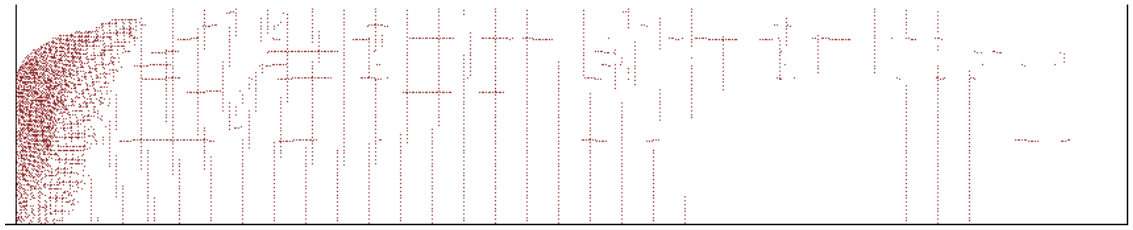

(c) S_{max}/H= 0.10

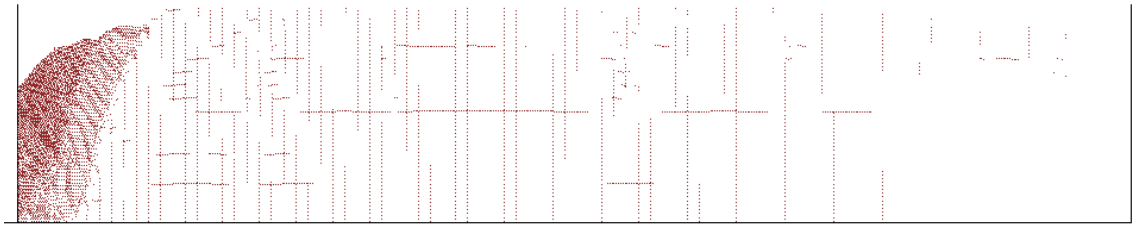

(d) $S_{max}/H=0.13$

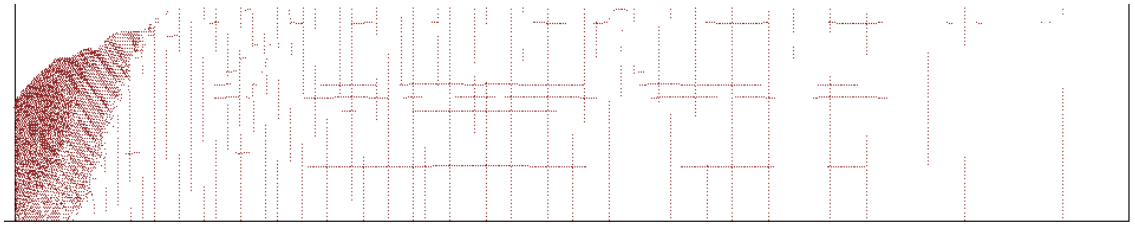

(e) $S_{max}/H=0.17$

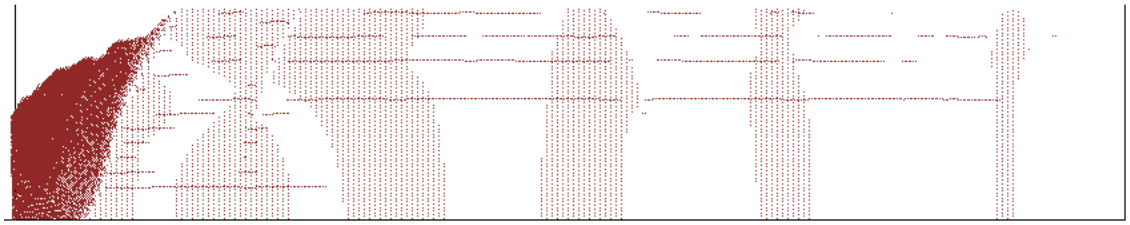

(f) $S_{max}/H=0.20$

Figure 4.4 Failure process of densely packed cohesionless soils in active T ($\phi=30^o$ and $\delta=0^o$), where S_{max} = the maximum displacement of the wall moved and H= the height of the wall

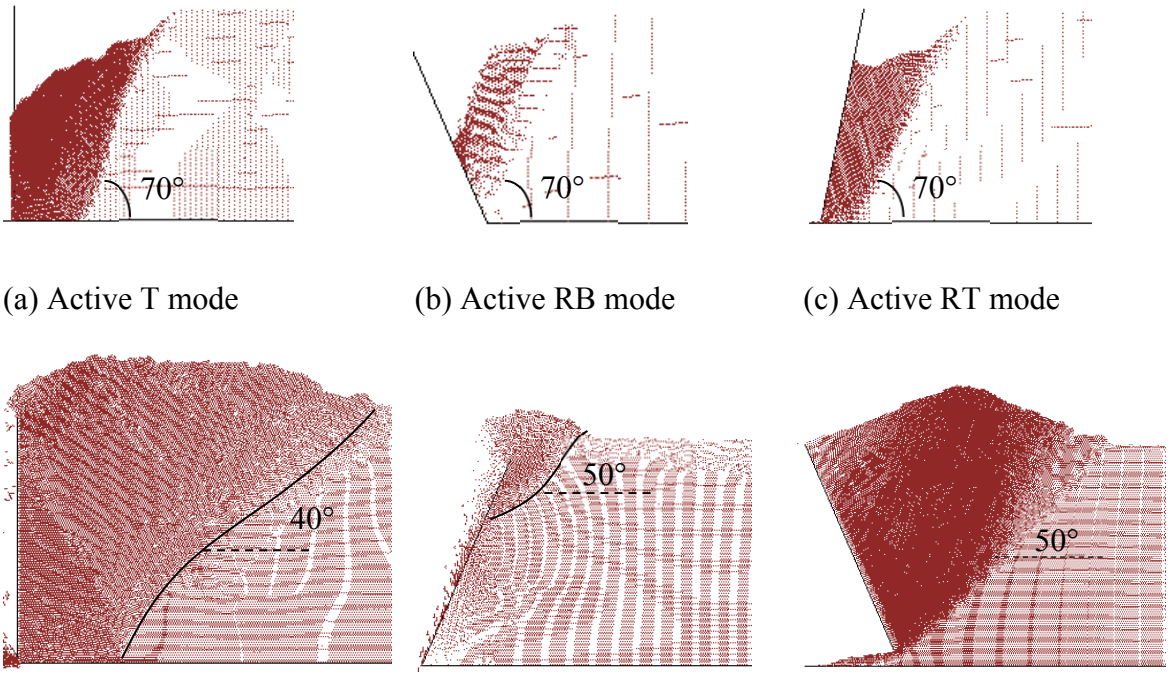

(a) Active T mode (b) Active RB mode (c) Active RT mode

(d) Passive T mode (e) Passive RB mode (f) Passive RT mode

Figure 4.5 Final failure patterns of densely packed cohesionless soils in active mode (S_{max}/H= 0.2) and passive mode (S_{max}/H= 0.4) (ϕ =30^o and $\boldsymbol{\delta}$=0^o)

In the passive cases, as the soils near the retaining wall is under compression, a dilatancy characteristic of the dense soils is exhibited and part of the soils move up and escapes from the system (which is actually not possible but may be present in DEM analysis). Compared with the active cases, the shear failure zone of passive cases is generally larger, however, the angles of shear planes in passive modes obtained from the model simulations are between 40°to 50° to the horizontal, which is different with the angle of the shear plane 45°-ϕ/2 (i.e. 30°) from the classical result, but it is similar to the results obtained by Weng et al. (2014).

Weng et al. (2014) have explored the evolution of lateral earth pressure using the distinct element method and investigated the effect of the key parameters such as particle size, internal friction angle and normal stiffness of the particles to the change of lateral pressure on dense and random packing pattern of particles. The outcome showed that (1) greater soil friction angle resulted in smaller K_a but

greater K_p, which agreed well with the classical theories; (2) the larger soil particle stiffness caused a decline of K_a but increase of K_p; (3) the increase of particle size gave a surge on K_a especially in random packing of particles and has only a small effect K_p. However, the failure planes in passive wall movement cases exhibited steeper than an angle of 45° - ϕ/2 to the horizontal (Figure 4.6). As the parameters of soil grains in PFC2D were justified by the sandbox test of aluminium rods, this result can be considered as acceptable. The failure patterns between Figure 4.5d and Figure 4.6 looks similar, while for the final failure stage from DEM in Figure 4.5d, the failure zone is larger than that by Weng et al. (2014) 's results.

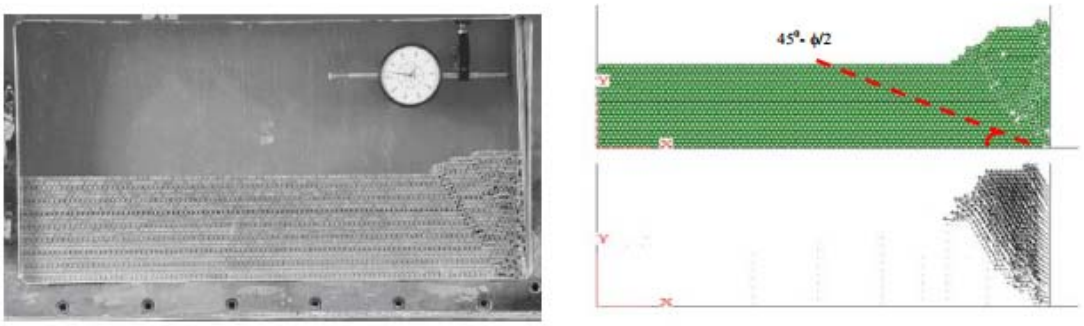

Figure 4.6 Failure patterns at passive T modes for the experiment (left) and simulation (right)

The phenomenon of acquiring smaller failure zone in the DEM model simulations than that in slip line method under passive cases is that in the slip line method, the whole soil domain is assumed to be fully plastic while not all the soil particles in DEM analysis have reached the fully plastic state, especially in the passive RB mode.

4.5 Back analysis of irregular dense packing soil on limited wall movement

a) Active mode

Figures 4.7 to 4.9 show the change of earth pressure along the wall height at different location of

the wall under active T, RB, RT modes. Different modes of wall movement result in different pressure distributions (Clayton et al. 2013). In Figure 4.7, the drop of the pressure in active T mode evenly occurred from the top to the bottom of the wall. The experiment of the change of active lateral pressure in T mode conducted by Fang & Ishibashi (1986) showed that the stress was nonlinear and the profile was approximately parabolic. The stress obtained from Figure 4.7 is slightly nonlinear, but most of it matches with the prediction of the slip line method. In addition, the stress profiles of both RB and RT modes are consistent with those results obtained by the other scholars. The basal stress of the soils in RB mode and the upper stress of the soils in RT mode do not achieve the active state. Hence, the slip line method may underestimate the stresses at the upper and lower portions of soils in RT and RB modes respectively.

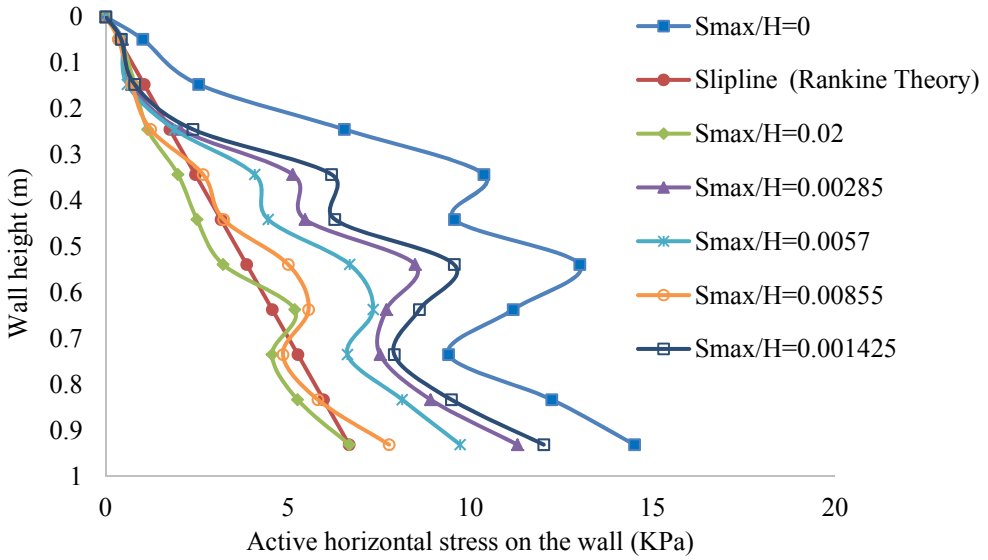

Figure 4.7 Horizontal stress profile against the wall in active T ($\phi = 30^o$ and $\boldsymbol{\delta} = 0^o$)

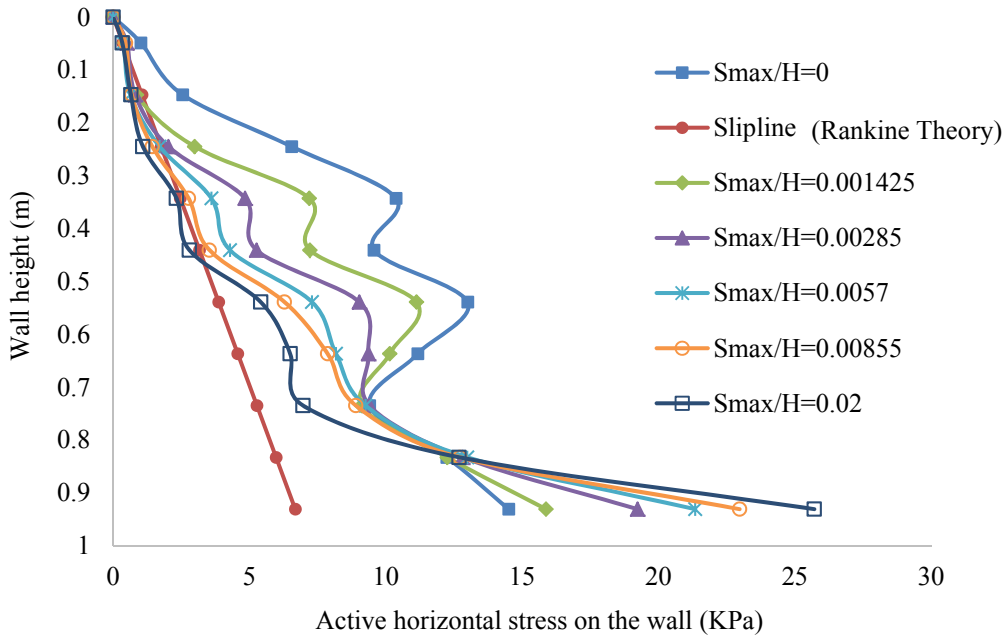

Figure 4.8 Horizontal stress profile against the wall in active RB ($\phi = 30^o$ and $\boldsymbol{\delta} = 0^o$)

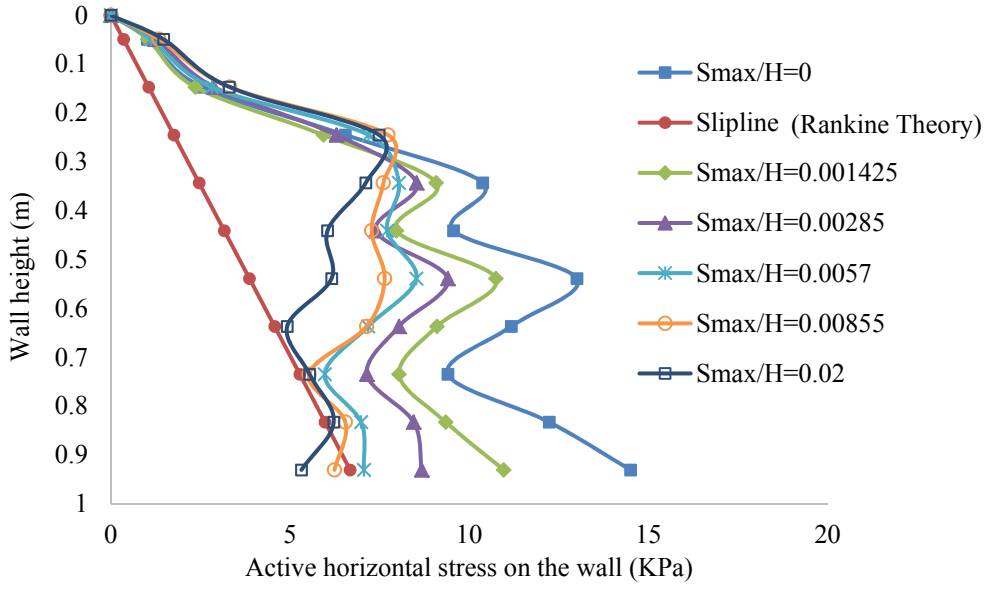

Figure 4.9 Horizontal stress profile against the wall in active RT ($\phi = 30^o$ and $\boldsymbol{\delta} = 0^o$)

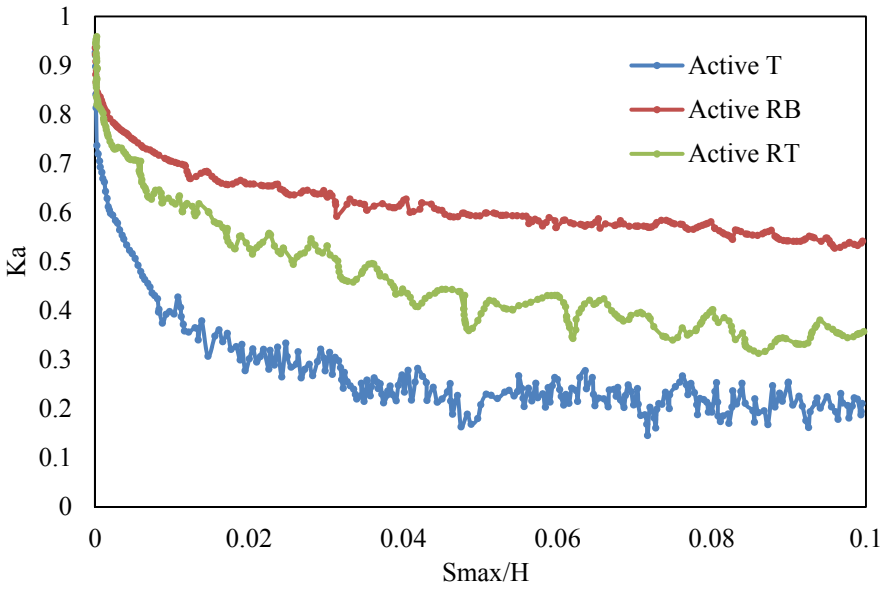

Figure 4.10 The variation of Ka in three different active wall movements

The percentage required for the full mobilization of active stress is between 0.25-1% of the wall height (Craig, 2004). Figure 4.10 clearly depicts that Ka started to level off at around 1% under the three kinds of active displacement modes, but the full mobilization of active stress occur at approximately 4% in the three modes. It exceeds the normal requirement of wall movement to achieve an active state and causes a delay effect, as the particles in the simulations require some time to follow the wall movement. The distinct difference of the magnitude of Ka in active modes is observed with the descending order of RB, RT and T modes. It is reasonable for the value of Ka in RB and RT modes to be higher than that in T mode, as only part of the backfill in the rotational modes is under expansion. In the at-rest condition of soils, the horizontal stress linearly increases with depth, therefore, as the bottom portion of soils in active RT is not supported by the wall, the pressure against the wall dropped quickly. Hence, active RT has the second lowest Ka. The resultant force position

against the wall under three kinds of active wall movement is shown in Figure 4.11. The position of the earth pressure is diverse in different displacement modes of the retaining wall. The point of the resultant of the active T mode slightly differs from the position of Coulomb theory 0.33H (also the slip-line plasticity theory), and it varies with the retaining wall movement modes. For the active RB mode, the position of resultant force is lower than that of the classical theory, while the resultant force in the active RT mode is located at a higher position than that of the classical theory, as shown in Figure 4.11.

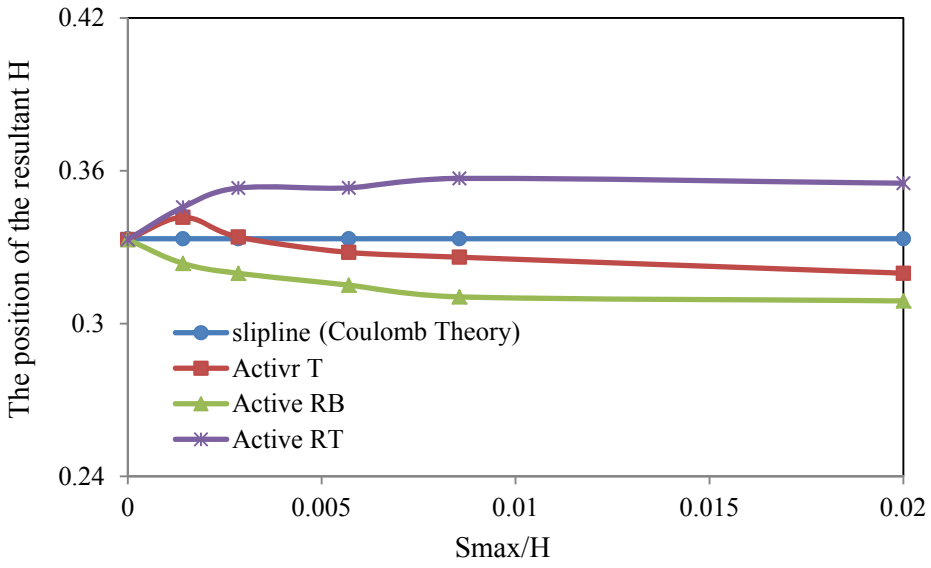

Figure 4.11 The position of resultant force of lateral earth pressure in active modes

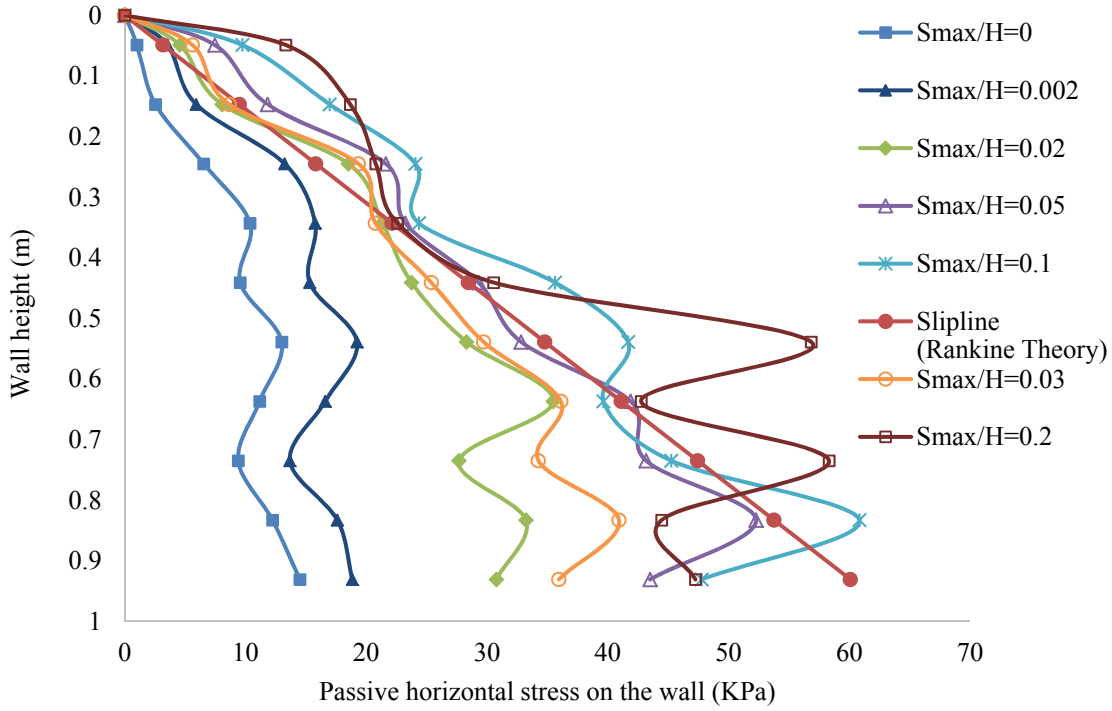

Figure 4.12 Horizontal stress profile against the wall in passive T (ϕ =30^o and $\boldsymbol{\delta}$=0^o)

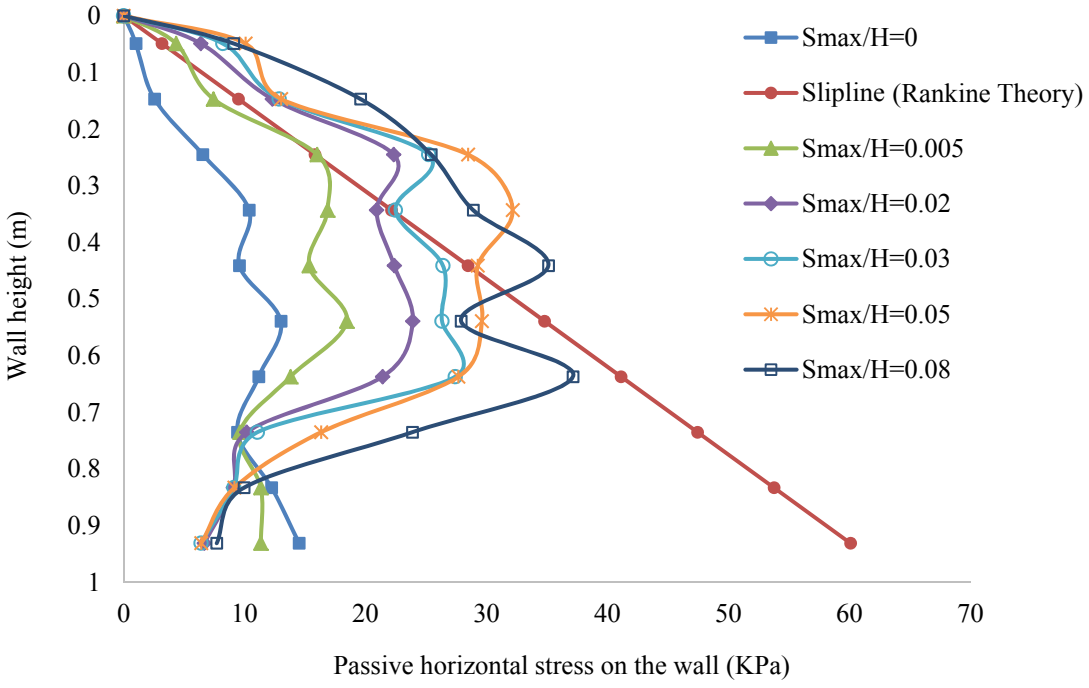

Figure 4.13 Horizontal stress profile against the wall in passive RB (ϕ =30^o and $\boldsymbol{\delta}$=0^o)

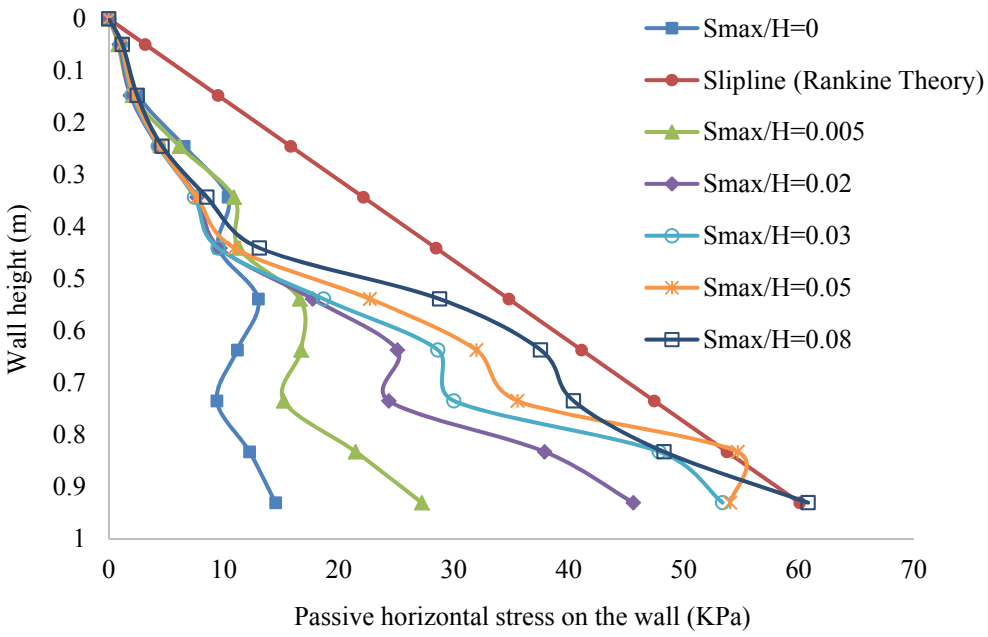

Figure 4.14 Horizontal stress profile against the wall in passive RT (ϕ =30^o and $\boldsymbol{\delta}$=0^o)

b) Passive mode

The passive pressure profiles in T, RB and RT modes along the wall are shown in Figures 4.12 to 4.14. The stress profile in T mode has a higher nonlinearity than the other two modes because the strain mobilization was non-uniform and complicated (Jiang et al.2014). The passive pressure against the bottom part of the wall in T mode exceeded the pressure of slip line method, but this is not common to occur in both model simulations and experiments. This may be caused by the stress localization and fluctuation of the backfill in PFC2D analysis. The lateral stress at the upper part of the wall slightly exceeded the stress predicted by slip line method in RB mode. On the experimental basis in other scholars' studies, the upper stress of soils in RB mode might exceed the estimated lateral pressure from the slip line method. In the RT mode, the stress calculated by slip line method

overestimates the actual lateral soil stress, and this is commonly observed.

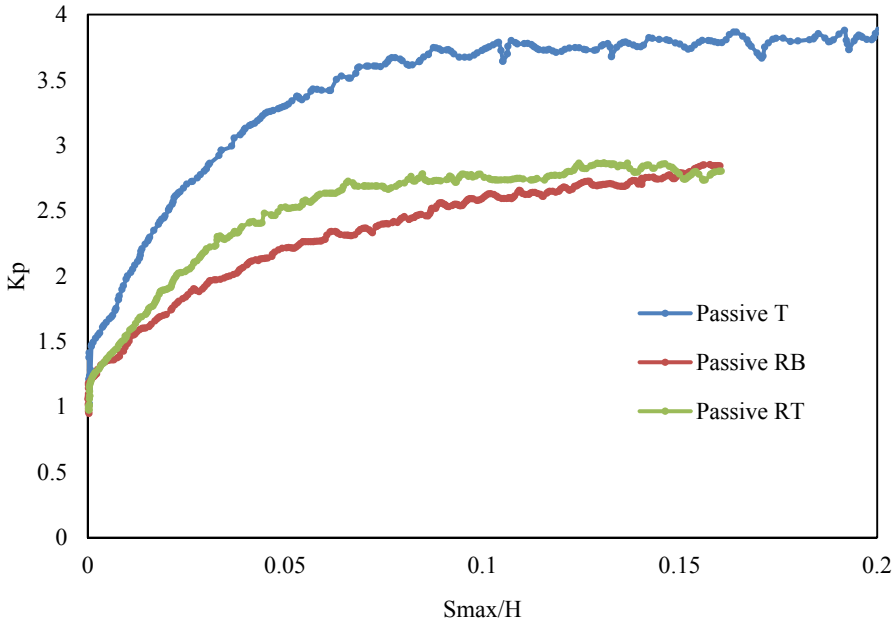

Figure 4.15 The variation of K_p in three different passive wall movements

Figure 4.15 shows the value of Kp in the passive modes. The relatively high Kp coefficient was observed at passive T as the strength of larger proportion of the backfill near the wall was highly mobilized. The magnitudes of Kp in RB and RT modes were relatively small because the lower portion of soils in RB mode and the upper portion of soils in RT mode did not reached the full passive state. In addition, a convergence of the coefficient of Kp in both RB and RT modes was noticed. The Kp coefficients of all these passive modes did not show peak values in spite of the initial void ratio 0.209 of the dense backfill. As the wall movement was limited even though it is large, the shear displacement of soils was not sufficiently large to cause the Kp to drop.

According to Craig (2004), 2-4% and 10-15% of wall movement is required for dense and loose

soils respectively to fully achieve passive conditions. However, the tendencies of the soils to achieve full passive states were about 15% of wall movement. The delay may caused by the late response of particles to the corresponding wall movements in PFC^{2D} simulations, which is the same situation in the active cases.

4.6 Variation of lateral earth pressure under different soil friction

(1) Active T mode

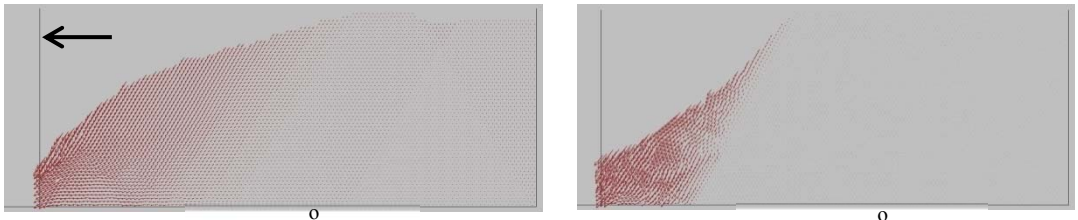

(a) $\phi = 0^{o}$ (b) $\phi = 40^{o}$

Figure 4.16 Eventual failure pattern of ultimate lateral pressure with different friction angles of sandy soil in active T mode (unit weight of soil≠0, contact bond strength=0)

From Figure 4.16, for higher friction angle of soil, less shear planes and disturbed zones formed. The failure patterns with lower friction angle ($\phi = 0^{o}$ and 30^{o}) tend to be progressive and soil collapses gently, while failure shape is found to be steeper with sudden collapse in higher friction angle cases ($\phi = 35^{o}$ and 40^{o}). Friction angle reflects the shearing resistance of soil. For soil particles with higher friction angle, they could uphold more earth pressure and soil unit weight, the disturbed area is subsequently decreased and less propagated.

(2) Active RB mode

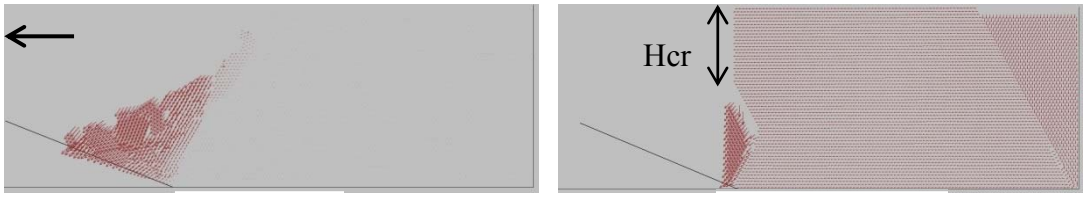

(a) $\phi = 0^{o}$ (b) $\phi = 30^{o}$

Figure 4.17 Eventual failure pattern of ultimate lateral pressure with different friction angles of sandy soil in active T mode (unit weight of soil≠0, contact bond strength=1000N)

In Figure 4.17, large amount of soil collapse when the friction angle is 0^{o}, but only partial sudden failure occurs in case of ϕ=30^{o}. This reflects that higher soil friction angle has more resistance to shear failure. It is also noted that local failure occurred in Figure 4.16b, and soil collapsed at unsupported vertical cut condition due to its own self-weight. The height from top to the soil above this local failure is called Critical Height (Hcr). Cohesion soil is bonding intensely without any collapse.

(3) Influence of soil friction on passive T mode

Figure 4.18 shows the variation of coefficient Kp with different soil friction angles at Smax/H=0.20. The trend and pattern of the curves with different soil friction angles remained unchanged. Greater interior friction angle of soil particle led to higher passive coefficient Kp. Compared the results in Figure 4.18 with Kp coefficients calculated by program KP by Cheng (2003), the results obtained from PFC2D were larger than that by the slip line method. However, as the friction angle is larger, the deviation between both methods is smaller, vice versa.

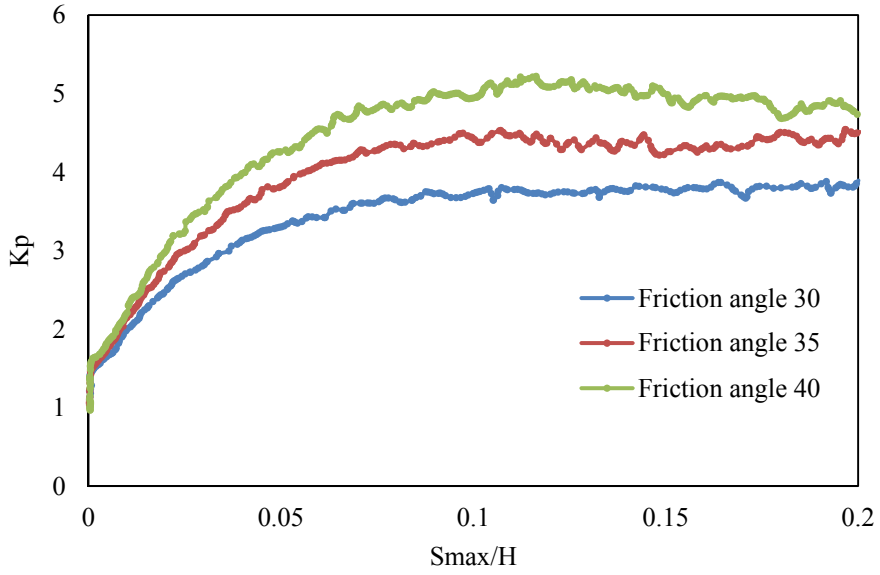

Figure 4.18 The variation of Kp in passive T at Smax/H=0.20 with different soil frictions ($\boldsymbol{\delta}=0^{o}$)

4.7 Slip line method for the ultimate lateral earth pressure under different wall friction in passive T mode

Cheng (2003) has developed an iterative finite difference program called KA/KP for the slip line problem on lateral earth pressure. From the results of program KP, the slip line fields for passive T mode of the soil with $\phi = 30^{o}$ are shown in Figures 4.19-4.21, under different retaining wall friction δ=0°, 15°, 30°.

1) Wall friction 0°

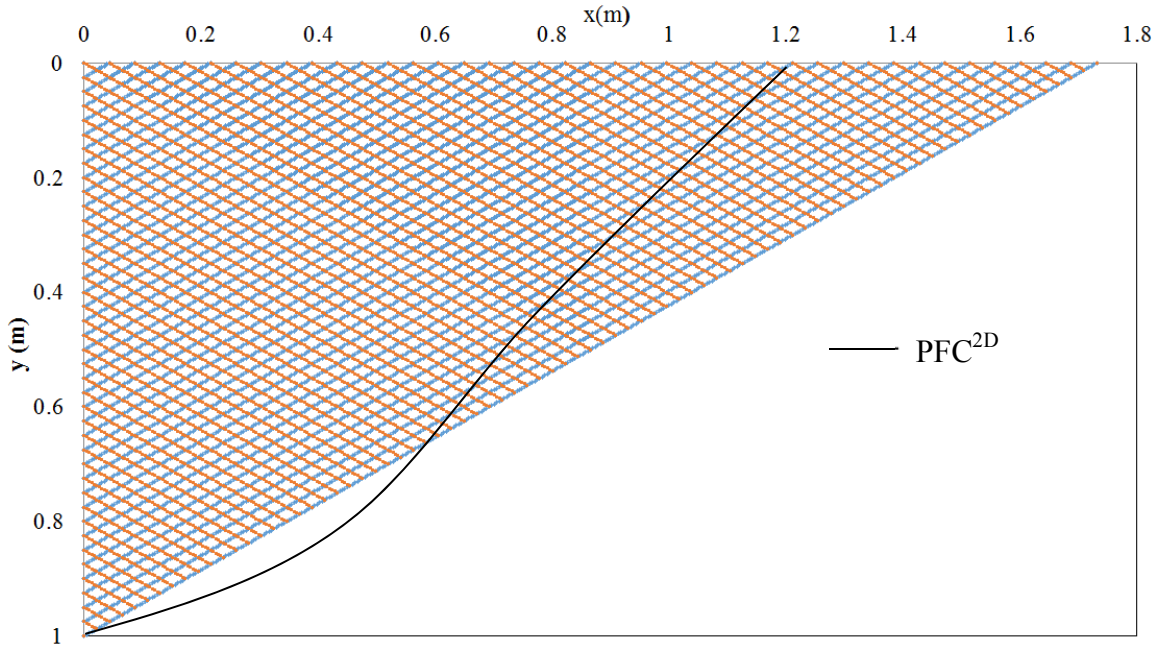

Figure 4.19 Comparison of failure zone between slip line and PFC2D in passive T (ϕ =30^o and $\boldsymbol{\delta}$=0^o)

2) Wall friction 15°

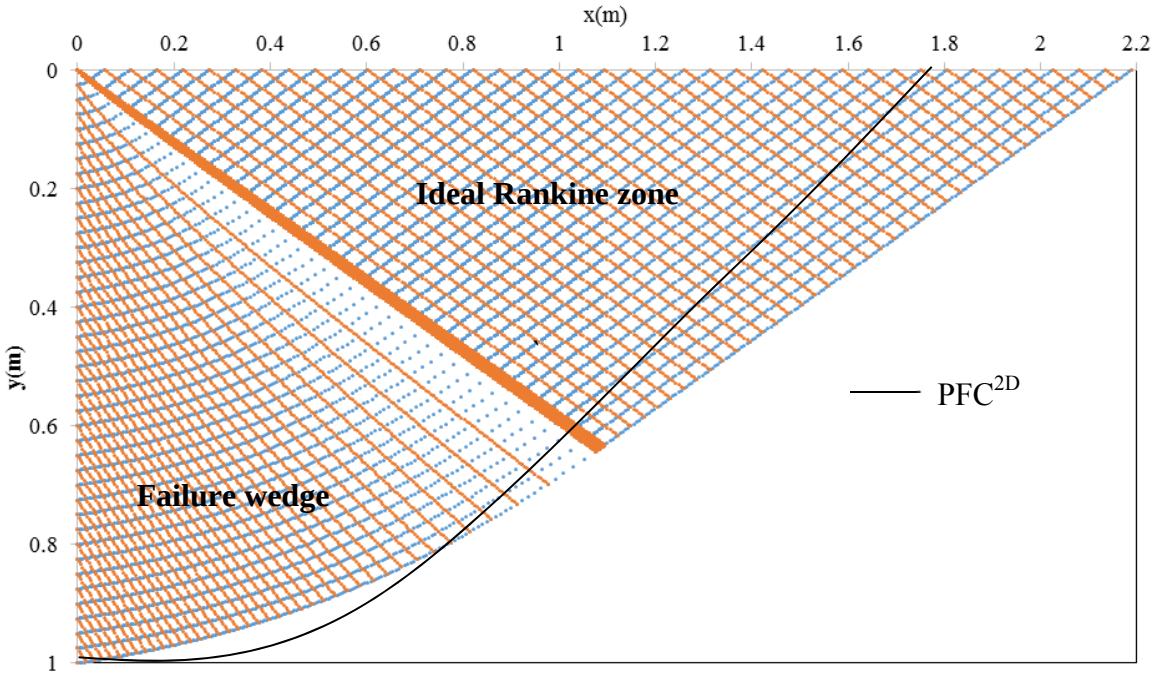

Figure 4.20 Comparison of failure zone between slip line and PFC2D in passive T (ϕ =30^o and δ=15^o)

3) Wall friction 30°

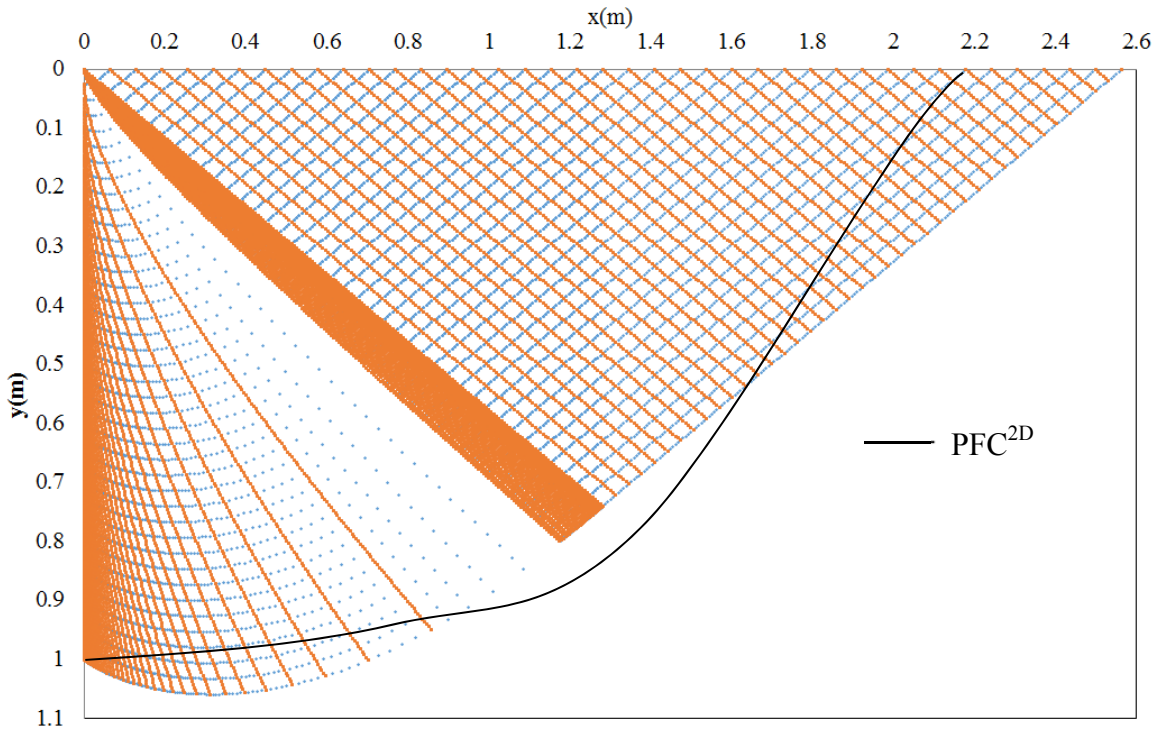

Figure 4.21 Comparison of failure zone between slip line and PFC2D in passive T (ϕ =30^o and δ=30^o)

As the wall friction angle increased, the failure zones obtained by both methods also increased, and the shape of the zones became more curved. With the effect of wall friction, two distinct zones such as a logarithmic spiral failure wedge and a straight upper part of ideal Rankine zone are shown. In the above three comparisons, the areas of the curved failure wedge obtained from the two methods were similar to each other, but the ideal Rankine zones from the slip line method were always larger than that from PFC2D. In the ideal Rankine zones generated by PFC2D, the upper edge of the zones was relatively steeper and closer towards the wall. This demonstrated that the failure zones by PFC2D fell within the expected failure zones by the slip line method, with only slight difference at the upper edge part of backfill.

4.8 Influence of retaining wall friction for passive earth pressure

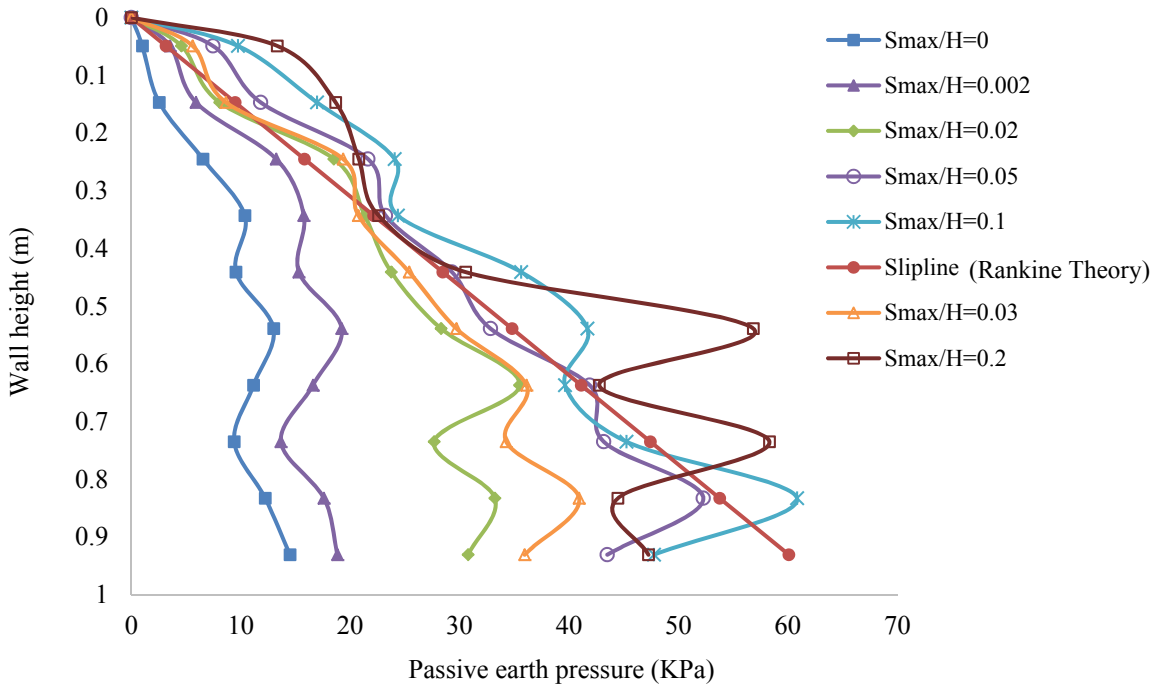

(a) Wall friction angle (δ=0 ^{o})

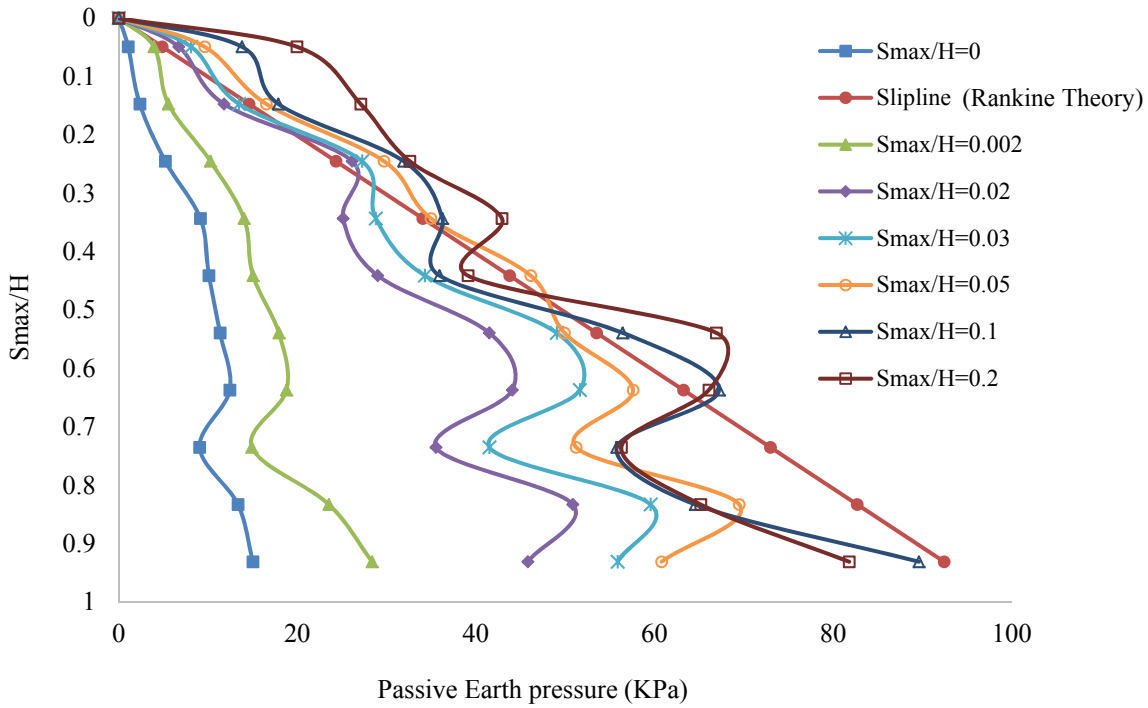

(b) Wall friction angle (δ=15 ^{o})

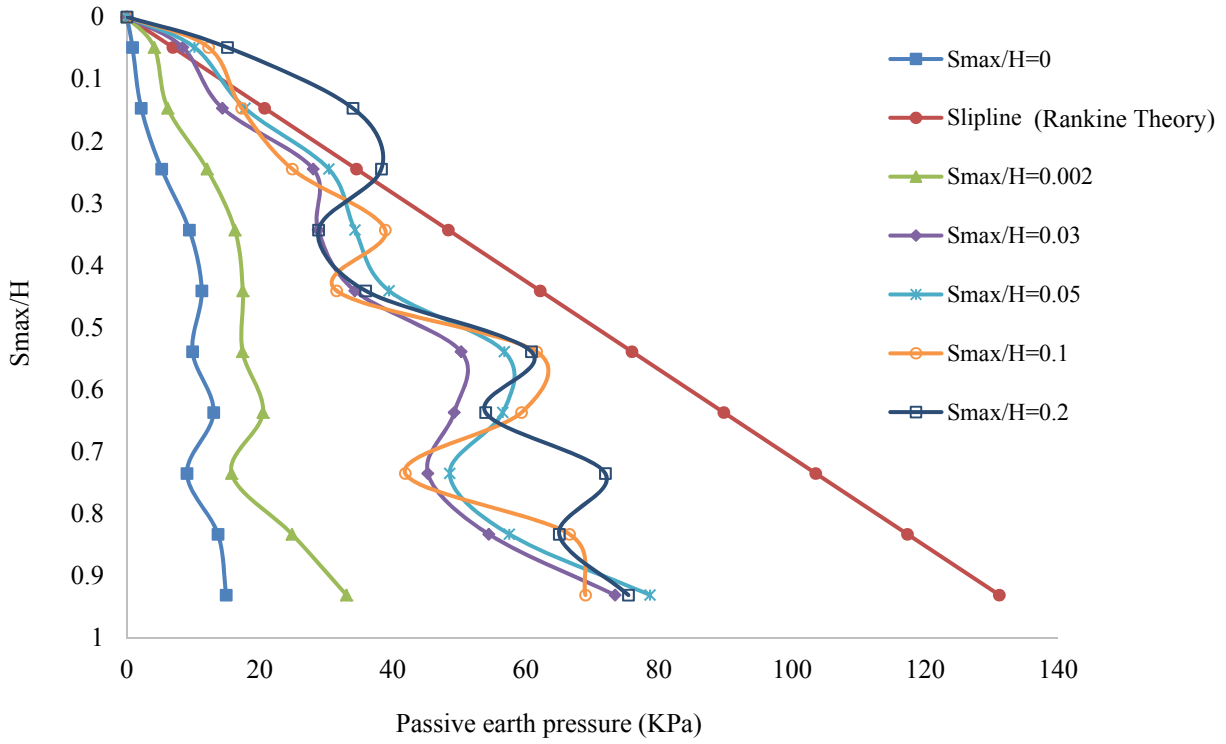

(c) Wall friction angle (δ=30 ^{o})

Figure 4.22 Stress profiles in passive T with different wall friction angle (ϕ =30^{o})

Figures 4.22a to 4.22c show the comparison of lateral passive pressure with the increase of wall friction angle in both PFC2D and slip line methods. The stress obtained from PFC2D was higher than that from slip line method without the presence of wall friction, especially for the lower part of the soils. With the increase in the wall friction angle, the slip line solution becomes the upper bound of the passive earth pressure. The distinct difference between the two methods gradually became noticeable with the depth of the backfill. In Figure 4.22c, the basal soil stress estimated by slip line method was about 1.5 times higher than that of PFC2D.

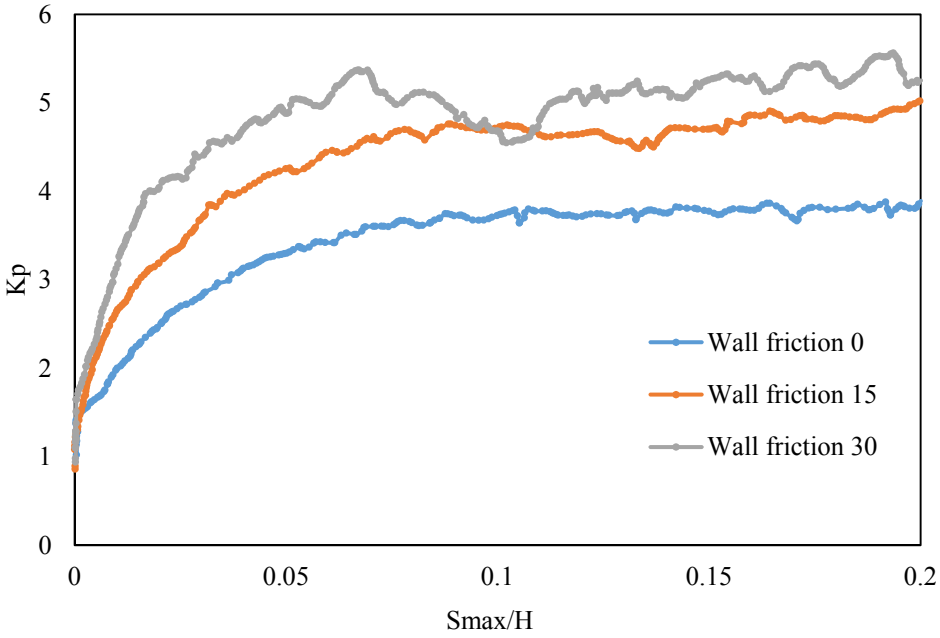

Figure 4.23 The magnitude of K_p in passive T at S_{max}/H=0.20 with different wall frictions

Similar observation is noticed in Figure 4.23. The influence of wall friction angles to the lateral earth pressure in passive translational mode is realized. The greater the exterior friction angle of the retaining wall, the larger will be the passive coefficient Kp. The increasing rate of Kp obtained from PFC2D became relatively slower with the increase in wall friction angle as compared with the increasing rate of Kp from the slip line method. As a result, a larger difference in the result between the slip line and DEM is found when the wall friction angle is large.

4.9 Conclusions

This study explored the influencing factors, including the packing type, the interior friction angle, and the exterior wall friction in the sandy backfill for the active and passive earth pressure of a retaining wall. The software PFC2D based on the distinct element method (DEM) is adopted. The earth pressure against a rigid retaining wall under various wall movement modes is analyzed with the irregular packing soils. The analysis shows that DEM has good capability in simulating and predicting

the macroscopic mechanical behavior of the sandy soil under different stress states. On such a basis, the lateral earth pressure evolution is further simulated, and the earth pressure law is also examined from the microscopic particle scale as well as the macroscopic scale.

The numerical results are showed as follows:

a) The distinct analysis model could effectively capture the variations of lateral earth pressure under both active and passive conditions, and the simulated failure patterns is consistent with those from the experimental sandbox tests carried out by Weng et al. (2014).

b) The position of the earth pressure is diverse in different displacement modes of the retaining wall. The point of the resultant of the active T mode slightly differs from the position of Coulomb theory 0.33H (also the slip-line plasticity theory), and it varies with the retaining wall movement modes. For the active RB mode, the position of resultant force is lower than that of the classical theory, while the resultant force in the active RT mode is located at a higher position than that of the classical theory.

c) The variation of the earth pressure coefficient Ka/Kp is affected by the wall displacement modes. In the active state, Ka drops rapidly at the beginning and then reaches a constant value with increasing wall displacement, while Kp rapidly increases and then gradually approaches a constant value in the passive state.

d) Different modes of wall movement result in different pressure distributions. The larger displacement of the wall moves away from the soil mass, the smaller total earth pressure is; the larger displacement of the retaining wall moves toward the soil mass, the greater resultant force of the earth pressure is.

e) The greater interior friction angle of soil particle led to the lower active coefficient Ka and to the higher passive coefficient Kp, which is agreed with that of the conventional limit equilibrium

theory, but the values of the two analytical methods exhibited significant differences.

f) The active earth pressure coefficient Ka increases with increasing particle size in the small strain state, while the larger particle size led to lower passive coefficient Kp. The increasing inter-particle stiffness decreases the active earth pressure coefficient Ka and increased the passive coefficient Kp. However the obvious difference becomes inconspicuous among the three cases of mean grain size of soil when the critical state is reached, even to the residual state when large displacement is considered.

g) When the soil assembly was arranged in dense packing, it exhibited much larger lateral pressure than that for the random packing mode.

h) Considering the influence of retaining wall friction in passive T mode, the greater exterior friction of the retaining wall, the larger passive coefficient Kp.

Furthermore, the comparison of active and passive lateral pressure and failure patterns under different wall displacement modes by DEM and slip line method has been achieved. The results show that the areas of the curved failure wedge obtained from the two methods are similar to each other, but the ideal Rankine zones from the slip line method are always larger than that from PFC2D. In the ideal Rankine zones generated by PFC2D, the upper edge of the zones is relatively steeper and closer towards the wall. This demonstrated that the failure zones by PFC2D fell within the expected failure zones by the slip line method with only slight difference at the upper edge part of backfill.

Both of Slip line method and DEM are useful in tackling the lateral earth pressure problems. The parameter calibration in DEM is relatively time consuming and difficult, however, the application of DEM is versatile and capable of determining the process from the initial stress state to the final plastic state of soils. The failure patterns and the coefficient of active and passive lateral earth pressure of soils in plasticity state are easily determined by using the program KA and KP developed by Cheng

(2003). Nevertheless, the flexibility of slip line method is not as good as that of DEM. From the DEM studies, it can concluded that the classical theories are not sufficiently accurate to estimate the lateral earth pressure precisely.

CHAPTER 5 THE USE OF INTERNAL AND EXTERNAL VARIABLES AND EXTREMUM PRINCIPLE IN LIMIT EQUILIBRIUM FORMULATIONS WITH APPLICATION TO BEARING CAPACITY AND SLOPE STABILITY PROBLEMS

5.1 Introduction

Limit equilibrium method (LEM) for slope stability problem is well known to be a statically indeterminate problem, therefore, slope stability methods must require assumptions on the internal forces or base forces (stress) before the problem can be solved. Broadly speaking, there are two major groups of "rigorous" methods in the LEM analysis: (1) internal variables in form of direction or the location of interslice forces; (2) external variables (boundary stress) in the form of base normal forces (stress) acting on a potential slip surface. Based on such assumptions, many types of geotechnical problems, from lateral earth pressure, bearing capacity and slope stability problems can be solved with good accuracy.

For the first group of methods, the Morgenstern-Price's (MP) method (1965) and the Janbu's rigorous method (1957, 1973) are the most common formulations. In the MP method (1965) which is a method popular to many engineers, the inclination of the total internal force is usually expressed as $\lambda f(x)$, where λ is a mobilization factor while $f(x)$ is a function specifying the normalized inclination of the interslice forces. This function has a value between 0 to 1 and x is the normalized distance with the value in the range 0 to 1.0. Since only the MP formulation (1965) is adopted the global moment equilibrium, the back-calculated thrust line may lie outside the soil mass which is physically not possible. This situation is equivalent to the violation of the local moment equilibrium, and due to the classical MP method cannot enforce the local moment equilibrium automatically.

In Janbu's rigorous method (1957, 1973), the distance between the thrust line and the base of the slip surface is assumed to be known, while the local moment equilibrium is used in the formulation. Abramson et al. 2002 indicate that moment equilibrium is considered about the centre of the base of each slice in the modern implementation of the Janbu's rigorous method. The local and overall moment equilibrium is hence implicitly satisfied, and the interslice shear forces can then be calculated. As the problem is actually over-specified by 1 unknown factor, the moment equilibrium of the last slice is not enforced in the Janbu's rigorous method (1973), therefore true moment equilibrium is still not maintained in this method. Besides these two methods, there are many other variants of slope stability/limit equilibrium methods that are usually based on these two important slope stability formulations. The solution will be a lower bound of the ultimate limit state in the failure stage, as long as a statically admissible stress field is defined over a domain. In this respect, as force (lumped the stresses over a finite length) instead of stress is considered in the classical LEM, LEM is an approximate but not an exact lower bound solution (Chen 1975).

For the second group of method, the representative method is the variational principle by Baker and Garber (1978) (BG). BG method minimizes the safety function with respect to both the potential slip surfaces $y(x)$ and potential normal stress $\sigma(x)$ acting on this surface, using equilibrium requirements as the constraints. It should be noted that in the BG formulation (1978), the failure mass bounded by the potential slip surface and the ground surface is not cut into slices, and complete equilibrium can be researched using this group of methods, which is not possible with the first group of methods. In the framework of LEM, this solution is a lower bound on the minimal safety factor. However, from a plasticity perspective, the results from all LEM are only the approximate lower bound solutions (Chen 1975) as these results are not necessarily kinematically admissible. In fact, LEM methods do not deal with strain and displacements, so the notion of kinematic admissibility cannot even be defined in LEM methods. It is important to realize that the variational technique by BG (1978) is just one of the many different available minimization procedures. The variational

approach is an analytical procedure which is convenient for the solution of simple slope stability problems, but it is difficult to use in the cases when the layered geometry or the ground/loading conditions are complicated. Cheng et al. (2009) have demonstrated the equivalence between a global optimization analysis and the variational principle; and the simpler global optimization analysis can be applied to general complicated cases without any problems.

Under the lower bound theorem in the limit analysis (Chen, 1975), the loads determined from the stress distribution alone are not greater than the actual collapse load, which satisfies: (a) the equilibrium equations, (b) the stress boundary conditions and (c) nowhere violates the yield criterion. Under the upper bound theorem, the loads determined by equating the external rate of work to the internal rate of dissipation, are not less than the actual collapse load, associated with a prescribed deformation mode (or velocity field), which satisfies: (a) the velocity boundary conditions and (b) the strain and velocity compatibility conditions. The lower bound theorem which does not contain energy dissipation, is also applicable to the limit equilibrium formulation. The major difference between the limit equilibrium and the limit analysis lies in the upper bound approach. In the upper bound of limit analysis, the energy balance is considered in determining the critical solution; but in the limit equilibrium formulation, the minimum resistance (force/moment) or factor of safety against failure is taken into account. Cheng et al. (2010) have demonstrated the equivalence of the maximum extremum and the ultimate limit of the system (where the maximum strength of a prescribed failure surface is utilized) by a simple footing on clay, based on the slip line solution. In the formulation by Cheng et al. (2010), which treats *f(x)* as a variable to be determined, the overall moment equilibrium is adopted, while the local moment equilibrium of an individual slice is not directly enforced. The local moment equilibrium is indirectly enforced by rejecting those *f(x)* which are associated with the thrust line outside of the soil mass. Cheng et al. (2010) have indicated that as long as a *f(x)* is prescribed, the solution will be a lower bound theorem to the ultimate limit state. Under the ultimate limit state, where the strength of a system is fully mobilized, *f(x)* is actually determined by this requirement, a

boundary condition which has not been used in the past. Cheng et al. (2010) have applied a modern heuristic optimization algorithm to determine *f(x)* for arbitrary problems, and have pointed out that every kinematically acceptable failure surface should have a factor of safety. The use of an inappropriate f(x) in the classical stability analysis will lead to failure to converge.

Cheng's approach (2010) can be classified as a hybrid formulation of the first and second groups of methods. The use of the maximum extremum of the system is conceptually similar to the second group of methods, but there are two major differences between the formulations proposed by Cheng et al. (2010) and Baker and Garber (1978). Baker and Garber (1978) simultaneously minimizes the factor of safety with respect to the base normal forces as well as the locations of the failure surfaces, while Cheng et al. (2010) determine the maximum extremum of the system for any specified failure surface. The BG approach (1978) does not enforce the acceptability of the internal forces; however, a reasonable distribution of the internal stress is obtained by this approach and also adopted by Baker (1981, 2005). Cheng et al. (2010) have enforced the acceptability of the internal forces during the extremum computation, which is different from the BG approach (1978).

In this chapter, the well-known plasticity slip line solutions for a bearing capacity problem are firstly used to determine *f(x)* and the thrust line for a ''horizontal slope''. Based on the ultimate load, the failure surfaces and *f(x)*or the thrust line from the slip line solutions, and the factors of safety will then be back-computed with Morgenstern and Price's method (1965) and Janbu's rigorous method (1957, 1973), and the equivalence between these two stability methods under the ultimate condition will be illustrated. It is well known that it is hard to achieve convergence of the thin slices with Janbu's rigorous method (1973). The present study shows that the international adaption of Janbu's rigorous method (1973) can be very sensitive to the location of the thrust line, and a method to improve the convergence has been proposed in this chapter.

It will be demonstrated that there is no difference between the use of external and internal variables in specifying a problem at the maximum extremum condition. It is believed that the use of the internal variables is preferable over the use of the boundary variables, on the condition of the imposition of the acceptability of the internal forces can be easily enforced. Furthermore, it will be illustrated clearly that the classical limit equilibrium methods with a prescribed internal/external force assumption will be a lower bound to the ultimate condition. The maximum extremum of the system from LEM is also testified to be equivalent to the slip line solution in the present study.

5.2 Interslice force function *f(x)* and thrust line for a horizontal slope problem

In the present study, a ‘‘horizontal slope’’ is taken into account under the action of an applied load. This case is actual, as the slip line solution (plasticity solution) is available for this ultimate ‘‘horizontal slope’’/bearing capacity problem. The slip line equations given by Equations (5.1) and (5.2) can be used to investigate the stresses at the ultimate condition. Sokolovskii (1965), Booker and Zheng (2000), Cheng (2003), Cheng and Au (2005), Cheng et al. (2007a) and many others scholars have provided solutions to slip line equations. In the present study, the slip line program SLIP, developed by Cheng and Au (2005) (which has been compared and verified with program ABC by Martin (2004) as well as many other published results), is used for the slip line analysis for a bearing capacity problem.

$$\alpha \ characteristics: -\frac{\partial p}{\partial S_\alpha}\sin 2\mu + 2R\frac{\partial \theta}{\partial S_\alpha} + \gamma(\sin(\varepsilon + 2\mu)\frac{\partial y}{\partial S_\alpha} + \cos(\varepsilon + 2\mu)\frac{\partial x}{\partial S_\alpha}) = 0 \qquad (5.1)$$

$$\beta \ characteristics: \frac{\partial p}{\partial S_\beta}\sin 2\mu + 2R\frac{\partial \theta}{\partial S_\beta} + \gamma(\sin(\varepsilon - 2\mu)\frac{\partial y}{\partial S_\beta} + \cos(\varepsilon - 2\mu)\frac{\partial x}{\partial S_\beta}) = 0 \qquad (5.2)$$

where $p=(\sigma_1+\sigma_3/2), R=(\sigma_1-\sigma_3/2)=p\sin\phi+c\cos\phi$, σ_1 and σ_3 are the major and minor principle stresses, respectively, S_α and S_β are the characteristic lines, as shown in Figure 5.1(a), c and ϕ are the cohesive strength and the friction angle of the soil, $\mu=(\pi/4-\phi/2)$, γ is the unit weight of the soil, θ is the direction of the principal stress to the y axis and ε is the angle between the body force and the y-axis. For simplicity, effective soil parameters c' and ϕ' are represented by c and ϕ in the present study.

The bearing capacity factors N_c, N_q and N_γ are classically determined by a simple superposition principle. Michalowski (1997) and Cheng (2002) have presented that this simple superposition is only a good approximation and is only slightly conservative even for high friction angle conditions. A bearing capacity problem can be viewed as a "horizontal slope" where the failure is induced by the bearing pressure applied from the foundation. This reason is obvious, but is not practically adopted for the engineering use by limit equilibrium analysis (due to poor results) because of its inability to specify a correct *f(x)*, as pointed out by Cheng et al. (2010). In the present study, these three factors corresponded to the ultimate condition, together with the corresponding *f(x)*, the thrust line and the base normal forces will be determined by slip line solutions. Once the stress field (p, R, θ) for the slip line field, shown in Figure 5.1(b), has been determined by Equations (5.1) and (5.2) using **SLIP** developed by Cheng (2005), the interslice force function and the thrust line location can be determined as follows:

STEP 1 : Calculate the normal stress (σ_x, σ_y) and shear stress (τ_{xy}) at any grid point by **SLIP** using the following relations:

$$\sigma_1 = p + r \tag{5.3}$$

$$\sigma_3 = p - r \tag{5.4}$$

Hence, by the Mohr-Coulomb relation

$$\sigma_x = p + R \cos 2\theta$$

$$\sigma_y = p - R \cos 2\theta$$

$$\tau_{xy} = R \sin 2\theta \qquad (5.5)$$

STEP 2 : For any specified section (with a given x-ordinate) as shown in Figure 5.1(c), determine the normal stress and the shear stress at equal vertical intervals by interpolation from the 4 grid points in the slip line field enclosing any given x and y coordinates using a bilinear equation similar to the 4-node quadrilateral element used in the finite element analysis.

STEP 3 : Calculate the interslice normal force E and shear force X in each specified section by integrating the normal stress and shear stress at an vertical interval Δy in a vertical direction (as shown in Figure 5.1(a)) by:

$$E = \sum \sigma_x \Delta y \qquad (5.6)$$

$$X = \sum \tau_{xy} \Delta y \qquad (5.7)$$

STEP 4 : The maximum ratio of X/E across all section determined from STEP 3 is denoted as the mobilization factor λ.

STEP 5 : Determine $f(x)$ across the slip surface by:

$$f(x) = \frac{X/E \ \left(at\ each\ location\ x\right)}{\lambda} \qquad (5.8)$$

STEP 6 : Obtain the average normal stress σ_{ar} at each differential element along the vertical direction by the stresses σ_{x1} at top and σ_{x2} at bottom of the element. Determine the lever arm h_t of the normal stresses above the base of the slip surface from

$$\sigma_{ar} = \frac{\sigma_{x1} + \sigma_{x2}}{2} \tag{5.9}$$

$$h_t = \frac{\sum\left[\sigma_{ar}\Delta y\left(h_i - y_i\right)\right]}{E} \tag{5.10}$$

where h_i, y_i are the average y-ordinates of the element and the y-ordinate of the slip surface at section i respectively. In the present analysis, a very fine grid is divided and used (1 mm for N_c and N_q and 0.1 mm for N_γ). With such a fine grid, simple interpolation within a subdomain, as shown in Figure 5.1c, and a simple trapezoidal rule as used in Equations (5.6) and (5.7), is good enough for the analysis.

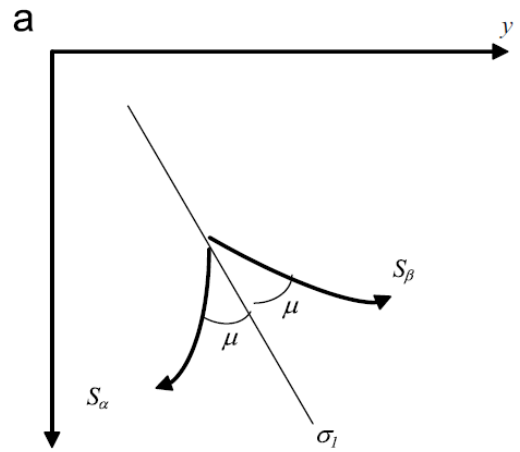

Major principal stress

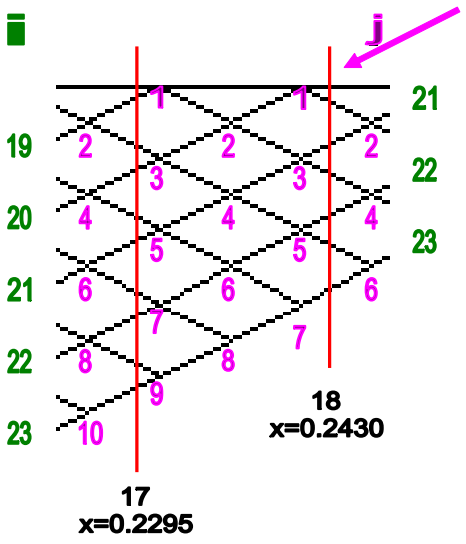

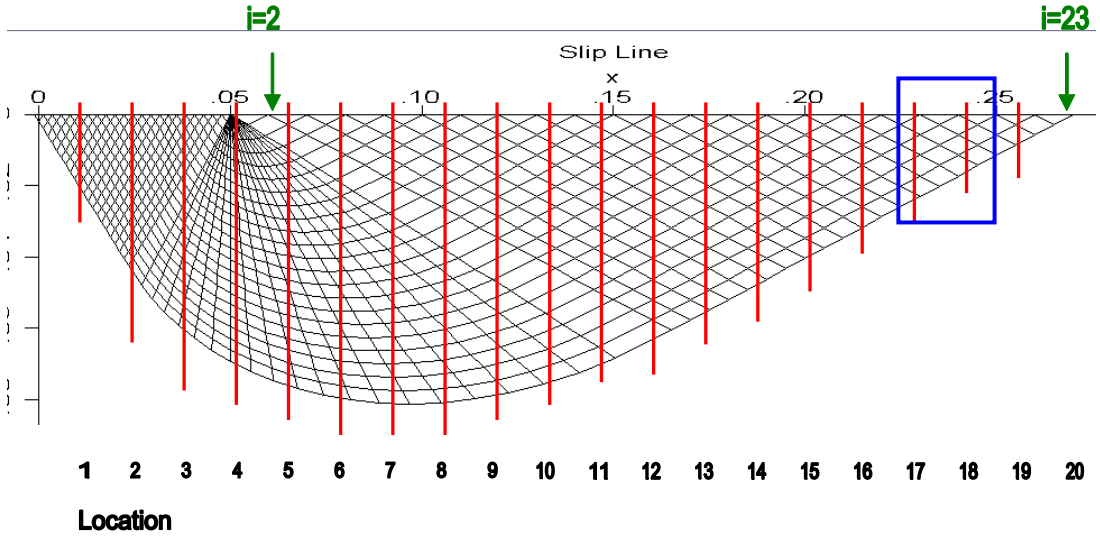

Figure 5.1 *(a) Typical slip line (b) Determination of f(x) and thrust line from slip line analysis and (c) Interpolation to obtain stress at any point from grid points in slip line field.*

For the assessment of the three bearing capacity factors, a direct super-position approach is presented, which is also the basis for the determination of these three factors. From the results of **SLIP**, *f(x)* for different ϕ is determined for different cases associated with N_c, N_q and N_γ. A typical slip line field for the case of N_c is shown in Figure 5.2, where the pressure on the ground surface at the left-hand side is determined from a slip line analysis. The slip line field obtained from **SLIP** is in accordance with the classical solution where active and passive wedges exist at the left- and right-hand sides of the problem, and a log-spiral zone exists in-between of these two wedges, as shown in Figure 5.2.

On the other hand, for the slip line field for N_γ as shown in Figure 5.3 with ϕ=30°, the active zone is actually curved, while the intermediate radial shear zone is not a true log-spiral zone with an inscribed angle less than 90°. When ϕ is further decreased to 10°, the radial shear zone becomes very

small and the active zone begins to dominate the problem. The bearing capacity factors from **SLIP** are very close to the slip line solutions from Sokolovskii (1965), as shown in Figures 5.3 and 5.4.

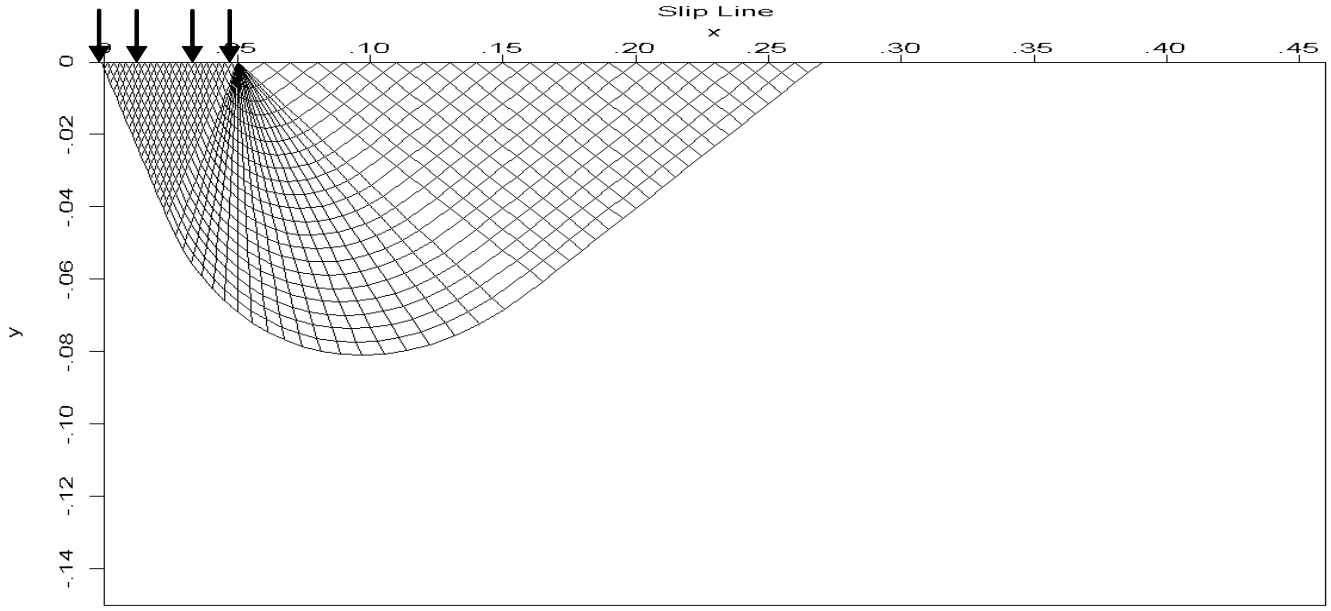

Figure 5.2 Slip line for case of factor N_c when ϕ=30°, N_c=30.18 from program SLIP & 30.14 from classical bearing capacity equation (using natural horizontal distance x instead of normalized distance x)

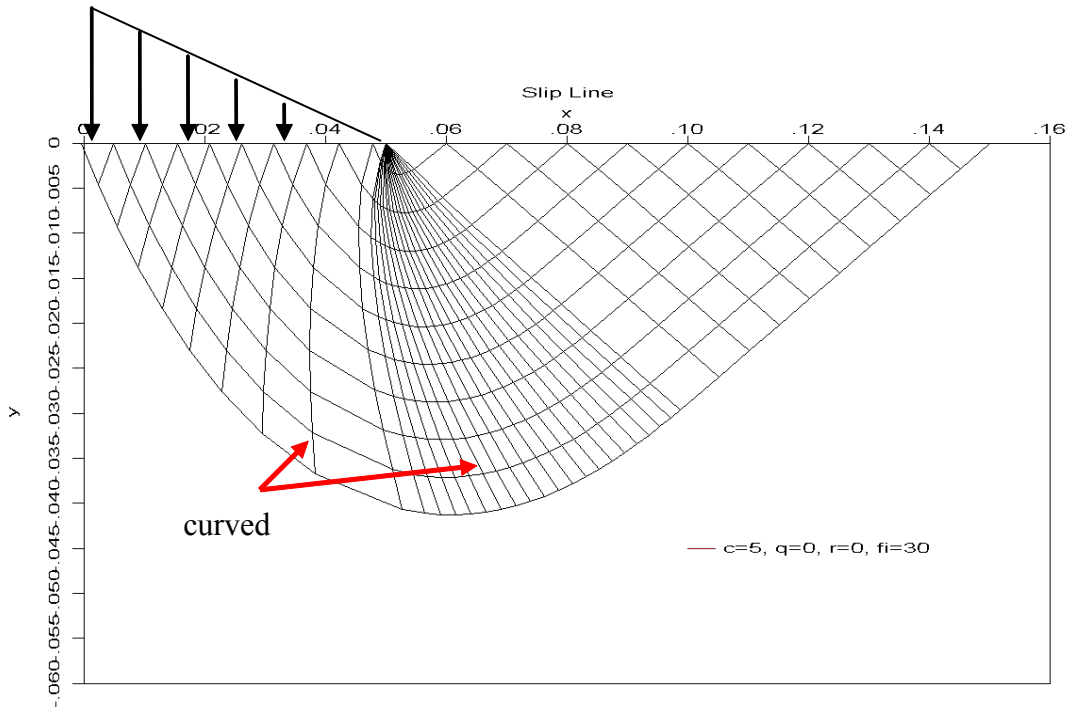

Figure 5.3 Slip line for case of factor N_γ when ϕ=30°, N_γ=15.32 from program SLIP & 15.3 from Sokolovskii (1965) (using natural horizontal distance x instead of normalized distance x)

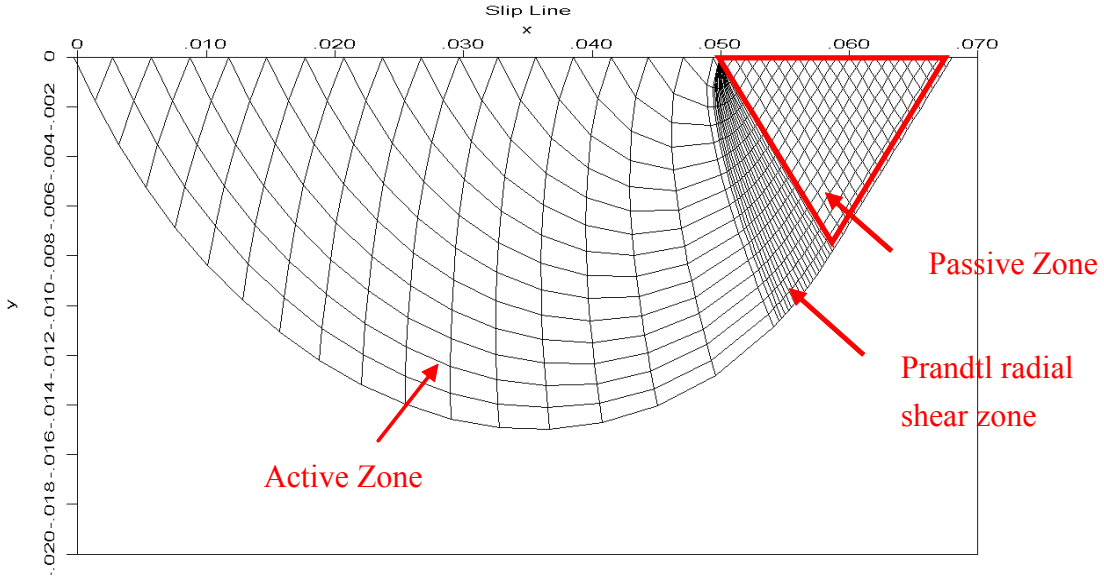

Figure 5.4 Slip line for case of factor N_γ when ϕ=10°, N_γ=0.54 from program SLIP & 0.56 from Sokolovskii (1965) (using natural horizontal distance x instead of normalized distance x)

The results of *f(x)* for the cases associated with the determination of N_c, N_q and N_γ are given in Figures 5.5, 5.6 and 5.7. In Figure 5.5 and 5.6, *f(x)* is symmetrical about x=0.5 when ϕ=0. At the left- and right-hand sides of the wedge, *f(x)* is zero as shown in Figures 5.5 and 5.6. These results are consistent with the slip line results in which the principal stresses are the vertical and horizontal stresses in the active and passive wedges respectively. When ϕ>0, *f(x)* moves towards the left-hand side of the figure when ϕ is increasing. These results are also obvious because the failure zone will become longer when ϕ is increasing. It is also interesting to note that *f(x)* is the same for factors N_c and N_q factors. These results are not surprising as the failure mechanisms for N_c and N_q are the same based on the classical plasticity solution. On the other hand, it can be observed from the results in

Figures 5.3 and 5.4 that the principal stresses for N_γ are the vertical and horizontal stresses only in the passive wedges. Hence, *f(x)* is zero only in the right-hand side in Figure 5.7.

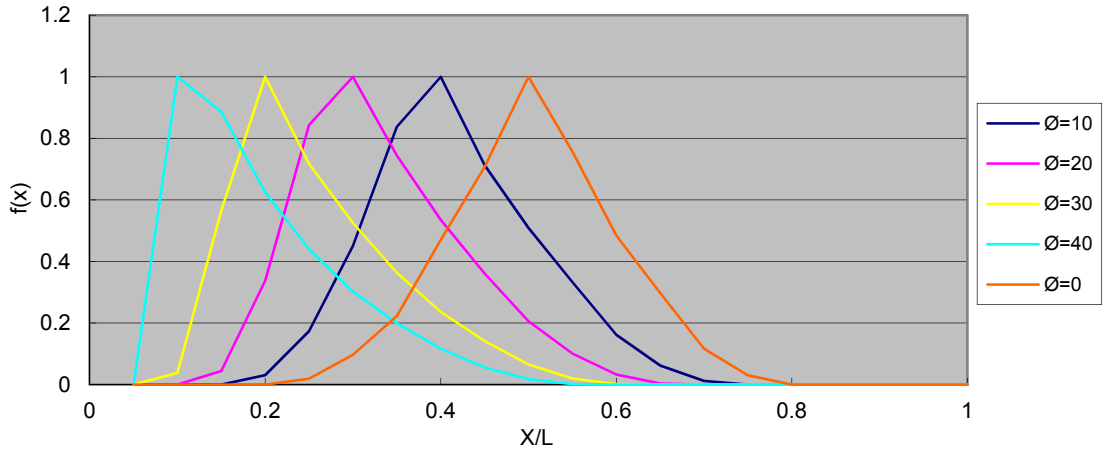

Figure 5.5 f(x) against different dimensionless distance x in case of factor N_c

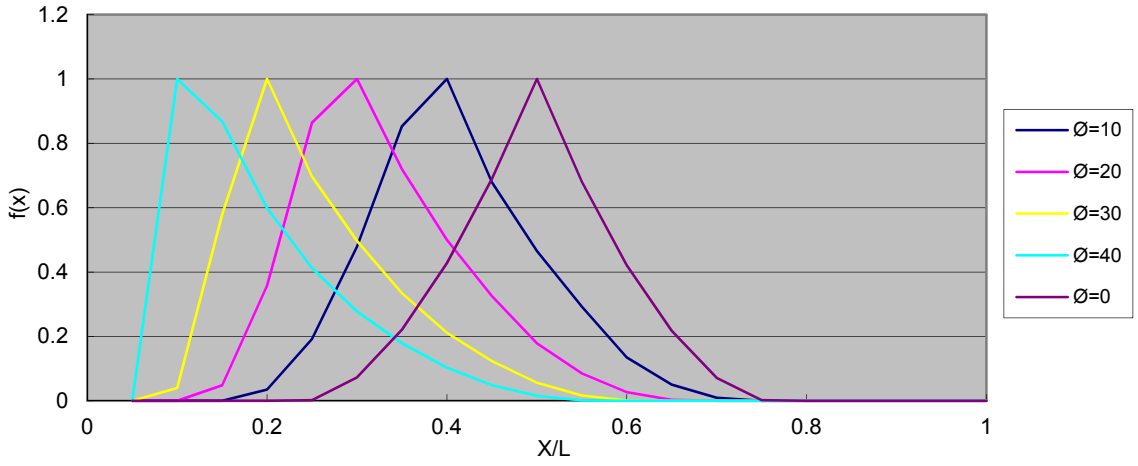

Figure 5.6 f(x) against different dimensionless distance x in case of factor N_q

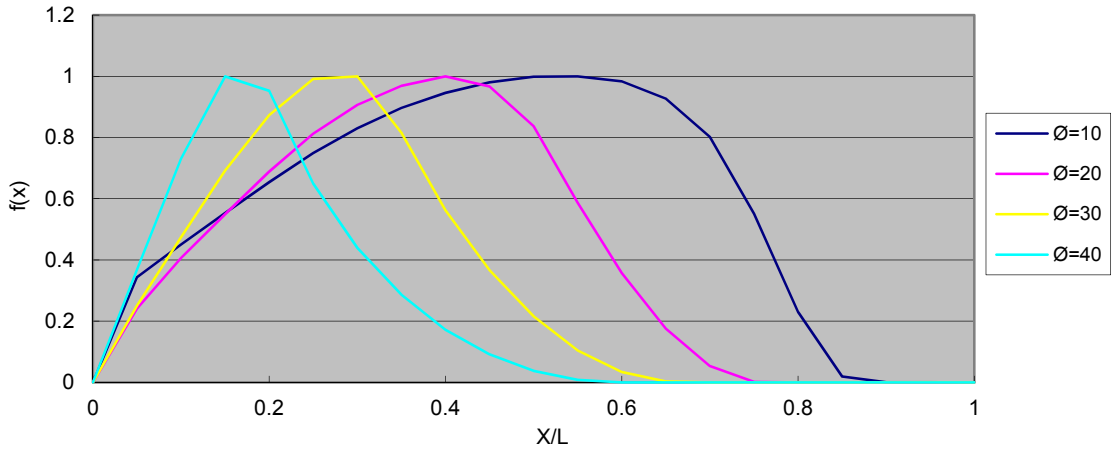

Figure 5.7 f(x) against different dimensionless distance x in case of factor N_γ

The results of the thrust line for N_c (and N_q) at ϕ= 0, 10, 20, 30 and 40° are given in Figure 5.8. The horizontal axis is the dimensionless distance x in the range of 0 to 1. The thrust line ratio (LOT) is always 0.5 in the passive wedge region at the right-hand side. In the very beginning of the active wedge, the thrust line ratios are very close to 0.5, but deviate slightly from 0.5 because of the minor error arising from the iteration analysis in the slip line analysis. Outside the foundation, LOT will firstly go below 0.5 and then gradually rebound to 0.5. The fluctuation of LOT outside the foundation is mainly caused by the radial shear zone. It should be noted that the thrust line is more sensitive to the size of the grid, while the ultimate bearing capacity factors from SLIP are relatively insensitive to the grid sizes used in the analysis. This situation is particularly important for the $N_\gamma$case, thus a very fine grid is adopted for the N_γ case or else there will be a larger fluctuation in the location of the thrust line.

The results of the thrust line ratio for N_q are the same as those for N_c which are shown in Figure 5.8. These results are in line with those for which *f(x)* is the same for the cases of N_q and N_c.

For the case of N_γ, the results are different from those of the previous two cases. Just beneath the foundation, the stresses are mainly induced by the ground pressure so that the thrust line value is slightly less than 0.5, which is obtained in Figure 5.9. At the passive zone, where there is no imposed

pressure, the vertical pressure is totally controlled by soil weight. Therefore, the thrust line ratio is 1/3, which implies a triangular pressure distribution; this is consistent with the demonstrations by Janbu (1973). It should be noted that the linear distribution of the ground pressure, as determined from the slip line analysis in Figure 5.3, applies only when c is taken as zero, which is also the way N_γ is defined. For simplicity, the coupling effect between the unit weight and cohesion c is not considered in the present study, but the present study is not limited to the case of c=0.

The results for the thrust line are consistent suggestion from Janbu (1973). Janbu (1973) proposed that LOT could be determined based on the earth pressure theory. For a general slope with the frictional material, the lateral earth pressure distribution is close to a triangular shape controlled by the unit weight of the soil; hence, a generally referred value for LOT is suggested as 1/3. In the present study, the horizontal and vertical pressure under half of the footing will be constant for both N_c and N_q where the unit weight of the soil is zero, thus, LOT should be exactly 0.5. The later part of the slip surface represents a passive earth pressure state in which the earth pressure distribution is similarly constant, and again LOT=0.5. There is a triangular-shaped earth pressure distribution in the passive zone for N_γ, hence, LOT=1/3.

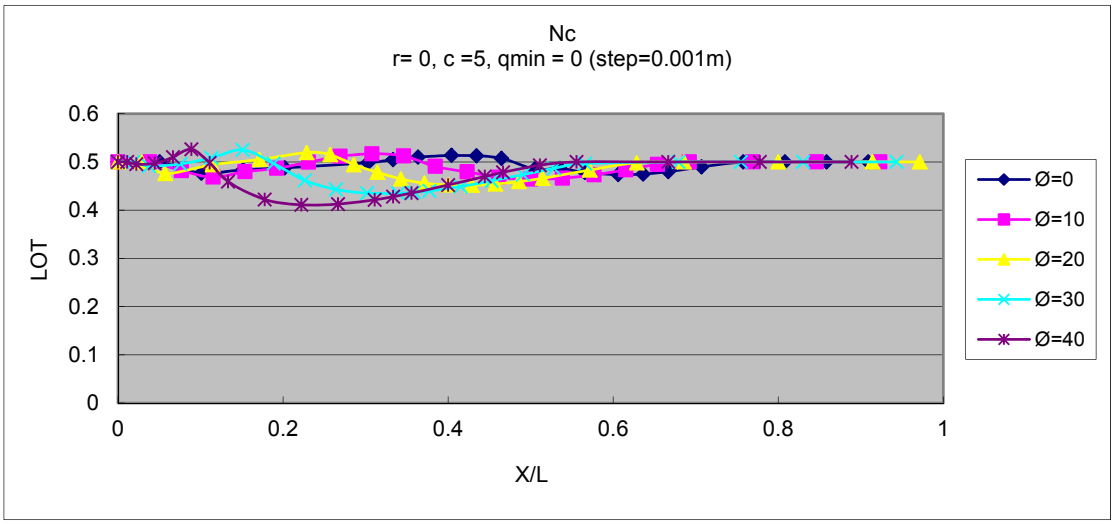

Figure 5.8 The thrust line for different friction angles for case N_c (x coordinate is x/L ratio) (same

results for Nq)

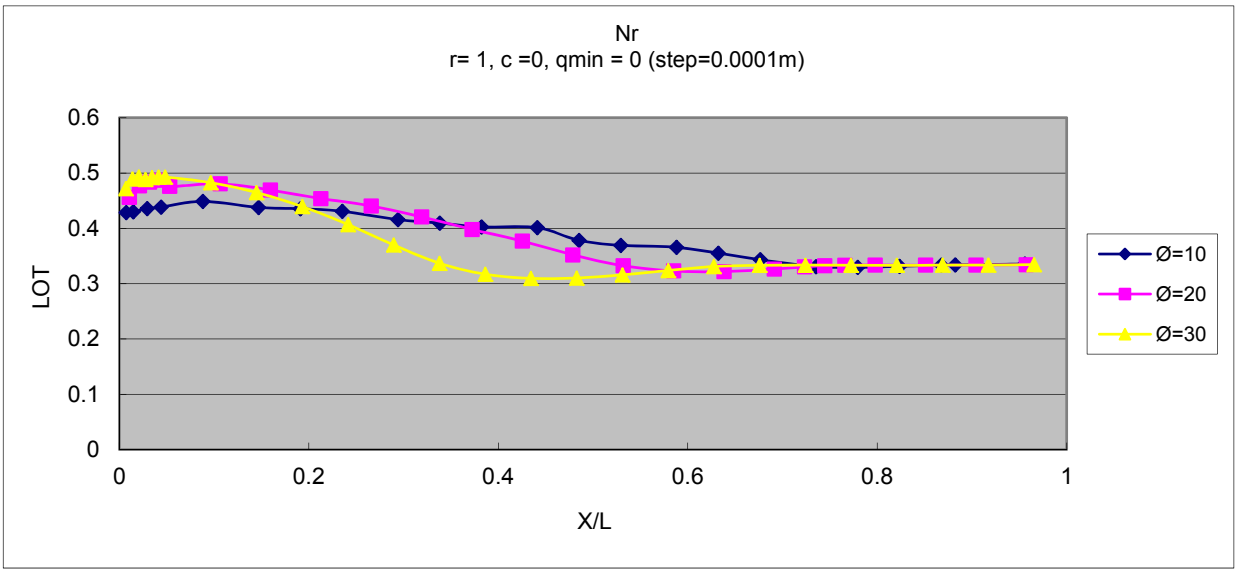

Figure 5.9 The thrust line for different friction angles for case N_γ (x coordinate is x/L ratio)

When *f(x)* or the thrust line is defined, the problem can be back-analyzed in the following ways. For the case of N_c, a uniform pressure with the value of cN_c is applied on ground surface without any surcharge outside the foundation. In the slope stability analysis, the unit weight of soil is set to zero. For the case of N_q, the unit weight of the soil and the cohesive strength are set to zero, a surcharge of 1 unit is applied outside the foundation, and the uniform foundation pressure is given by unit N_q in the analysis. For the case of N_γ, the cohesive strength and the surcharge outside the foundation are set to zero, a triangular pressure (see Figure 5.3) with a maximum value equal to γBN_γ is applied on the ground surface (average pressure is $0.5\gamma BN_\gamma$). Based on the f(x) shown in Figures 5.5, 5.6 and 5.7, and the failure surfaces obtained by the slip line solutions, the back-computed factors of safety is nearly 1.0 for all the cases. These results are obvious in the reason that the solutions from the slip line equations are the ultimate solutions of the system. On the other hand, when the thrust line ratios shown in Figures 5.8 and 5.9 are used in Janbu's rigorous method (1973), there are major difficulties

in the convergence with the international adaption of Janbu's rigorous method (1973) (equations by Janbu are approximations only). The majority of the analysis using Janbu's rigorous method (1973) cannot converge based on the exact thrust line location from the slip line solution. It is found by a series of investigations that the solutions can be very sensitive to the thrust line location, and another procedure which can truly satisfy the moment equilibrium have finally been proposed (instead of the approximations by Janbu, 1973).

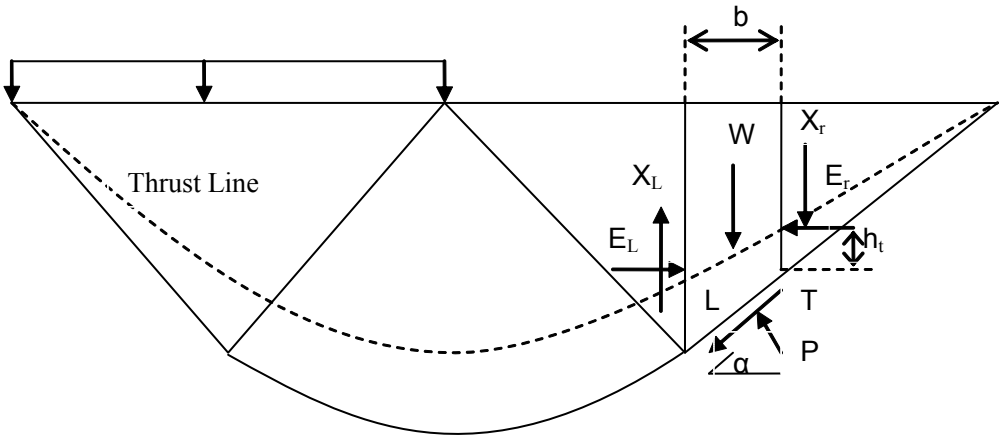

Figure 5.10 Slip surface and slices in the "horizontal slope"

For the slice shown in Figure 5.10, P and T are the base normal and the shear forces, respectively, l is the base length of the slice, E_L and X_L are the interslice normal and shear forces at the left, respectively, while E_r and X_r are the interslice normal and shear forces at the right, respectively, h_t is the height of the thrust line above the base of the slice at the right, W is the weight of the soil mass and α is the base angle of the slice base. Based on the Coulomb relation applied to force, which is the common approach for slope stability analyses, we obtain

$$T = \frac{1}{F}\left(cl + \left(P - ul\right)\tan\varphi\right) \tag{5.11}$$

For the vertical force equilibrium,

$$P\cos\alpha - T\sin\alpha = W + \left(X_r - X_L\right) \tag{5.12}$$

Rearranging and substituting for T gives

$$P = [W + (X_r - X_L) + \frac{1}{F}(cl\sin\alpha - ul\tan\phi\sin\alpha)] / m_\alpha \tag{5.13}$$

where $m_\alpha = \cos\alpha - \sin\alpha\frac{\tan\varphi}{F}$

For the horizontal force equilibrium,

$$-P\sin\alpha - T\cos\alpha = E_r - E_L \tag{5.14}$$

Rearranging, and substituting for T gives

$$P = [-(E_r - E_L) - \frac{1}{F}(cl\cos\alpha - ul\tan\phi\cos\alpha)] / i_\alpha \tag{5.15}$$

where $i_\alpha = \sin\alpha + \frac{1}{F}\tan\varphi\cos\alpha$

For the force equilibrium, resolving the forces parallel to the base of the slice along the base shear force direction yields

$$-T - (E_r - E_L)\cos\alpha = (W + (X_r - X_L))\sin\alpha \tag{5.16}$$

Rearranging Equation (5.16) gives

$$X_r - X_L = -W - \frac{1}{\sin\alpha}(T + (E_r - E_L)\cos\alpha) \tag{5.16a}$$

The moment equilibrium about the center of the base of the slice gives

$$X_L \frac{b}{2} + E_L \left(h_j - \frac{\tan\alpha \cdot b}{2} \right) + X_R \frac{b}{2} = E_r \left(h_{j+1} + \frac{\tan\alpha \cdot b}{2} \right) \qquad (5.17)$$

Rearranging Equation (5.17) yields

$$X_L + X_R = -E_L \left(2\frac{h_j}{b} - \tan\alpha \right) + E_r \left(2\frac{h_{j+1}}{b} + \tan\alpha \right) \qquad (5.17a)$$

For the overall force equilibrium in the horizontal and vertical directions, in the absence of surface loading, the internal forces will balance out and produce

$$\sum(E_r - E_L) = 0 \qquad \sum(X_r - X_L) = 0 \qquad (5.18)$$

From Equations (5.16) and (5.18)

$$\sum\left(X_r - X_L\right) = \sum\left(-W - \frac{1}{\sin\alpha}(T + (E_r - E_L)\cos\alpha) \right) = 0 \qquad (5.19)$$

Hence, the factor of safety is given by

$$F_f = \frac{\sum(cl + (P - ul)\tan\phi)}{\sum(-W\sin\alpha - (E_r - E_L)\cos\alpha)} \qquad (5.20)$$

The iteration solution starts from a good estimate of the initial factor of safety and the first interslice normal force E_L. From Equations (5.13) and (5.15), P and X_L for the first slice are then computed. Once X_L is known, Equations (5.16) and (5.17) can be used to compute X_r and E_r. The process is continued until all the internal forces and the factor of safety have been computed. The advantage of this solution procedure is that no finite difference scheme is required. Here are some notices about this new modified method:

1) This solution procedure is still sensitive to the location of the thrust line, but it is better than Janbu's rigorous method (1973) for thin slices.

2) A good initial choice for the factor of safety needs to be defined. In general, the factor of safety from Janbu's simplified method can be applied as the initial solution.

3) A good initial suggestion for the first interslice normal force should be supplied in the beginning, and this value can be estimated by Morgenstern–Price's solution.

Based on these proposed procedures, all the problems can converge nicely with the factors of safety close to 1.0 for all cases. For normal slopes, the convergence of Janbu's rigorous method (1973) is relatively ok. But for a horizontal slope, Janbu's rigorous method (1973) for thin slices is very poor in terms of the convergence for the present problem. Some of the results are shown in Figure 5.11. When the thrust line ratio based on the slip line solution is used, the factor of safety from the original Janbu's rigorous method (1973) is 0.964 instead of 1.0, which indicates that true moment equilibrium has not been achieved in the original Janbu's rigorous method (1973). From Figure 5.11(b) and (c), it is seen that the interslice shear force is not zero when x is less than 0.5 m from Janbu's rigorous method in Nordic countries, and that some of the $f(x)$ are actually less than zero, which are different from the results from the slip line analysis. When the thrust line ratio is 0.5 or based on that from the slip line solution, the corresponding f(x) obtained is a close approximation of that from the slip line analysis (except for the initial part). On the other hand, if a more rigorous consideration of the moment equilibrium is given, using the approach suggested above, the factor of safety is 1.0, while the $f(x)$ and internal forces obtained are virtually the same as those from the slip line analysis. That means, a correct thrust line will correspond to a correct $f(x)$, and the choice of internal or external variables is not important under the ultimate condition.

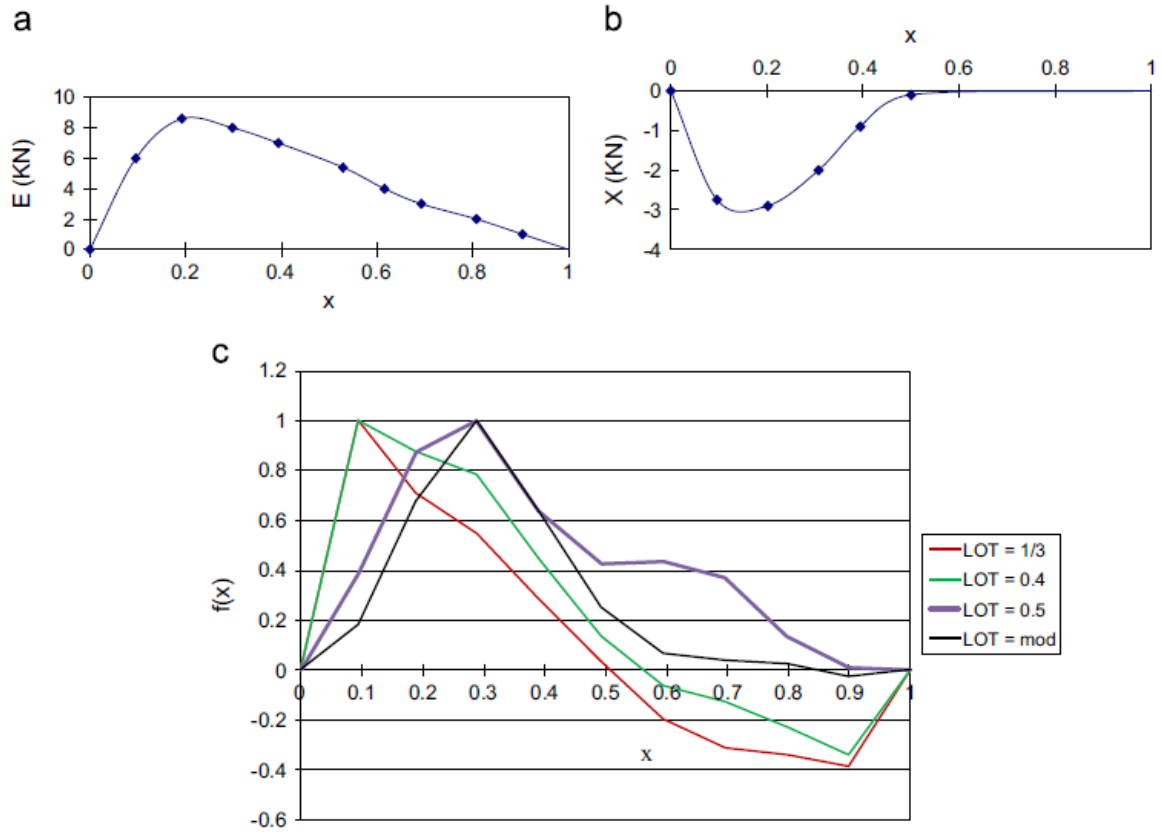

Figure 5.11 (a) E for thrust line ratio=1/3 for factor N_c when ϕ=30°, (b) X for thrust line ratio=1/3 for factor N_c when ϕ=30°, and (c) f(x) based on different thrust line ratios

It is interesting to note that all the factors of safety for the three bearing capacity factors are very close to 1.0 (0.001–0.002 different from 1.0) using either *f(x)* or the thrust line from the ultimate condition. That means, as long as the ultimate condition is given consideration, there is no difference between the uses of *f(x)* or the thrust line in defining a problem. In this respect, Morgenstern–Price's method (1965) and Janbu's method (1973) are judged to be equivalent methods when specifying a problem under the ultimate condition. Other than the ultimate condition, the choice of *f(x)* or the thrust line will give different factors of safety (well known in limit equilibrium analyses) as the solutions are only typical lower bound solutions. Since iteration analyses are sensitive to the thrust line location, the

use of *f(x)* for normal routine engineering analyses and designs is advantageous in that it is easier to achieve convergence for normal cases.

5.3 Boundary forces in limit equilibrium analysis

Baker and Garber (1978) have proposed the use of base normal forces as the variables in the variational principle formulation of slope stability problems. For N_q where ϕ=30°, the base normal stresses under an external surcharge of 1 kPa outside the foundation are determined by the slip line method which is shown in Figure 5.12.

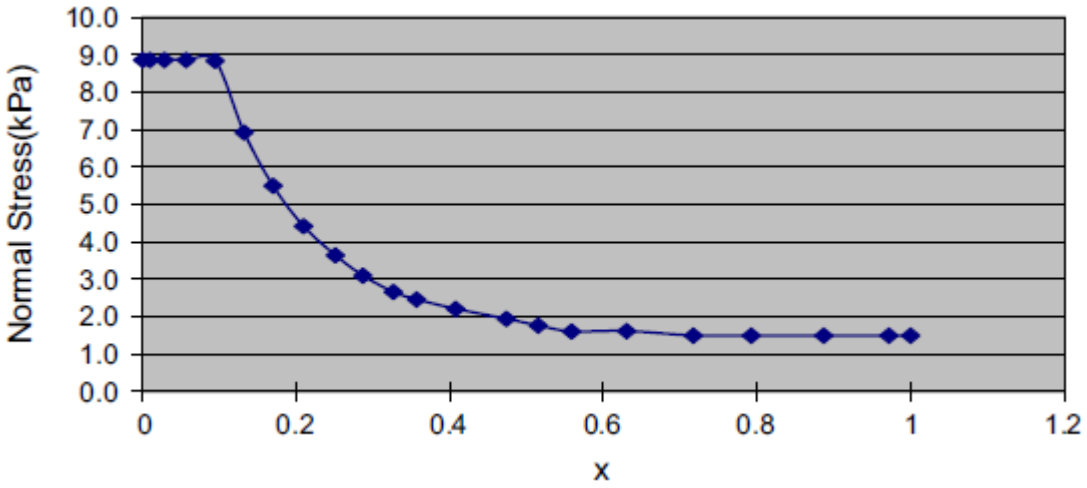

Figure 5.12 Base normal stresses distribution along the slip surface for factor N_q where ϕ'=30° and q=1 kPa

Based on the stresses determined from the slip line analysis, the base normal stresses, and hence, the forces for the slices, can be determined correspondingly. Once *P* is known, based on

$\sum(E_r - E_L) = 0$ and using Equation (5.14), the factor of safety can be computed by force equilibrium as

$$F = \frac{\sum\left(cl + P\tan\phi\right)\cos\alpha}{\sum -P\sin\alpha} \tag{5.21}$$

Based on the base normal stress in Figure 5.12, which has been tested against different grid size used for the slip line analysis, the factor of safety from Equation (5.21) is exactly equal to 1.0, which is as expected. However, using *P* or the thrust line as the control variables is less satisfactory compared to using the interslice force function in the optimization analysis. When the thrust line is defined, the moment equilibrium of the last slice is not used in the analysis, so the true moment equilibrium cannot be satisfied (the well-known problem of Janbu's rigorous method (1973)). It should be pointed out that for the original Janbu's moment equilibrium (1973), the moment equilibrium of the slice interface, instead of the slice, is considered so that there is no problem for the last slice, but the moment equilibrium for each slice is not strictly enforced. The use of *P* also suffers from this limitation. Once *P* is prescribed, *F* will be known from Equation (5.21). Based on the force equilibrium in the horizontal and vertical directions, as well as the moment equilibrium, the interslice normal and shear forces, as well as the thrust line, will be defined for the first slice. These results can then be used to compute the internal forces between slices 2 and 3. The computation progresses until the last slice for which both the force and the moment equilibrium cannot be enforced automatically. To apply the base normal force as the control variables in the extremum evaluation, the base normal forces for *N*-1 slices (*N*=total number of slices) are taken as the variables, while the base normal forces for the last slice will be determined from a trial and error process when the equilibrium of the last slice is satisfied. The same principle can also be applied to the thrust line, where the thrust line for only *N*-2 interfaces are prescribed and the thrust line for the last interface is obtained by a trial and error process until the moment equilibrium has been achieved. The use of *f(x)* is simpler in that the majority of the back-computed thrust lines are acceptable, so that the solution for the prescribed *f(x)*

can be adopted directly without the trial and error process. If the thrust line is not acceptable, then the solution is simply rejected and another trial *f(x)* can be considered.

5.4 Lower bound solution and maximum extremum from limit equilibrium analysis

For the previous problems where *f(x)* or the thrust line from the ultimate limit state is used, the factors of safety of the system will be very close to 1.0. As discussed by Cheng et al. (2010), whenever *f(x)* is prescribed, the solution will always be the lower bound, which can be illustrated by the results in Table 5.1. The maximum extremum corresponds to the state for which a system will exercise its maximum resistance before failure, and this condition is simply the ultimate condition of the system (Cheng et al., 2010). It is interesting to note that as f increases, the rate of decrease in the factor of safety increases, and the factors of safety corresponding to N_c and N_q can be considered to be the same. The maximum difference for the factors of safety corresponding to N_c and N_q with the ultimate limit state solution (1.0) is about 10%. On the other hand, the factor of safety corresponding to N_γ is close to 1.0 (bearing in mind that the failure surface is not the classical wedge/log-spiral mechanism).

Table 5.1 Factor of safety corresponding to the three bearing capacity factors based on f(x)=1

ϕ (°)	N_c	N_q	N_γ
0	0.941	0.941	-
10	0.941	0.941	1.0
20	0.937	0.936	0.989
30	0.925	0.924	0.968
40	0.894	0.892	0.939

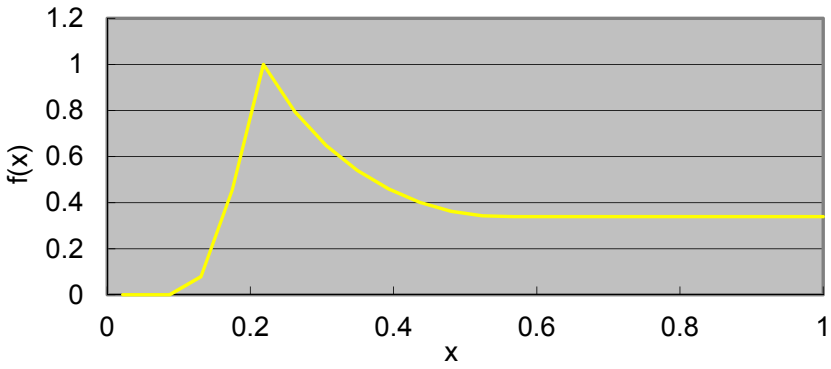

Figure 5.13 f(x) for factor N_c with a sloping ground of 15°

Based on the stresses at yield at the two ends of a failure surface, Chen and Morgenstern (1983) have established a requirement which states that the inclination of the internal forces at the two ends of a failure surface must be parallel to the ground slope. For the previous problems, *f(x)* is zero at the two ends and it satisfies this requirement. Consider a bearing capacity problem (equivalently a slope stability problem) for a soil with c=0 and ϕ=30°, and the ground is sloping at an angle of 15°. The solution to this problem is given by Sokolovskii (1965) as

$$N_c = \left[\frac{1+\sin\phi}{1-\sin\phi} e^{(2\alpha-\pi)\tan\phi} - 1 \right] \cot\phi \qquad (5.22)$$

where α=165° in the present problem. If the Spencer's method (1967) is used, a factor of safety 0.951 with λ=0.281 is obtained for this slip surface, which should bear a factor of safety 1.0 by the classical plasticity solution. Based on the slip line solution by **SLIP**, *f(x)* for this problem is given in Figure 5.13, and $\lambda f(x)$, at the end of the failure surface, is 0.268, which is exactly tan15°; the results clearly satisfy the requirement by Chen and Morgenstern (1983). If Spencer's method (1967) is used in the global minimum analysis, the minimum factor of safety is 0.825 with λ=0.219. The critical failure surface based on Spencer's method (1967), shown in Figure 5.14b, is slightly deeper than the classical slip line solution, shown in Figure 5.14(a). More importantly, the critical solution based on Spencer's method (1967) appears to be a wedge type of failure which is different from the classical solution. The low factor of safety from Spencer's method (1967) has illustrated the importance of *f(x)* in the analysis.

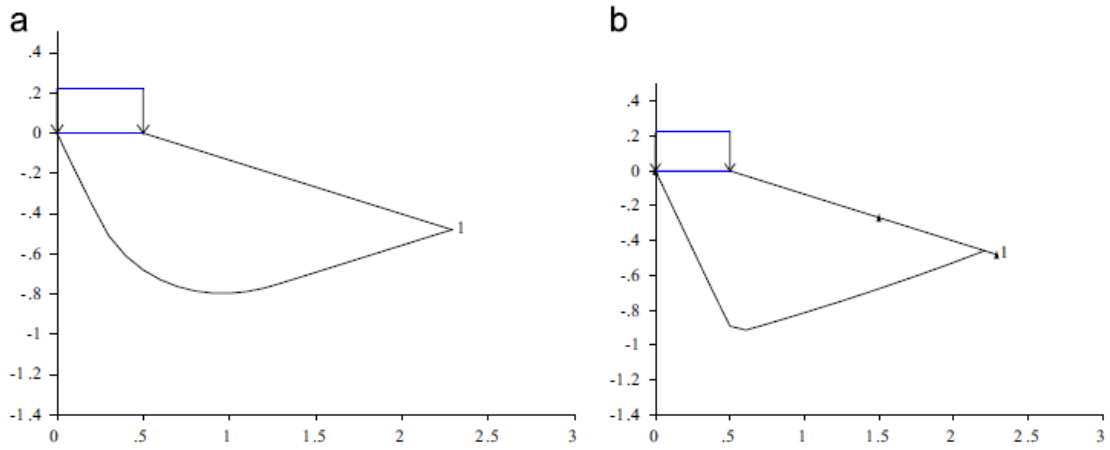

Figure 5.14 (a) Failure surface based on classical plasticity solution using f(x) from Figure 5.13 (λ=0.79 and FOS=1.0) and (b) critical failure surface based on the Spencer's method (λ=0.219, FOS=0.825)

Based on the previous problems and the present problem, it is established that the maximum extremum of a system is very close to the ultimate limit state of the system. For a prescribed failure mechanism, the system will exercise its maximum strength before failure, and this is conceptually the lower bound theorem. Either *f(x)* or the thrust line corresponding to the ultimate limit state will be sufficient to define the system, and *f(x)* and the thrust line can be determined if the method by Cheng et al. (2010) is adopted.

The results in Table 5.1 and Figure 5.15 have clearly illustrated the concept of lower bound analysis, and every prescribed *f(x)* with acceptable internal forces will give a lower bound solution to the problem. On the other hand, if unacceptable internal forces are accepted for any prescribed set of *f(x)*, thrust line or base normal forces, it is actually possible to obtain a low factor of safety or a value higher than 1.0 which is in conflict with the assumption of the lower bound analysis. In this respect, the acceptability of the internal forces, which is not explicitly imposed in the methods by Morgentern and Price (1965), Janbu (1973) or Baker and Garber (1978), is actually important if arbitrary internal

or external variables are imposed in a stability analysis. The lower bound concept can be visualized clearly by Figure 5.15, which shows all the temporary factors of safety during the simulated annealing analysis in searching for the maximum factor of safety using *f(x)* as the variables in the extremum determination for factor N_q when ϕ=30°. *f(x)* is set to 1.0 for the initial trial in the optimization analysis, and the factors of safety are far from 1.0 initially. As the global optimization analysis proceeds, the extremum of the system will tend towards the theoretical value of 1.0, and no factor of safety exceeding 1.0 can be found. The results, shown in Figure 5.15, comply well with the assumption of the lower bound analysis, and they further support the adoption of the maximum extremum as the lower bound solution. A further demonstration of the extremum principle is shown for a very thin slice for a 30° slope with ϕ=30°. According to classical soil mechanics, the factor of safety for this thin slice should be 1.0. From the maximum extremum principle, a factor of 1.0014 is obtained for the slip surface (a minor difference from 1.0 as a circular arc is actually used). From the results in Figures 5.15 and 5.16, it is clear that the maximum resistance of the system has been mobilized in the maximum extremum analysis, and that the extremum principle will not over-predict the factor of safety of the system. Besides the use of *f(x)*, the thrust line and the base normal forces from the slip line analysis, Cheng has also adopted the maximum extremum principle and have obtained factors of safety close to 1.0 for the three bearing capacity factors. Using the maximum extremum principle, all the factors of safety corresponding to the three bearing capacity factors are very close to 1.0 by using either *f(x)*, the thrust line or the base normal forces. These results further demonstrate that the results from the maximum extremum principle practically correspond to the ultimate condition of a system from a limit equilibrium viewpoint.

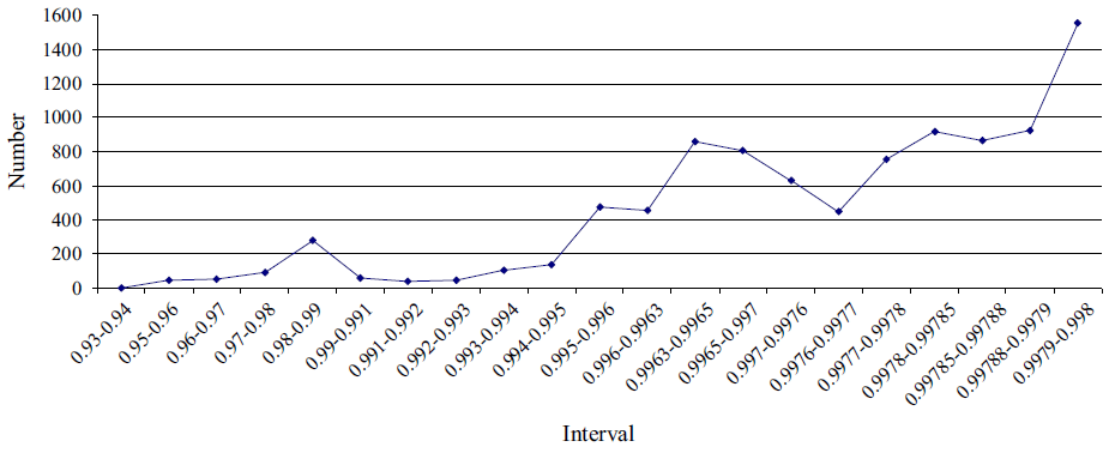

Figure 5.15 Distribution of acceptable factor of safety during simulated annealing analysis for factor N_q with ϕ=30° using f(x) as variable

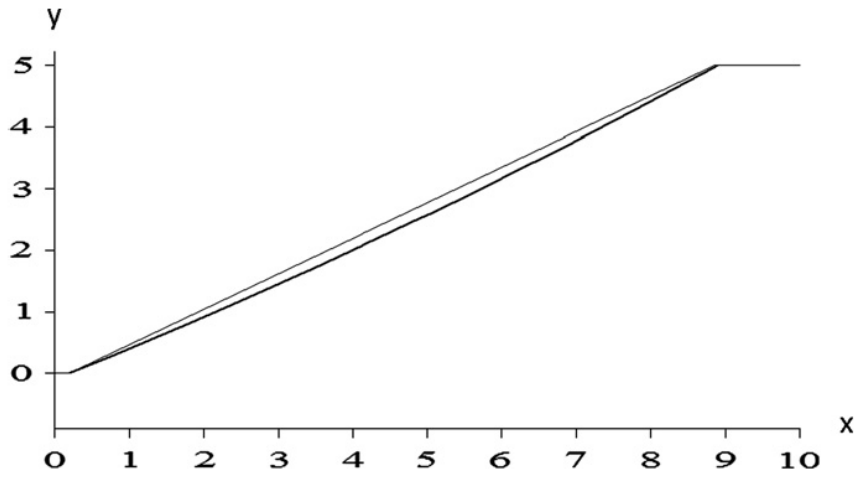

Figure 5.16 Factor of safety from extremum principle for a cohesionless soil with ϕ=30°

5.5 Discussions

In this study, it is demonstrated that even though a limit equilibrium problem can be formulated in various ways (through slope stability analysis), giving different results for the analyses, there will be no difference between different formulations if the ultimate condition is considered. For demonstration, the classical bearing capacity problem, where the slip line solution is available, has been used for illustration. Since the stresses are determinate for this problem, all the internal or external variables at the ultimate condition could be evaluated. The problem is then re-considered by taking *f(x)* as the control variables in the limit equilibrium and determining the maximum extremum. Based on this study, the following have been found.

1. It is demonstrated that a classical bearing capacity problem is equivalent to a horizontal slope stability problem if *f(x)*, the thrust line or the external boundary forces *P* are known at the ultimate condition. The use of *f(x)*, the thrust line or the external boundary forces are simply different ways to specify a limit equilibrium slope stability problem, and the uses of *f(x)*, the thrust line or the base normal forces as the control variables are actually equivalent at the ultimate condition.

2. It has been demonstrated in the present study that *f(x)* are the same for N_c and N_q factors from both the slip line methods and the extremum principle; these results are not surprising as the failure mechanisms for N_c and N_q are actually the same. It is also demonstrated that *f(x)* for N_c and N_q are zero at the two ends and take the maximum value at an x ratio less than 0.5. On the other hand, *f(x)* for N_γ takes the maximum value at a different *x* ratio. For N_c and N_q, the thrust line ratio cluster is around 0.4–0.5, while for N_γ, the thrust line ratio starts at a value between 0.4 and 0.5 and decreases gradually to 1/3 outside the foundation.

3. Based on the *f(x)*, thrust line or the base normal forces, the factors of safety using the MP (1965), Janbu's rigorous method (1973) or the BG method (1978) are very close to 1.0, as obtained from the slip line analysis. That means, as long as the ultimate condition is considered, there is no

practical difference between the uses of the internal or the external variables in defining a problem. It is illustrated in the present study that different formulations should give the same results under the ultimate condition.

4. The interslice force functions obtained from the slip line method in this study are not simple functions which have fully complied with the requirements by Chen and Morgenstern (1983). The inclination of the internal forces at the two ends of a failure surface is always parallel to the ground slope in the present study. On the other hand, $\lambda f(x)$ is set to 1.0 in Spencer's method (1967), which can be viewed as an approximate lower bound of the true failure mechanism. When Spencer's method (1967) is used, poor results are obtained for the bearing capacity problem, which indicates that the precise values for the internal or external variables can be very important in some problems. Considering critical and highly complicated problems, the classical approach by using a simple $f(x)$ may not be adequate.

5. Cheng et al. (2010) have also clearly illustrated that the solution will be a lower bound of the ultimate condition, as long as $f(x)$ is prescribed; hence, the classical limit equilibrium methods are practically lower bound theorems to the ultimate condition.

It should be pointed out that the extremum principle by Cheng et al. (2010) can be regarded as a form of the variational principle (Cheng et al., 2011; Sieniutycz and Farkas, 2005). However, the determined maximum factor of safety may deviate slightly from the true ultimate limit state, as the Coulomb theory is applied as a constraint along the vertical interface instead of any arbitrarily small domain. For a true ultimate limit state, the Mohr–Coulomb relation should be applicable through-out the whole medium domain instead of applying it to lumped global interslice normal and shear forces. In this respect, the maximum extremum principle proposed by Cheng et al. (2010), is only a good approximation to the ultimate condition, as the yield condition is checked globally at each domain interface instead of being enforced at each infinitesimal domain. Nevertheless, the method by Cheng

et al. (2010) provides a good solution with minimum effort by offering a practical solution to a problem without a complete discretization of the solution domain. In the strength reduction analysis of a slope, the factor of safety is varied all the time until the system cannot maintain stability. Stress will redistribute during the nonlinear elasto-plastic analysis, and as long as the stress can be redistributed without violating yield and equilibrium, the trial factor of safety can be furtherly increased. It should be noted that the concept of the extremum theorem is actually consistent with the concept of the strength reduction method in this respect. Hence, it is not surprising that the factors of safety from the strength reduction analysis in ultimate condition are always greater than those from the lower bound Spencer's analysis (Cheng et al., 2007b).

The use of the classical slope stability methods (limit equilibrium-based methods) will not yield good results for bearing capacity problems (plasticity-based solutions), which is well known among many engineers and has also been illustrated by Cheng et al. (2010). Thus, it is not surprising that very few engineers adopt slope stability analysis methods to determine the bearing capacity, which actually this approach is not recommended for use in Hong Kong. In this study, it is indicated that the maximum extremum of the limit equilibrium method is practically equivalent to the plasticity solution so that the limitation in applying the slope stability method to a bearing capacity determination will be removed. Cheng and Au (2005) and Graham et al. (1988) consider a special application of the present approach to the bearing capacity problem of a buried foundation adjacent to a slope with a horizontal set-back. An approximate slip line solution has been adopted by Graham et al. (1988) and Cheng and Au (2005) (see Figure 5.17) as part of the solution domain has not yielded and is not yet controlled by the slip line equations. As shown in Figure 5.17, Point C1 needs to be obtained by trial and error analysis. In order to solve the plasticity slip line equation, the weight of the triangular zone of the soil and the external surcharge is assumed to be known the external pressure acting on A1C1. The zone A1B1C1 is totally considered as an external loading without any consideration given to the strength contribution which appears not to be reasonable, but without this assumption, there is no way to solve

the slip line equation. Using the present approach, a fully yielded solution domain is not required, and the slope stability solution based on the maximum extremum can be used to assess the bearing capacity of the footing. The results shown in Table 5.2 show that the present approach provides a good bearing capacity factor which is not possible for the classical Spencer's method using $f(x)$=1.0, and Spencer's method always underestimates N_γ.

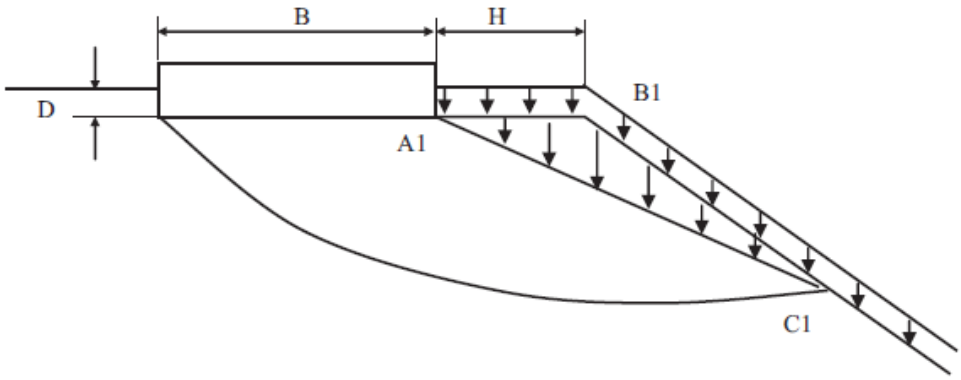

Figure 5.17 *Approximate modeling of footing with embedment and set back by the slip line method*

5.6 Conclusions

Although some of the case studies in this study are based on the use of horizontal slopes, as their analytical solutions are available for comparisons, the results from the present study are generally valid. This has been demonstrated by the problems as shown in Figures 5.14 and 5.17. Based on the present study, the Morgenstern–Price's method (1965) and Janbu's rigorous method (1973) can be viewed as the same under the ultimate condition. These two methods have been illustrated to be equivalent under the ultimate condition, as they are controlled by both yield and equilibrium equations, except for the ease of mathematical manipulation. Besides that, it has also been demonstrated that the application of the base normal forces can be an alternative to Morgenstern–Price's (1965) and Janbu's rigorous methods (1973). Hence, for the ultimate condition, the choice of the assumption is physically not important. On the other hand, if the ultimate condition is not considered, there are practical

differences between the use of *f(x)*, the thrust line or the base normal forces in LEM, and every prescribed assumption giving acceptable internal forces will be a lower bound theorem to the ultimate limit state of the problem, which can be clearly illustrated in Figure 5.16. The present study has demonstrated the equivalence between the slip line solution and the LEM for a medium domain which is fully in the plastic condition, provided that the maximum extremum from the LEM is applied in the comparison. The hyperbolic partial equations governing the α and β characteristic lines, as given by Equations (5.1) and (5.2), can be well approximated by tuning *f(x)* in the slope stability analysis until the critical solution has been obtained with the simple force and the moment equilibrium. It is an interesting and useful application of the lower bound concept used for more general problems where the classical slip line method cannot work. For a homogeneous problem with a continuous stress field, the conclusions from the present study will be valid. It should be kept in mind that for nonhomogeneous problems with discontinuous stress fields, the present conclusion is not valid, but the difference between the application of *f(x)*, the thrust line and the base normal force is still small at ultimate condition.

CHAPTER 6 EQUIVALENCE BETWEEN BEARING CAPACITY, LATERAL EARTH PRESSURE AND SLOPE STABILITY PROBLEMS BY SLIP-LINE AND EXTREMUM LIMIT EQUILIBRIUM METHODS

6.1 Introduction

Lateral earth pressure, ultimate bearing capacity and slope stability problems are three important and classical problems which are well considered by the use of the limit equilibrium method, limit analysis method and method of characteristics in the past. It is interesting to note that these three topics are usually considered separately in most of the books or research studies, and different methods of analyses have been proposed for individual problem even though they are governed by the same requirements for the ultimate conditions. Since the governing equations and boundary conditions for these problems are actually the same, the author views that each problem can be viewed as the inverse of the other problems which will be demonstrated in the present chapter. Actually, the classical limit equilibrium method has already been demonstrated to be equivalent to the plasticity solution in chapter 5 of this thesis. The present work is an extension of the chapter 5's works and the slip line method so as to unify the three major geotechnical problems under one single formulation.

For bearing capacity and lateral earth pressure problems, the use of slip line method is more common, as the geometry under consideration is usually more regular in nature. For slope stability problem where the geometry is usually irregular with complicated soil reinforcements and external loads, the use of the slip line method is practically not possible. Engineers usually adopt the limit equilibrium method (an approximate slip line form) with different assumptions on the internal force distribution ($f(x)$) for the solution of the problems. Morgenstern (1992) has commented that for most practical problems, the uses of different assumptions on the internal forces are not important. Cheng et

al. (2010) and Cheng et al. (2011) have developed the extremum principle and have demonstrated the equivalence of the maximum extremum from the limit equilibrium method and the classical plasticity solution by a simple footing on clay. Cheng et al. (2010) treat *f(x)* as a variable to be determined, and complete equilibrium is enforced during the search for the maximum extremum of a system. Cheng et al. (2010) have also pointed out that the limit equilibrium solution will be lower bound theorems to the ultimate limit state, as long as a *f(x)* is prescribed. When the strength of a system is fully mobilized under the ultimate condition, *f(x)* is actually determined by this requirement which is a boundary condition not been used in the past. Cheng et al. (2010) have pointed out that every kinematically acceptable failure surface should have a factor of safety. Failure to converge in the classical limit equilibrium analysis is caused by the use of an inappropriate *f(x)* in the analysis.

In this chapter, the author will first demonstrate the equivalence between the classical lateral earth pressure and bearing capacity problem by the slip line method. The equivalence between the lateral earth pressure problem and slope stability problem will then be illustrated by the use of extremum principle. Based on these results, it can be concluded that the three classical problems are equivalent in the basic principles, and each problem can be viewed as the inverse of the other problems.

6.2 Iterative finite difference solution of the slip line problem

Bearing capacity for shallow foundation has been studied by many researchers using different methods. Except for the term N_γ (weight term), N_c and N_q terms for the cohesive strength and surcharge are the same among different researchers (except Terzaghi, 1943) by using different methods of analysis. Sokolovskii (1965), Booker and Zheng (2000) and Cheng and Au (2005) have solved the bearing capacity problem under various conditions by the method of characteristics. Martin (2005) has pointed out that the method of characteristics can be used to establish the exact plastic

collapse load for any combination of the parameters c, φ, γ, B and q for the exact bearing capacity calculations, and a powerful program ABC has been produced for such analysis. For lateral earth pressure, Chen (1975), Absi and Kerisel (1990), Cheng (2003), Subra and Choudhury (2006), Shukla et al. (2009), Liu et al. (2009a, 2009b), Peng and Chen (2013), Liu (2014), Vo and Russell (2014, 2016) and many others have also obtained three active/passive earth pressure coefficients for plane strain problem based on the limit analysis and the method of characteristics. Cheng et al. (2007b) have also obtained the three lateral earth pressure coefficients for axi-symmetric problem based on the method of characteristics. In general, the basic numerical method is adopted by all the authors with various modifications or tricks applied to individual case.

Under static and seismic condition, when using method of characteristics for the evaluation of the bearing capacity and lateral earth pressure, many scholars have considered these problems. Kumar and Mohan (2002) have examined the effect of horizontal earthquake body forces on the bearing capacity of foundations in a rigorous manner by employing the method of stress characteristics. Then Kumar and Chitikela (2002) have also studied the seismic passive earth pressure coefficients using the method of characteristics. Cheng (2003) has proposed a rotation of axes in the solution of slip line equations for determination of lateral earth pressure with the presence of seismic loading under general conditions. Cascone and Casablanca (2016) have evaluated the static and seismic bearing capacity factors for a shallow strip footing and considered the seismic condition by means of the pseudo-static approach.

Slip line method (or method of characteristics) considers the yield and equilibrium of a soil mass controlled by the Mohr-Coulomb's criterion, and it is a typical lower bound method. A typical slip line system is shown in Figure 6.1, and the equations are governed by the α and β characteristic equations given by Sokolovskii (1965):

$$\alpha \text{ characteristic}: \quad -\frac{\partial p}{\partial S_\alpha}\sin 2\mu + 2R\frac{\partial \theta}{\partial S_\alpha} + \gamma[\sin(\alpha+2\mu)\frac{\partial y}{\partial S_\alpha} + \cos(\alpha+2\mu)\frac{\partial x}{\partial S_\alpha}] = 0 \qquad (6.1)$$

$$\beta \text{ characteristic}: \quad \frac{\partial p}{\partial S_\beta}\sin 2\mu + 2R\frac{\partial \theta}{\partial S_\beta} + \gamma[\sin(\alpha-2\mu)\frac{\partial y}{\partial S_\beta} + \cos(\alpha-2\mu)\frac{\partial x}{\partial S_\beta}] = 0 \qquad (6.2)$$

where γ is the unit weight of soil; $\mu = (\pi/4 - \varphi/2)$, c and φ are the cohesive strength and friction angle of soil, θ is the angle between the direction of major principal stress and the y-axis, S_α and S_β are the arcs along the α and β lines, α is the angle between the direction of the body force and the vertical direction (y-axis), p and R are the mean stress and radius of the Mohr-circle at the state of failure defined by

$$p = \frac{\sigma_1 + \sigma_3}{2} \quad ; \quad R = \frac{\sigma_1 - \sigma_3}{2} = p\sin\varphi + c\cos\varphi \qquad (6.3)$$

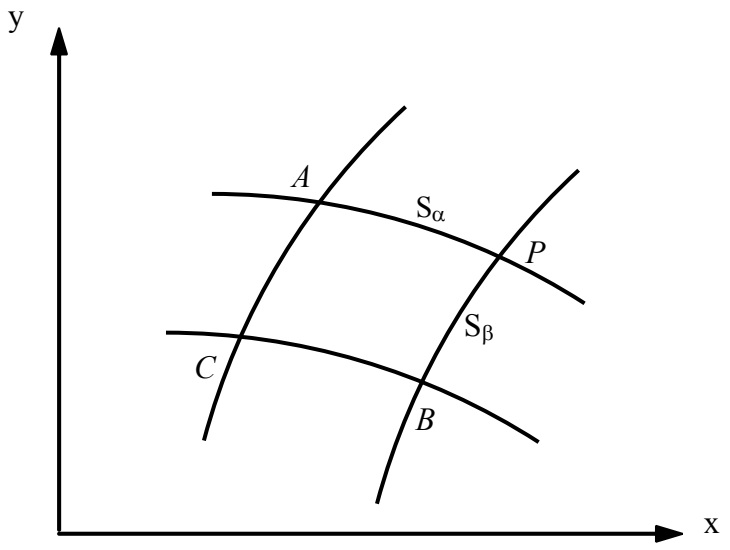

Figure 6.1 α and β lines in slip line solution

If the self-weight of soil is neglected (i.e. γ=0), Equations (6.1) and (6.2) can be simplified as follows:

$$-\sin 2\mu \frac{\partial p}{\partial S_\alpha} + 2R\frac{\partial \theta}{\partial S_\alpha} = 0 \tag{6.4}$$

$$\sin 2\mu \frac{\partial p}{\partial S_\beta} + 2R\frac{\partial \theta}{\partial S_\beta} = 0 \tag{6.5}$$

Integrates the above equations along the α and β lines gives:

$$\ln \bar{p} - 2\theta \cot 2\mu = C_\alpha \Rightarrow \ln \bar{p} - 2\theta \tan\varphi = C_\alpha \text{ (along } \alpha \text{ line)} \tag{6.6}$$

$$\ln \bar{p} + 2\theta \cot 2\mu = C_\beta \Rightarrow \ln \bar{p} + 2\theta \tan\varphi = C_\beta \text{ (along } \beta \text{ line)} \tag{6.7}$$

where $\bar{p} = p + c\cot\varphi$, c is cohesive strength of soil and C_α and C_β are constants. The sign convention used in the present chapter is compressive stress being positive, while the angles θ and others are taken as positive if measured in a counter-clockwise direction. Equations (6.6) to (6.7) will be used to derive the expressions for N_q, N_c, K_{aq} and K_{ac} in the following sections. Generally speaking, by solving Equations (6.1) and (6.2), solutions to many geotechnical problems have been developed and used. It is interesting to note that while there are many works towards the application of method of characteristics in various geotechnical problems, there is none which is devoted to the unification of these geotechnical problems. Bearing capacity, slip line and slope stability problems are treated as individual topics in all the previous works.

Boundary condition in slip line analysis

For a more general condition, the friction along the interface between the soil and the footing or the retaining wall is considered. If a pressure *p'* act on one point M on the soil surface and the angle

between *p'* and the normal line to boundary is δ (i.e. friction angle, Figure 6.2a), *p'* can be described as:

$$p' = \sqrt{(\sigma_n + c\cot\varphi)^2 + \tau_t^2} \tag{6.8}$$

where σ_n and τ_t are normal and shear stress acting on the point M respectively.

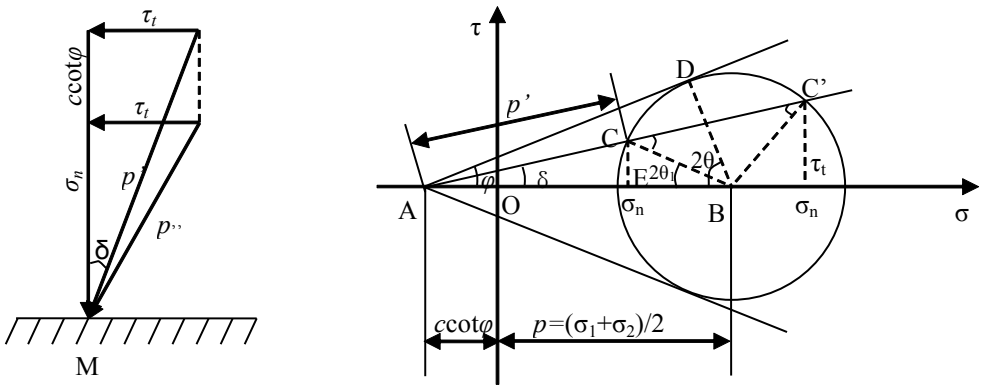

(a) (b)

Figure 6.2 The stress state of point M on a rough surface

The stress state at the point M can be represented by the Mohr circle as shown in Figure 6.2b. AD is the Mohr-Coulomb line and the angle between AD and horizontal line AB is φ. AC represents stress *p'*, and the angle between AC and horizontal line is δ (∠CAB), and δ is taken as positive in Figure 6.2a in a clockwise direction, which corresponds to an active pressure condition. The line AC intersects the Mohr circle at point C, and the abscissa and ordinate of the point C are σ_n and τ_t respectively. Line OB denotes the characteristic stress *p*, ∠ABD = 2θ, ∠ABC = $2\theta_1$, and angle θ_1 is inclination angle between the major principal stress and boundary. It can easily be seen from the geometrical relationship in the Figure 6.2b that:

$$\tau_t = p'\sin\delta \tag{6.9}$$

$$\overline{\sigma_n} = \sigma_n + c\cot\varphi = p'\cos\delta \tag{6.10}$$

Therefore, Equation (6.9) divided by Equation (6.10) gives,

$$\frac{\tau_t}{\sigma_n + c\cot\varphi} = \frac{\sin\delta}{\cos\delta} = \tan\delta \tag{6.11}$$

For convenience, δ in Equation (6.11) is a boundary condition which is defined in terms of τ_f, σ_n, c and φ instead of purely τ_f, σ_n for simplicity. This boundary condition is usually the footing or the back of a retaining wall (surface AO in Figure 6.3) where σ_n is constant (γ is neglected here). The true friction can be transformed to the apparent friction δ easily. According to the geometrical relationship in Figure 6.2b,

$$\overline{\sigma_n} = \sigma_n + c\cot\varphi = \overline{AB} - \overline{BE} = \overline{AB} - \overline{BC}\cos 2\theta_1 = \overline{AB} - \overline{BD}\cos 2\theta_1 \tag{6.12}$$

$$\tau_t = \overline{CE} = \overline{BC}\cos 2\theta_1 = \overline{BD}\sin 2\theta_1 \tag{6.13}$$

From triangle ABD, it is known that,

$$\overline{AB} = p + c\cot\varphi \tag{6.14}$$

$$\overline{BD} = \overline{AB}\sin\varphi = (p + c\cot\varphi)\sin\varphi \tag{6.15}$$

Substitute the above equations in Equations (6.12) and (6.13),

$$\overline{\sigma_n} = \sigma_n + c\cot\varphi == (p + c\cot\varphi) - (p + c\cot\varphi)\sin\varphi\cos 2\theta_1 \tag{6.16}$$

$$\tau_t == (p + c\cot\varphi)\sin\varphi\sin 2\theta_1 \tag{6.17}$$

So, Equation (6.17) divided by Equation (6.16) gives:

$$\frac{\tau_t}{\sigma_n + c\cot\varphi} = \frac{(p + c\cot\varphi)\sin\varphi\sin 2\theta_1}{(p + c\cot\varphi) - (p + c\cot\varphi)\sin\varphi\cos 2\theta_1} = \frac{\sin\varphi\sin 2\theta_1}{1 - \sin\varphi\cos 2\theta_1} \tag{6.18}$$

Solve Equations (6.11) and (6.18) simultaneously,

$$\frac{\sin\delta}{\cos\delta}=\frac{\sin\varphi\sin 2\theta_1}{1-\sin\varphi\cos 2\theta_1} \tag{6.19}$$

Rearrange Equation (6.19) give,

$$\frac{\sin\delta}{\sin\varphi}=\sin\left(2\theta_1+\delta\right) \tag{6.20}$$

The general solution to Equation (6.20) is,

$$2\theta_1+\delta=2m\pi+\Delta \tag{6.21}$$

and $$2\theta_1+\delta=\left(2m+1\right)\pi-\Delta \tag{6.22}$$

where $\Delta=\arcsin\frac{\sin\delta}{\sin\varphi}$. Combine the above two solutions,

$$2\theta_1+\delta=2m\pi+k\Delta+\left(1-k\right)\frac{\pi}{2} \tag{6.23}$$

or $$\theta_1=m\pi+\frac{1}{2}\left(k\Delta-\delta\right)+\left(1-k\right)\frac{\pi}{4} \tag{6.24}$$

where k=±1; m is an integer and generally m=0 or m=±1. According to the triangle ABC in Figure 6.2b,

$$p+c\cot\varphi=p'\frac{\sin\Delta}{\sin\left(\Delta-k\delta\right)}=\frac{\left(\sigma_n+c\cot\varphi\right)}{\cos\delta}\frac{\sin\Delta}{\sin\left(\Delta-k\delta\right)} \tag{6.25}$$

Based on Equations (6.25) and (6.24), the pressure and friction angle on the soil boundary can be converted into the characteristic pressure p and θ_1. For the angle θ between the major principal stress σ_1 and boundary, if the boundary is horizontal, $\theta=\theta_1$. If the boundary inclines to the horizon at α, $\theta=\theta_1+\alpha$. It is noted here that the sign (±) of k is defined based on the direction of displacement of the boundary when the soil attains the limit equilibrium state. When the boundary of soil move in the direction of *p'*, k=-1; when the boundary of soil move in the opposite direction of *p'*, k=1. In other

words, if the soil is in active failure state, k=-1; otherwise, the soil is in the passive failure state and k=1.

For the case of a smooth soil surface (δ=0) with tangential stress (shear stress) τ_t= 0, the characteristic pressure on the boundary OA can be simplified as,

$$p = \frac{(\sigma_n + c\cot\varphi)}{1-\sin\varphi} - \cot\varphi = \frac{\sigma_n + c\cos\varphi}{1-k\sin\varphi} \tag{6.26}$$

Equation (6.26) is obtained because of the relation $\underset{\delta\to 0}{Lim}\frac{\sin\Delta}{\sin(\Delta-\delta)} = \frac{1}{1-\sin\varphi}$.

6.3 Bearing capacity factors and active earth pressure coefficients for rough interface

The ultimate limit state of a bearing capacity and lateral earth pressure problem is shown in Figure 6.3. For the ultimate bearing capacity problem, q_2 is the surcharge on the ground surface, and q_1 is an unknown to be determined. By contrast, when active lateral earth pressure problem is considered, q_1 is the surcharge acting behind the retaining wall, and q_2 is the lateral earth pressure to be determined.

Except for the known and unknown variables and the direction in solving the problem (from left to right or from right to left), the governing equations and conditions for the bearing capacity and lateral earth pressure problems are actually similar. Friction angle is considered in the present study, i.e. the friction angle at the interface OA is δ_1; and the friction angle at the interface OD is δ_2. The total slipping wedge can be divided into three limit equilibrium regions, i.e. active failure region OAB, transition region OBC and passive failure region OCD. It is also interesting to note that the present concept is somewhat similar to the concept of P_{pc}, P_{pq}, and $P_{p\gamma}$ as adopted by Terzaghi (1943), but the

pressure on the inclined surface in the present work is normal to the inclined surface (or with an angle of friction to the normal) while the concept of P_{pc}, P_{pq}, and $P_{p\gamma}$ are always vertical pressures. Furthermore, the failure mechanism as assumed by Terzaghi (1943) is different from many other researchers or the plasticity solution as obtained in the present work.

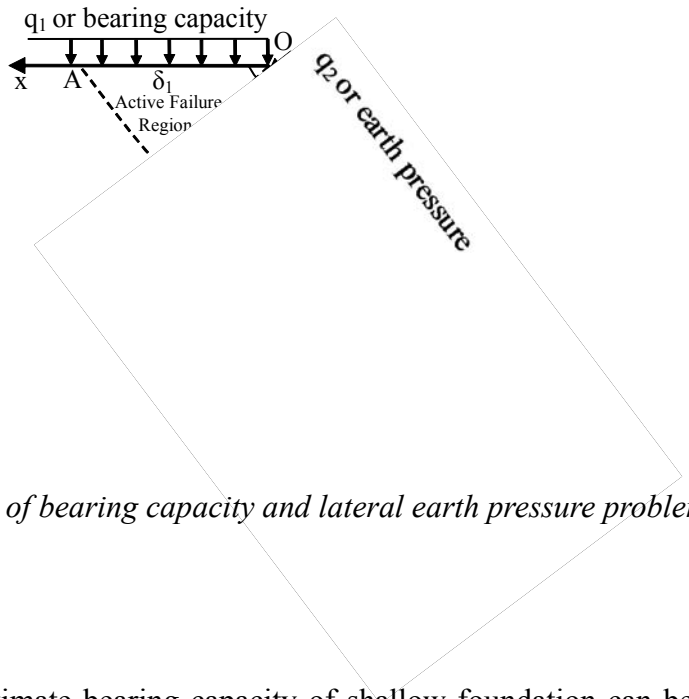

Figure 6.3 Unified model of bearing capacity and lateral earth pressure problem

For a plane strain case, the ultimate bearing capacity of shallow foundation can be determined from the 'superposition' approach which has been shown to be an approximate but good assumption for normal problems by Michalowski (1997) and Cheng (2002). For a strip footing loaded vertically in the plane of symmetry, the ultimate bearing capacity pressure q_u is given by the bearing capacity factors N_γ, N_c *and* N_q as:

$$q_u = q_{u\gamma} + q_{uc} + q_{uq} = \frac{1}{2}\gamma B N_r + cN_c + qN_q \tag{6.27}$$

Similarly, the total active earth pressure is considered a combination of the effects due to the weight of the soil ($p_{a\gamma}$), the cohesive strength of soil (p_{ac}) and the surcharge loading (p_{aq}). The lateral active earth pressure coefficients $K_{a\gamma}$, K_{ac}, *and* K_{aq} and the total active earth pressure can be expressed as,

$$p_a = p_{a\gamma} + p_{ac} + p_{aq} = \gamma h K_{ar} - cK_{ac} + qK_{aq} \tag{6.28}$$

To derive N_q from the bearing capacity model, assume c=0 and γ=0 and a uniform surcharge q_2 is applied along interface OD. The boundary conditions along the slope surface OA (active boundary) are:

$$p = p' \frac{\sin\Delta}{\sin(\Delta - k\delta)} = \frac{q_{uq}}{\cos\delta_1} \frac{\sin\Delta_1}{\sin(\Delta_1 + \delta_1)} \tag{6.29}$$

$$\theta = \theta_1 = \pi - \frac{1}{2}(\Delta_1 + \delta_1) + \frac{\pi}{2} \tag{6.30}$$

The boundary conditions along the slope surface OD (passive boundary) are:

$$p = \frac{q_2}{\cos\delta_2} \frac{\sin\Delta_2}{\sin(\Delta_2 - \delta_2)} \tag{6.31}$$

$$\theta = \theta_1 + \alpha = \pi + \frac{1}{2}(\Delta_2 - \delta_2) + \alpha \tag{6.32}$$

According to Equations (6.6) or (6.7), substitute the above boundary conditions into the equation (6.7) respectively and the following relation can be obtained,

$$\begin{aligned} &\ln\left(\frac{q_{uq}}{\cos\delta_1} \frac{\sin\Delta_1}{\sin(\Delta_1 + \delta_1)}\right) + 2\left(\pi + \frac{\pi}{2} - \frac{1}{2}(\Delta_1 + \delta_1)\right)\tan\varphi = \\ &\ln\left(\frac{q_2}{\cos\delta_2} \frac{\sin\Delta_2}{\sin(\Delta_2 - \delta_2)}\right) + 2\left(\pi + \frac{1}{2}(\Delta_2 - \delta_2) + \alpha\right)\tan\varphi \end{aligned} \tag{6.33}$$

From the above equation, N_q can be derived,

$$N_q = \frac{\cos\delta_1}{\cos\delta_2} \frac{\sin(\Delta_1 + \delta_1)\sin\Delta_2}{\sin(\Delta_2 - \delta_2)\sin\Delta_1} \exp\left[(2\alpha - \pi + \Delta_1 + \delta_1 + \Delta_2 - \delta_2)\tan\varphi\right] \tag{6.34}$$

Similar procedure can be used to derive N_c. Consider the case where q_2=0 and γ=0, the boundary conditions at the base of the footing become:

$$p + c\cot\varphi = \frac{q_{uc} + c\cot\varphi}{\cos\delta_1}\frac{\sin\Delta_1}{\sin(\Delta_1 + \delta_1)} \tag{6.35}$$

θ is unchanged and is same as Equation (6.30). The boundary conditions along the slope surface OD become:

$$p + c\cot\varphi = \frac{c\cot\varphi}{\cos\delta_2}\frac{\sin\Delta_2}{\sin(\Delta_2 - \delta_2)} \tag{6.36}$$

θ is unchanged and is same as Equation (6.32). Similarly to the previous process in deriving N_q, substitute the above boundary conditions into Equation (6.7) gives N_c as:

$$N_c = \left\{\frac{\cos\delta_1}{\cos\delta_2}\frac{\sin(\Delta_1 + \delta_1)\sin\Delta_2}{\sin(\Delta_2 - \delta_2)\sin\Delta_1}\exp\left[(2\alpha - \pi + \Delta_1 + \delta_1 + \Delta_2 - \delta_2)\tan\varphi\right] - 1\right\}\cot\varphi \tag{6.37}$$

For the lateral earth pressure problem, K_{aq} is derived by assuming c=0 and γ=0. The boundary conditions on the surface OA are:

$$p = p'\frac{\sin\Delta}{\sin(\Delta - k\delta)} = \frac{q_1}{\cos\delta_1}\frac{\sin\Delta_1}{\sin(\Delta_1 + \delta_1)} \tag{6.38}$$

θ is the same as Equation (6.30). The boundary conditions on the interface OD are:

$$p = \frac{p_{aq}}{\cos\delta_2}\frac{\sin\Delta_2}{\sin(\Delta_2 - \delta_2)} \tag{6.39}$$

θ is the same as Equation (6.32). Substitute the above boundary conditions into Equation (6.7), and K_{aq} can be derived as:

$$K_{aq} = \frac{\cos\delta_2}{\cos\delta_1}\frac{\sin(\Delta_2 - \delta_2)\sin\Delta_1}{\sin(\Delta_1 + \delta_1)\sin\Delta_2}\exp\left[(\pi - 2\alpha - \Delta_1 - \delta_1 - \Delta_2 + \delta_2)\tan\varphi\right] \tag{6.40}$$

Considering another case where q_1=0 and γ=0, the boundary conditions on the surface OA become,

$$p + c\cot\varphi = \frac{c\cot\varphi}{\cos\delta_1}\frac{\sin\Delta_1}{\sin(\Delta_1+\delta_1)} \tag{6.41}$$

θ is the same as Equation (6.30). The boundary conditions along the slope surface OD become,

$$p + c\cot\varphi = \frac{-p_{ac} + c\cot\varphi}{\cos\delta_2}\frac{\sin\Delta_2}{\sin(\Delta_2-\delta_2)} \tag{6.42}$$

It is to be noted here that the lateral earth pressure induced by cohesive strength is negative, so a sign (-) is added to p_{ac}. θ is the same as Equation (6.32). Similar to the previous process in deriving K_{ac}, substituting the above boundary conditions into Equation (6.7) gives:

$$K_{ac} = \left\{1 - \frac{\cos\delta_2}{\cos\delta_1}\frac{\sin(\Delta_2-\delta_2)\sin\Delta_1}{\sin(\Delta_1+\delta_1)\sin\Delta_2}\exp\left[(\pi - 2\alpha - \Delta_1 - \delta_1 - \Delta_2 + \delta_2)\tan\varphi\right]\right\}\cot\varphi \tag{6.43}$$

By comparing Equation (6.34) with Equation (6.40), it is clear that the relation between N_q and K_{aq} for general rough interface is given as,

$$N_q \cdot K_{aq} = 1 \tag{6.44}$$

Combining Equation (6.37), (6.40) and (6.43) together, it is noted that the following relation among N_c, K_{aq} and K_{ac} can be developed,

$$N_c = K_{ac} / K_{aq} \tag{6.45}$$

Equation (6.45) can also be viewed from another point of view. The active pressure along OD induced from the uniform surcharge q_1 along AO will be negative for the cohesive strength. If q_1 is chosen such that the lateral earth pressure on OD is exactly 0, this condition will correspond to the ultimate bearing capacity induced by cohesive strength.

Using this concept, Equation (6.45) is also determined from Equations (6.37), (6.40) and (6.43). The bearing capacity factors N_c and N_q are hence demonstrated to be related to the active lateral earth pressure coefficients K_{ac} and K_{aq} by Equations (6.44) and (6.45). For the terms N_γ and $K_{a\gamma}$ related to

self weight of soil, analytical expression is not possible and numerical computation will be adopted for the comparisons which will be explained in the later section.

6.4 Bearing capacity factors and active earth pressure coefficients for smooth interface

For the case of smooth soil interfaces (δ_1=0 and δ_2=0), the boundary conditions become much simpler. On the passive failure boundary (OD), the characteristic pressure p and θ can be simplified as,

$$p = \frac{\sigma_n + c\cos\varphi}{1-\sin\varphi} \text{ and } \theta = \frac{\pi}{2} \tag{6.46}$$

On the active failure boundary (OA), p and θ is simplified as,

$$p = \frac{\sigma_n + c\cos\varphi}{1+\sin\varphi} \text{ and } \theta = \alpha \tag{6.47}$$

With the above boundary conditions, Equations (6.1) and (6.2) can be solved from right to left which give N_q for smooth surface as

$$N_q = \frac{1+\sin\varphi}{1-\sin\varphi} e^{(2\alpha-\pi)\tan\varphi} \tag{6.48}$$

K_{aq} is given by solving Equations (6.1) and (6.2) from left to right as:

$$K_{aq} = \frac{1-\sin\varphi}{1+\sin\varphi} e^{(\pi-2\alpha)\tan\varphi} \tag{6.49}$$

Equations (6.48) and (6.49) also meet the relation defined by Equation (6.44). Sokolovskii (1965) has proved that the bearing capacity N_c for general inclined ground is given by,

$$N_c = \left[\frac{1+\sin\varphi}{1-\sin\varphi} e^{(2\alpha-\pi)\tan\varphi} - 1\right]\cot\varphi \tag{6.50}$$

Similar relation can also be derived for K_{ac} by solving Equations (6.1) and (6.2) from left to right as:

$$K_{ac} = \left[1 - \frac{1-\sin\varphi}{1+\sin\varphi} e^{(\pi-2\alpha)\tan\varphi}\right]\cot\varphi \tag{6.51}$$

Using K_{aq} from Equation (6.49) and K_{ac} from Equation (6.51), Equation (6.45) is exactly equal to Equation (6.50). It is noted here that Equations (6.48) ~ (6.51) are actually the simplifications of Equations (6.34), (6.37), (6.40) and (6.43). Equations (6.49) and (6.51) also comply with the Caquot's (1934) theorem of corresponding state that

$$K_{ac} = \frac{1-K_{aq}}{\tan\phi} \tag{6.52}$$

6.5 Verification of equivalence by finite difference programs

For a further verification of the above results, the analytical expressions and the unification of the active lateral earth pressure and bearing capacity problems are further checked by the use numerical computation. Cheng (2003) has developed an iterative finite difference program called KA for the slip line problem in a previous study on lateral earth pressure. For the numerical study in this section, another program ABC which is coded by Martin (2004a,b), Martin (2005) for bearing capacity problem based on the method of characteristics is used for comparison. The programs KA and ABC are written with the same basic theory except that program KA has an axes transformation technique as proposed by Cheng (2003) to account for the earthquake load which is not available in program ABC. For details about these programs, the readers are suggested the works by Cheng (2003) or the user guide of program ABC.

First of all, consider the case without friction on the interface. As shown in Table 6.1, for N_q and K_{aq}, the values using the formula or the finite difference programs are very close to each other, and the relation between N_q and K_{aq} is consistent with Equation (6.44). The results from KA are just the same as Equation (6.49) which is first proposed by Sokolovskii (1965). The minor differences between the analytical expressions and the numerical results can be attributed to the results of discretization, and the differences are very small and are negligible. The numerical results have further supported the validity of the previous results and the unification of the lateral earth pressure and bearing capacity problem. Table 6.2 shows that the results from ABC and KA are very close to the solutions from the analytical equations, and the relation between K_{ac} and N_c meet the requirement from Equation (6.45).

However a requirement on the iterative finite difference analysis is noticed in the present study. Cheng (2003) has found that the active pressure coefficients are not sensitive to the precise location of the slip line, and no iteration in the finite difference scheme is required for practical purpose (passive pressure coefficient is very sensitive and at least two iterations are required for a good accuracy). When lateral earth pressure program KA is used for bearing capacity problem, the transition zone is much larger and the precision of analysis becomes important. For the present study, iteration in program KA is required and convergence is deemed to be satisfied when the change of the coordinates of the slip line is less than 0.1%. In general, several iterations will be required for the analysis, and the number of iterations increases with the friction angle which is as expected. With the use of iteration analysis, the numerical results from KA (active pressure program) agree well with the analytical expressions for bearing capacity problem as given in this chapter. For shallow foundations with sloping ground or active lateral earth pressure problem, the inverse relation between the above two classical soil mechanical problems also holds well which is illustrated by the results as shown in Tables 6.3 and 6.4. The relations as shown in Tables 6.1 to 6.4 are interesting, and this has illustrated the nature of the problem which are governed by Equations (6.1) and (6.2) for both types of problems. Classically, the determination of the bearing capacity or lateral earth pressure by solving Equations

(6.1) and (6.2) are actually equivalent to solving these two equations by iterative finite difference methods from left to right or from right to left. The same governing equations are however exactly the same for the two types of problems.

For the more general cases with friction on the interface between soil and wall/footing, the inverse relation between the bearing capacity and active earth pressure problems is also confirmed which is shown in Tables 6.5-6.8. Through the above results, it is clear that each problem is the inverse of the other, and the choice of the problem depends on the way the problem is being viewed and solved. In other words, the variables of one problem are just the variables of the corresponding image problem.

Table 6.1 Verification of the relationship between K_{aq} and N_q on level ground (smooth), and K_{aq} x N_q is very close to 1.0 for all cases

φ	N_q		K_{aq}	
(°)	Equation(6.48)	ABC	Equation(6.49)	KA
10	2.471	2.471	0.405	0.405
20	6.399	6.34	0.156	0.156
30	18.401	18.407	0.054	0.054
40	64.195	64.256	0.016	0.016
50	319.057	319.92	0.003	0.003

Note: c=0, γ=0, α=180°.

Table 6.2 Verification of the relationship between K_{ac} and N_c on level ground (smooth), and $N_c = K_{ac} / K_{aq}$ is satisfied

φ	N_c		K_{ac}	
(°)	Equation(6.50)	ABC	Equation(6.51)	KA
10	8.345	8.345	3.377	3.382
20	14.835	14.836	2.318	2.329
30	30.14	30.149	1.638	1.648
40	75.313	75.385	1.173	1.178
50	266.882	267.606	0.836	0.838

Note: γ=0, q=0, α=180°.

Table 6.3 Verification of the relationship between K_{aq} and N_q on sloping ground (smooth condition), and K_{aq} x N_q is very close to 1.0 for all cases

α	N_q	K_{aq}	
(°)	Equation(6.48)	Equation(6.49)	KA
170	15.042	0.066	0.066
160	12.297	0.081	0.081
150	10.052	0.099	0.100
140	8.218	0.122	0.122
130	6.718	0.149	0.149

Note: c=0, φ=30°, γ=0.

Table 6.4 Verification of the relationship between K_{ac} and N_c on sloping ground (smooth), and N_c = K_{ac} / K_{aq} is satisfied

α	N_c	K_{ac}	
(°)	Equation(6.50)	Equation(6.51)	KA
170	24.322	-1.617	1.626
160	19.567	-1.591	1.599
150	15.679	-1.560	1.566
140	12.501	-1.521	1.526
130	9.903	-1.474	1.477

Note: φ=30°, q=0, γ=0.

Table 6.5 Verification of the relationship between K_{aq} and N_q on level ground (rough), and K_{aq} x N_q is very close to 1.0 for all cases

δ_1 (°)	δ_2 (°)	N_q	K_{aq}	
		Equation(6.34)	Equation(6.40)	KA
0	5	19.285	0.0519	0.0518
0	10	20.093	0.0498	0.0497
0	15	20.834	0.0480	0.0479
0	20	21.505	0.0465	0.0464
0	25	22.083	0.0453	0.0452
0	30	22.456	0.0445	0.0444
5	0	21.167	0.0472	0.0472
10	0	23.838	0.0419	0.0419
15	0	26.299	0.0380	0.0379
20	0	28.416	0.0352	0.0351
25	0	30.020	0.0333	0.0332
30	0	30.829	0.0324	0.0322
5	5	22.184	0.0451	0.045
10	10	26.030	0.0384	0.0383
15	15	29.776	0.0336	0.0335
20	20	33.209	0.0301	0.0300
25	25	36.027	0.0277	0.0276
30	30	37.622	0.0266	0.0263

Note: c=0, φ=30°, γ=0.

Table 6.6 Verification of the relationship between K_{ac} and N_c on level ground (rough), and $N_c = K_{ac} / K_{aq}$ is satisfied

δ_1	δ_2	N_c	K_{ac}	
(°)	(°)	Equation(6.37)	Equation(6.43)	KA
0	5	31.671	1.642	1.652
0	10	33.07	1.646	1.656
0	15	34.353	1.649	1.660
0	20	35.516	1.652	1.663
0	25	36.516	1.654	1.666
0	30	37.162	1.655	1.672
5	0	34.931	1.650	1.660
10	0	39.557	1.659	1.670
15	0	43.819	1.666	1.677
20	0	47.485	1.671	1.682
25	0	50.265	1.674	1.685
30	0	51.666	1.676	1.687
5	5	36.692	1.654	1.664
10	10	43.353	1.666	1.676
15	15	49.841	1.674	1.683
20	20	55.787	1.680	1.692
25	25	60.668	1.684	1.697
30	30	63.432	1.686	1.702

Note: φ=30°, q=0, γ=0.

Table 6.7 Verification of the relationship between K_{aq} and N_q on sloping ground (rough), and K_{aq} x N_q is very close to 1.0 for all cases

α	N_q	K_{aq}	
(°)	Equation(6.34)	Equation(6.40)	KA
170	24.341	0.0411	0.041
160	19.898	0.0503	0.0502
150	16.266	0.0615	0.0614
140	13.297	0.0752	0.0751
130	10.87	0.0920	0.091

Note: c=0, φ=30°, γ=0.

Table 6.8 Verification of the relationship between K_{ac} and N_c on sloping ground (rough), and $N_c = K_{ac} / K_{aq}$ is satisfied

α	N_c	K_{ac}	
(°)	Equation(6.37)	Equation(6.43)	KA
170	40.428	1.661	1.672
160	32.733	1.645	1.656
150	26.442	1.626	1.636
140	21.299	1.602	1.611
130	17.096	1.573	1.580

Note: φ=30°, q=0, γ=0.

6.6 Relation between N_γ and $K_{p\gamma}$

For N_γ, Sokolovskii (1965) and Cheng and Au (2005) and others determined it by solving Equations (1) and (2) from right to left. For the ultimate pressure at the bottom of the footing on a level ground, the slip line program SLIP by Cheng and Au (2005) starts at with a uniform distributed load (very small and tends to zero, similar to that by Martin 2004) along OD (which is horizontal now) and the construction of the slip-line field begins from the right hand side to the left hand side. The ultimate bearing stress along OA due to the weight of soil and friction angle of the soil will be a triangular pressure along OA, which are given by Sokolovskii (1965), Booker and Zheng (2000) and Cheng and Au (2005). However, the image passive pressure problem can be determined by applying a small uniform distributed load (tends to zero) on line OA as shown in Figure 6.4 and solving the slip line equations from left to right. The passive pressure along line OD from passive pressure determination is virtually the same as the bearing stress on line OA from bearing capacity determination from the program output from SLIP and KP. This approach is conceptually the reverse of the classical method of characteristics for solving the bearing capacity problem, but it is not explicitly considered in the past.

A typical slip line system for the lateral pressure problem is shown in Figure 6.4, which is actually the same as the slip lines obtained by Cheng and Au (2005) or Martin (2004) for bearing capacity problem. Just from Figure 6.4 alone, it is actually not possible to tell whether it is a bearing capacity problem or a lateral earth pressure problem (even though the ways of solution are the inverse). The mean pressure acting on OA is the ultimate bearing pressure due to the self weight of soil and N_γ is then determined accordingly. The present results are actually equal to that from the Prandtl's mechanism (Prandtl, 1920), and the results are compared with the classical solution by Sokolovskii (1966), Hansen (1970), Vesic (1973), Meyerhof (1963) and Chen (1975). Based on the slip line

program ABC developed by Martin (2004a,b) for bearing capacity determination and the slip line lateral earth pressure program KP developed by Cheng (2003), the equivalent N_γ for level ground and sloping ground are given in Tables 6.9 and 6.10. Since N_γ from SLIP is defined by the average value of the bearing stress along OA from bearing capacity determination (after Sokolovskii 1966) from the Prandtl's mechanism (Prandtl, 1920), numerically, it is the same as the passive pressure $K_{p\gamma}$ from KP, or

$$N_\gamma = K_{p\gamma} \tag{6.53}$$

N_γ can be considered as the corresponding passive earth pressure coefficient, and the classical bearing capacity equation $\gamma BN_\gamma/2$ can be considered as equivalent to $K_p\gamma H^2/2$. The classical definition of bearing capacity $\gamma BN_\gamma/2$ is a hence better definition as compared with using γBN_γ, as it actually reflects the fact that bearing capacity and passive pressure problems are just image problem of each other.

The author should point out a major issue for the results as given by Martin (2004a,b) and some other researchers in Table 6.9, for which the failure mechanism is based on an asymmetric failure mode. Although most of the available solutions based on the method of characteristics use an asymmetric failure mechanism, Graham et al. (1988) have actually adopted a near symmetric failure mechanism for problem with a sloping ground with the method of characteristics. Cheng and Au (2005) have pointed out that the results by Graham et al. (1988) are not good as compared with experimental results due to the use of symmetric failure mechanism. However, the results by Sokolovskii (1965) and other famous classical results (used by many engineers and many design codes) as given in Table 6.9 are actually based on a symmetric failure mechanism. In this respect, the author present the result from KP with a symmetric failure mechanism in Table 6.9. If the author adopts asymmetric failure similar to that by Martin (2004a,b), the results from program SLIP will be

equal to that by ABC. From Tables 6.9 and 6.10, it is clear that N_γ can also be determined from the lateral earth pressure program KP by Cheng. It is interesting to note that when α equals to 145°, N_γ should equal to 0 when c=0. This result is correctly reflected in the active pressure program KA or program ABC but is not correct in the Vesic's (1973) and Hansen's (1970) bearing capacity factors for purely cohesionless soil. It should also be noted that the results by program SLIP and KP for bearing capacity and lateral earth pressure determination by Cheng and Au (2005) and Cheng (2003) and are virtually the same in Tables 6.9, 6.10 and 6.11. While Cheng developed these programs for different purposes, the extension of these programs will give similar results if they are properly used.

Based on the results from above, it can be concluded that the bearing capacity problem and lateral earth pressure problem are inverse image problems which can be unified under the same formulation. It is true that it is more convenient to obtain the three bearing capacity factors in the traditional way by solving Equations (6.1) and (6.2) from right to left, but it is also completely possible to solve the bearing capacity problem by solving the problem from left to right as a lateral earth pressure problem at the expense of slightly more effort in the computation. In fact, for problem as shown in Figure 6.3, if there is loading along AO but no loading along OD, this kind of problem has been considered as bearing capacity problem as well as slope stability problem in different research papers in the past (Cheng et al. 2013b). In this respect, the classification of such a problem is sometimes arbitrary in the past, and this also illustrates that there is no difference between a bearing capacity problem and a slope stability problem by nature.

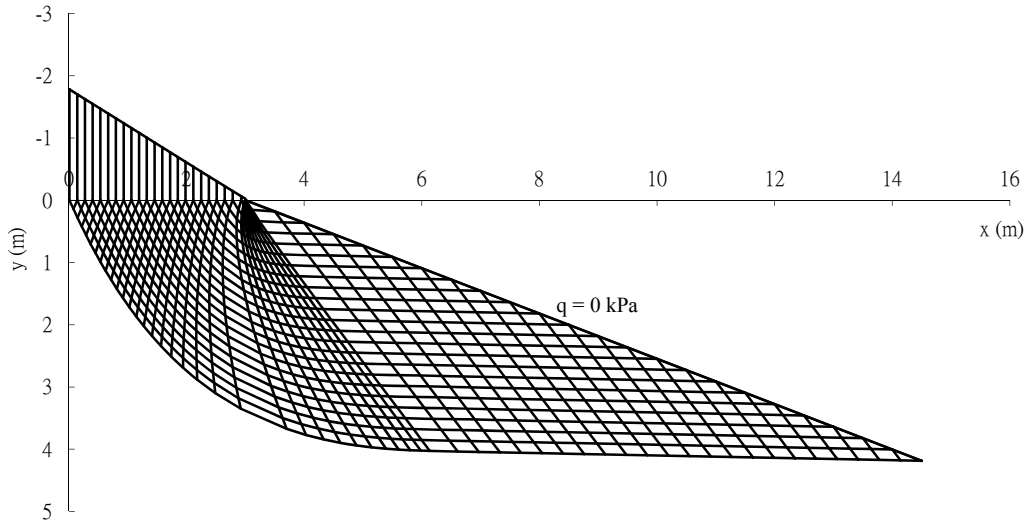

Figure 6.4 Typical slip line pattern for lateral earth pressure problem with triangular surcharge

Table 6.9 Comparison of N_γ on level ground for smooth foundation by various methods of analysis (based on asymmetric failure)*

φ\N_γ	ABC	Sokolovskii (1965)	Hansen (1970)	Bolton & Lau (1993)	Vesic (1973)	Chen (1975)	KP
10	0.281*	0.56	0.39	0.29	1.22	0.72	0.56
20	1.579*	3.16	2.95	1.6	5.39	3.45	3.158
30	7.653*	15.3	15.07	7.74	22.4	15.2	15.3
40	43.19*	86.5	79.54	44	109.41	81.79	86.5
50	372*	--	568.33	389	762.7	--	748.1

Table 6.10 Comparison of N_γ for different methods of analysis (φ=35°) for sloping ground (correction factors by Vesic 1973 and Hansen 1970 are used)

$\alpha \backslash N_\gamma$	Vesic (1973)	Hansen	KP
180	48.03	33.93	17.59
170	32.59	21.38	11.25
160	19.43	12.42	7.44
150	8.58	6.18	4.86
145	4.32	3.9	0

6.7 Comparisons between slip line and limit equilibrium extremum principle

Cheng et al. (2010) have demonstrated that the extremum principle provides a good approximation to the ultimate condition, and the results by extremum principle are very close to (usually equal to) the slip line solutions in general. In fact, Cheng et al. (2013a) have demonstrated that the extremum principle is equivalent to the solution of partial differential equations, and the slope stability problem and bearing capacity problem can be viewed as equivalent problem under the extremum condition (Cheng et al. 2013b). In this section, the previous work by Cheng et al. (2013b) is further extended to the problem of lateral earth pressure. To determine the lateral earth pressure from the extremum principle, a prescribed slip surface is first defined and the maximum factor of safety is

determined with the extremum principle by adjusting *f(x)* in accordance with the approach by Cheng et al. (2010). The critical slip line is then determined by the minimum factor of safety from different trial slip line which is the typical upper bound approach for slope stability analysis. The lateral force between the retaining wall and the soil is varied until the minimum factor of safety is 1.0. Under this condition, the frictional force and the lateral earth pressure arising from the extremum limit equilibrium principle should be a good approximation (usually exactly equal to) of the results from slip line analysis. Refer to Figure 6.5, the α line corresponding to AB is obtained for a specific height from the extremum limit equilibrium method. Different α lines are constructed by the extremum limit equilibrium method, then the β lines can be constructed by drawing lines at an angle of ($\pi/2-\varphi$) to the α lines. In this way, the slip line system is obtained by the classical limit equilibrium method using the extremum principle (Cheng et al. 2010). Similarly, the same approach can be used to determine the bearing capacity factors from slip line solutions.

To determine N_c factor, a surcharge is applied underneath a foundation with a value equal to cN_c without any external surcharge while the self weight is maintained at zero. For factor N_q, the self weight and cohesive strength are maintained at zero while a surcharge of 1 unit is applied outside the foundation and the foundation load is maintained at N_q. If the slip surface based on the classical Prandtl's or Hill's mechanism (Chen 1975) is used, the factors of safety as determined for different φ are exactly 1.0 if the extremum principle is used and *f(x)* is kept on varying until the maximum factor of safety is found. For the term N_r, a triangular pressure is applied underneath the foundation, and the maximum pressure is adjusted until the critical factor of safety from extremum limit equilibrium method is 1.0. The critical slip surface is allowed to be automatically determined from the extremum principle in this analysis, and the resulting critical slip surface with a factor of safety 1.0 from the extremum principle will be very close to that by slip line analysis. The bearing capacity factors N_r obtained from different approaches are given in Table 6.11. For example, for φ=10°, the slip line

system using a very fine grid for the case of N_r is given in Figure 6.6. The failure zone at the right of Figure 6.6 is a typical triangular zone underneath the footing with a curved narrow transition zone, and this slip surface is far from the Hill's or Prandtl's mechanism as adopted by Chen (1975). The slip surface from the extremum principle is close to that as shown in Figure 6.6, and the N_r from extremum principle limit equilibrium slope stability analysis is also very close to that by the slip line method. For N_c and N_q, if the slip surfaces are not specified but is searched from the extremum principle in the way as suggested by Cheng et al. (2007a, 2010), the critical slip surfaces from extremum limit equilibrium solution are exactly equal to that from the slip line solution as shown by Cheng et al. (2013b).

Table 6.11 Bearing capacity N_r from different methods (solution from Slip is based on Cheng and Au (2005) using slip line solution, solution from Sokolovskii is also based on slip line solution, solution from Chen is based on limit analysis, present solution (automatic) is based on extremum principle with search for critical slip surface)

φ (°)	Program SLIP	Sokolovksii (1965)	Chen (1975)	Present (Automatic search)
10	0.56	0.56	0.72	0.57
20	3.16	3.16	3.45	3.18
30	15.31	15.3	15.2	15.3
40	86.8	86.5	81.79	86.6

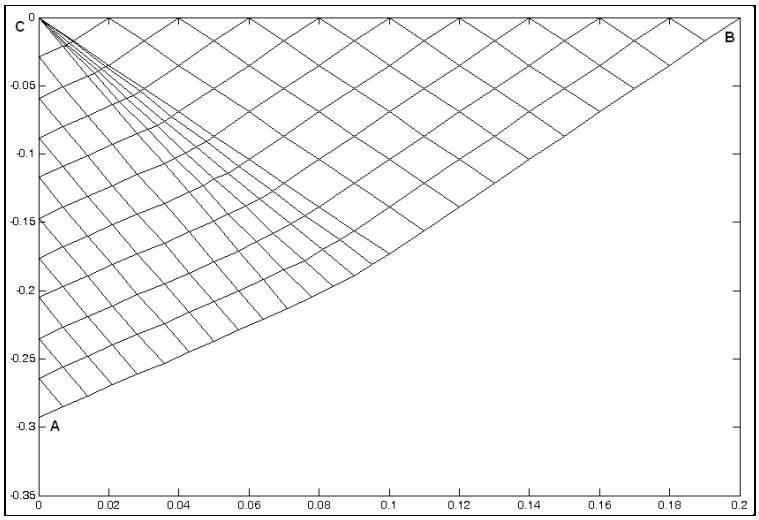

Figure 6.5 Construction of slip line from limit equilibrium method (φ=30°, δ=20°)

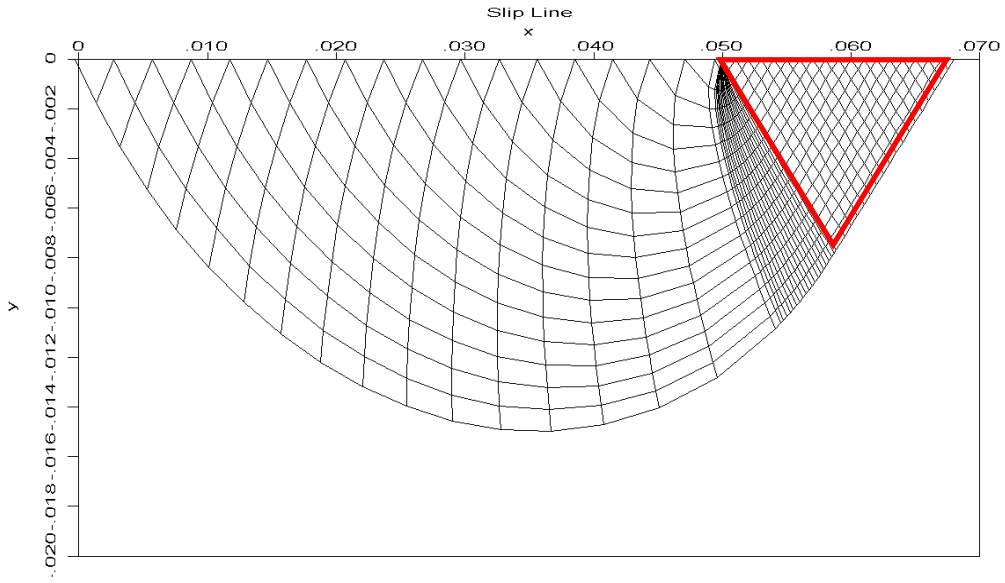

Figure 6.6 Slip line for the bearing capacity problem when φ=10°

It is also interesting to note that the lower bound principle has been clearly illustrated in the present analysis. For the case of factor N_c using the Prandtl's mechanism, the author has analyzed the intermediate results during the extremum analysis. *f(x)* is kept on changing during the analysis, with an initial value of 1.0 for all x_i during the simulated annealing optimization analysis. With *f(x)*=1.0, the factor of safety is actually 0.925 which is far from 1.0. As *f(x)* is changed, the factor of safety converges towards 1.0 during the simulated annealing analysis, but no factor of safety greater than 1.0 can be obtained. The same results are also obtained for the case of N_q as well. The results as shown in Figure 6.7 are actually good illustration of the lower bound principle.

For the lateral earth pressure, consider the case of a vertical wall with a wall friction δ and the ground is inclined at an angle α above the horizontal direction. The active pressure coefficient can be determined from slope stability method in the following way. Refer to Figure 6.5, a normal force FORCE on the retaining wall AC is assumed, then the wall friction is given by FORCEXtanδ. The normal and tangential forces are applied at the vertical boundary AC, and soil mass ABC is considered as a slope stability problem. For any prescribed failure surface, the extremum of the factor of safety (by treating *f(x)* as variable) from limit equilibrium analysis is obtained. Upper bound analysis is then carried out to determine the minimum factor of safety. If the minimum factor of safety from the extremum is not equal to 1.0, the value of FORCE will be adjusted until a minimum factor of safety 1.0 is achieved. The lateral earth force and hence lateral pressure coefficient is then determined. From the results as shown in Table 6.12, it is clear that there is no practical difference between a lateral earth pressure problem and a slope stability problem, provided that the critical extremum solution from slope stability analysis is used for comparison.

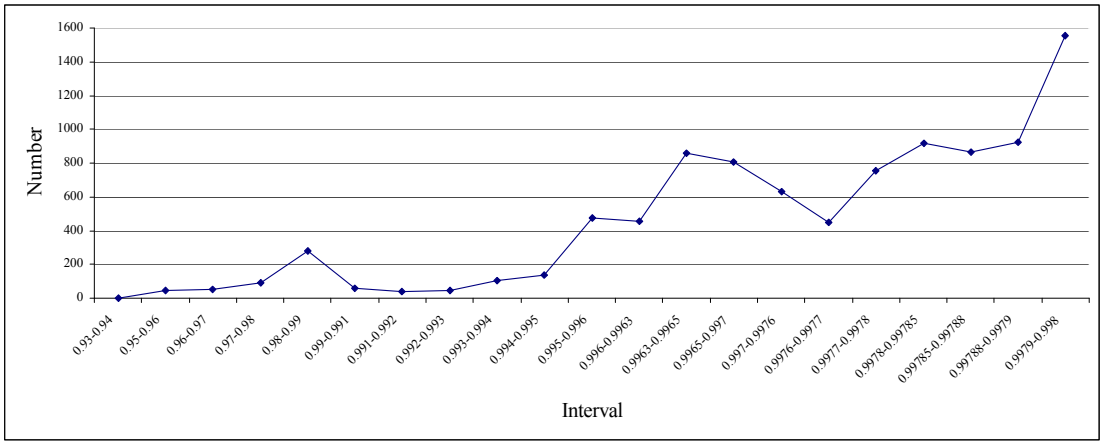

Figure 6.7 Distribution of acceptable factor of safety during simulated annealing analysis for N_c (same results for N_q) with $\varphi=30°$ using f(x) as the variable

Table 6.12 Active pressure coefficients from slip line analysis and extremum principle

φ (°) (α=10°, δ=10°)	Slip line	Extremum Principle
20	0.531	0.54
30	0.35	0.353
40	0.225	0.228
φ (°) (α=15°, δ=10°)		
20	0.61	0.615
30	0.379	0.382
40	0.23	0.232

6.8 Discussion

In this chapter, the method of characteristics has been applied to study two classical and important geotechnical problems: active lateral earth pressure problem and ultimate bearing capacity problem. The active lateral earth pressure and bearing capacity problems are demonstrated to be equivalent, except for the ease of mathematically manipulation. Based on the slip line theory, the coefficients N_q, N_c, K_{aq} and K_{ac} are derived and the relations among them are established. Two finite difference programs ABC and KA are further used to confirm the validity of the results as derived in the present study. Cheng and Au (2005) have found that iterative analysis is required for normal bearing capacity problem but not for lateral active earth pressure (Cheng 2003). When the retaining wall gradually becomes horizontal and behaves as a bearing capacity problem, it is found that iterative analysis will be necessary for the active pressure program to achieve a good result (similar to slip line analysis of bearing capability problem). Other than the ways in solving Equations (6.1) and (6.2), there are no practical difference between the two classical geotechnical problems, and the two problems can actually be viewed as equivalent problems under the ultimate condition.

It is demonstrated that classical bearing capacity and active lateral earth pressure problems are actually the same, as they are controlled by both the yield and equilibrium equations. Based on the present study, for a normal shallow foundation problem, it can be viewed as a lateral earth pressure problem and vice versa. The surcharge (ultimate bearing capacity) behind an imaginary retaining wall which generate a net upward stresses outside the foundation (or equivalently the retaining wall) will be the ultimate limit state of the system. A bearing capacity problem can hence be viewed as a lateral earth pressure problem in this manner.

The author has demonstrated the lower bound principle in Figure 6.7 using the extremum analysis. Based on the minimum of the extremum from limit equilibrium method, the author has also demonstrated that there are no practical differences between the slope stability problem and the lateral

earth pressure and bearing capacity problems, provided that the extremum from the slope stability analysis is used in the comparisons. Based on the present study, it can be concluded that the three geotechnical problems are practically the same problem – the ultimate condition of the system where the maximum resistance of the system is fully mobilized. In this respect, the three geotechnical problems can be considered as equivalent under the ultimate condition.

It is interesting to note that there are many previous laboratory tests conducted for slopes with surcharge on top as well as bearing capacity problem with inclined ground, as reported in various literature. Actually, the two types of tests are exactly the same, but different researchers prefer to consider the same problem as either slope stability problem or bearing capacity problem. For example, Vesic (1973), Shield et al. (1977) and Graham et al. (1988), Cheng and Au (2005) have considered a bearing capacity problem with an inclined ground by laboratory tests as well as numerical analysis. Empirical correction factors have also been put forward for bearing capacity with inclined ground by Vesic (1973), Meyerhof (1963), Hansen (1970) which are well received by the engineers. On the other hand, the same problem is also termed as slope with a top surcharge by many researchers. For example, Kusakabe et al. (1981), Buhan and Garnier (1988) termed the problem as a slope stability problem but are actually determining the bearing capacity factors in their works. It is also interesting to note that the laboratory slope tests with a top surcharge by Manna et al. (2014) and Li and Cheng (2015) are practically the same as the bearing capacity laboratory bearing capacity tests by Shield et al. (1977). In the limit analysis or slip line analysis of this problem, Graham et al. (1988) and Cheng et al. (2015) have considered only failure mechanism without actually classifying the problem as a bearing capacity or slope stability problem. In the laboratory bearing capacity/slope stability tests by Yoo (2001), the author also does not have a clear distinction between slope stability and bearing capacity problem. Based on these previous works, it is clear that there is not a real difference between the slope stability and bearing capacity problem in literature, which is also illustrated clearly in the present work.

6.9 Conclusion

In the past, there are various applications of plasticity theory, limit equilibrium or limit analysis to various geotechnical stability problems. It is surprising that all the authors treat different geotechnical problem separately while the basic nature of these geotechnical problems is actually governed by the same ultimate requirement. Sokolovskii (1965) has hinted that the three problems are equivalent in nature, but has not actually given the results explicitly to demonstrate the equivalence of the problems. The classical plasticity slip line formulation is actually a lower bound problem where the maximum resistance of a system is fully mobilized. For classical slope stability problem where a *f(x)* is prescribed, the solution is a lower bound to the true collapse state which is clearly illustrated in Figure 6.7 and is also discussed by Cheng et al. (2010). By varying *f(x)* until the maximum resistance of the system is fully mobilized, the corresponding solution is practically equivalent to the plasticity slip line solution. The three classical geotechnical problems can then be unified, and such unification is not surprising because the fundamental principles behind the three problems are exactly the same: equilibrium and yield. By using an extremum limit equilibrium slope stability program, the author has also determined the bearing capacity factors and lateral earth pressure coefficients which are exactly the same as those classical plasticity slip line solutions. The classification of a problem is hence just a matter of convenience instead of the difference in the nature of the problem.

CHAPTER 7 SUMMARY, CONCLUSIONS AND SUGGESTIONS FOR FUTURE WORK

7.1 Summary of main work and contributions

In all the classical textbooks and research works, lateral earth pressure, ultimate bearing capacity and slope stability problems have been treated as independent problems. Based on the project supervisor's previous works, there is a feeling that there are close relations between these three types of problems, as they are both based on the same yield criterion and equilibrium condition. The present study is devoted to the ultimate limit state analysis of these three main geotechnical engineering problems, using discrete element method, plasticity and extremum principle in limit equilibrium formulations. Some of the results are also compared with finite element and laboratory tests for verification. Many important and new results are obtained from the present study, and some of these results are both innovative and new and have useful contributions to the better understanding about the ultimate limit state and the failure mechanism of these three classical geotechnical engineering problems.

The summary of works is grouped under four main areas as below.

(1) Slip-line method, adaptive finite element limit analysis and discrete element analysis are used to study the bearing capacity problem of a shallow foundation in Chapter 3 and to investigate the shear failure development from elastic condition to plastic condition, then extend to large displacement condition. The large scale failure mechanism and movement of soil in the bearing capacity problem of a strip footing are also studied. The numerical results obtained by the discrete element method based particle flow analysis are then compared with the plasticity solution, the slip-line method as well as the laboratory tests.

The contributions of this part have shown that there are noticeable differences between the continuum and discontinuum analyses, and the well-known log-spiral transition zone is not apparent in both the discrete element approach as well as the laboratory tests. With the increase in the friction angle of soil, the transition zone is becoming more a wedge zone than a log-spiral zone as found from the present study. In this respect, the initial state of a system does affect the ultimate condition which is neglected in the ultimate limit analysis.

(2) Discrete element method and slip line method are adopted to analyze the retaining wall lateral pressure behavior of soil in Chapter 4 under different boundary conditions and friction angles between a wall and soil particles. The large displacement failure mechanism and movement of soil with the lateral earth pressure of a backfill is further investigated, and the influence of the micro-parameters on the lateral earth pressure of soil is also observed. The numerical results obtained are then compared with the classical methods as well as the slip-line method and laboratory tests.

(3) For classical limit equilibrium method, some assumptions are required in order to solve for the problem. At the maximum extremum condition, it is found that there is no difference between the use of external and internal variables in specifying a problem. The use of the internal variables is preferable over the use of the boundary variables as the imposition of the acceptability of the internal forces can be easily enforced. The classical limit equilibrium methods with a prescribed internal/external force assumption is also demonstrated to be a lower bound to the ultimate condition. The maximum extremum of the system from LEM is also indicated to be equivalent to the slip line solution in Chapter 5.

(4) Based on the method of characteristics, the equivalence between the classical lateral earth pressure and bearing capacity problem is demonstrated in Chapter 6. The equivalence between the lateral earth pressure problem and slope stability problem is then illustrated by the use of extremum principle. Based on these results, it can be concluded that the three classical problems are equivalent

in the basic principles in terms of the failure mechanism under the ultimate limit state of the system, and each problem can be viewed as the inverse of the other problems.

The most important contribution of this study is to demonstrate the equivalence between bearing capacity, lateral earth pressure and slope stability problems by slip line method and extremum limit equilibrium methods in terms of the failure mechanism under the ultimate condition of the system. Through the method of characteristics, K_{ac}, K_{aq} and $K_{p\gamma}$ are demonstrated to be related to N_c, N_q and N_γ, so these two problems can be unified, and each problem can be viewed as the inverse of the other problem. The extremum principle is also applied to demonstrate the equivalence between the lateral active pressure, bearing capacity and slope stability problems. These three problems can be considered as equivalent in the basic principles, and the classification of a problem is simply a matter of convenience. This work is an interesting and useful compliment of the classical geotechnical analysis.

7.2 Conclusions

The conclusions of the present study can be summarized as follows:

(1) For the elasticity analysis of the bearing capacity problem, the general behaviors of soil particles analyzed by Discrete Element Method match well with that from the theoretical elasticity method. For the plastic condition, the slip-line method differs from the adaptive finite element limit analysis if the unit weight of soil is considered, else, the results from the two different methods will be similar. For the slip line method, a triangular bearing pressure is predicted from the solution of the slip line equations which is based on the assumption of zero external surcharge as the boundary condition. On the other hand, the adaptive finite element limit analysis imposes a uniform bearing pressure as the

boundary condition which is however a back-computed result from the slip line solution. This is the reason for the difference in the bearing pressure from the two different methods of analysis.

(2) The progressive failure progress of the bearing capacity problem is studied and can be concluded as follows: as the uniform loading is applied to the footing acting on the soil, firstly there is a small disturbed area under the footing, then plastic area is extended showing clearer view of Plastic Zone I and Zone II, and finally Zone III appears. Next, shear failure surface becomes continuous, followed by upheaval on ground surface. As the settlement keep increasing, plastic zones extend to the surrounding area, so that secondary failure surface occurs and multiple failure zones show up, and the plastic failure transfers to a larger disturbed area followed by further upheaval. Such results are also compatible to the various model test results as published in literature.

(3) For the case of uniform loading on shallow foundation for dense sands, elastic footing settlement takes place in the very beginning, inducing compression to soil particle to overcome the interlocking effect and resulting in soil mass volume increase as well as increase in the porosity (shear dilatancy effect). As the loading increases, that will be followed by slipping (shear failure), volume expansion and upheaval on the ground surface.

(4) The log-spiral zone is found to be distorted in the slip line analysis but not the finite element limit analysis when the weight of soil is important, but else log-spiral will be the rigorous solution from these two methods. It is also found that the classical log-spiral failure zone for the bearing capacity problem is not found from the DEM analysis (no matter weight of soil is important or not) as well as from some of the published model test results or the in-house laboratory tests. From the DEM analysis and limited laboratory tests, the log-spiral zone appears to be replaced by a wedge failure zone. The classical plasticity formulation which neglects the stress-strain relation as well as the initial insitu stress condition is found to be not able to fully reflect the behavior of soil. Nevertheless, the log-spiral failure mechanism still appears to be a good approximation in general.

(5) For the lateral pressure behavior of soil under different boundary conditions and interior and exterior friction of soil and retaining wall, different modes of wall movement result in different earth pressure distributions. The larger the displacement of the retaining wall toward the soil mass, the greater will be resultant force of the earth pressure. The larger displacement of the wall moves away from the soil mass, the smaller will be the total earth pressure. For the large displacement failure mechanism and movement of soil with the lateral earth pressure of a backfill, among these three active modes, active T mode gives the largest and active RB obtains the smallest with regard to the area of shear failure zone. As the mobilization of shear strength in soils is proportional to the area of failure zone, the smallest active pressure occurs in active T mode , while active RB mode has the highest active pressure. In the passive cases, as the soils near the retaining wall is under compression, a dilatancy characteristic of the dense soils is exhibited.

(6) The position of the earth pressure is diverse in different displacement modes of the retaining wall under the numerical discrete element analysis. The point of the resultant of the active T mode slightly differs from the position of Coulomb theory 0.33H (also the slip-line plasticity theory). For the active RB mode, the position of resultant force is lower than that of the classical theory, while the resultant force in the active RT mode is located at a higher position than that of the plasticity theory.

(7) The active earth pressure coefficient Ka increases with increasing particle size in the small strain state, while the larger particle size led to the lower passive coefficient Kp. The increasing inter-particle stiffness decreases the active earth pressure coefficient Ka and increased the passive coefficient Kp. However the obvious difference becomes inconspicuous among the three cases of mean grain size of soil when the critical state is reached, even to the residual state when large displacement is considered.

(8) The comparison of active and passive lateral pressure and failure patterns under different wall movement modes by DEM and slip line method has shown that the areas of the curved failure wedge obtained from the two methods are similar to each other, but the ideal Rankine zones from the

slip line method are always larger than that from PFC2D. In the ideal Rankine zones generated by PFC2D, the upper edge of the zones is relatively steeper and closer towards the wall. This demonstrated that failure zones by PFC2D fell within the expected failure zones by the slip line method with only slight difference at the upper edge part of backfill.

(9) It is well known that limit equilibrium method requires assumptions for the solution. The unknowns can be specified on the boundary of the slip surface or inside the soil mass, and there is no theoretical ground for the choice of variables up to the present. Booker and Zheng (2013) prefer the use of external variables simply because of the mathematical manipulation, but they never give the physical ground for the use of external variables formulation. On the other hand, the use of internal variables formulation is adopted for most of the slope stability problems in literature, and the reason also appears to be simply due to the mathematical convenience. Even though a limit equilibrium problem can be formulated in various ways (slope stability analysis, trial wedge or similar) giving different results for the analyses, it is found from the present study that there will be no difference between different formulations if the ultimate condition is considered. The classical bearing capacity problem has been used for illustration, where the slip line solution is available. Since the stresses are determinate for this problem, all the internal or external variables at the ultimate condition could be evaluated. The problem is then reconsidered by taking f(x) as the control variables in the limit equilibrium and determining the maximum extremum. The use of the interslice force function f(x), the thrust line or the base normal forces should provide an equivalent concept at the ultimate/failure state. The well-known bearing capacity solutions are used to determine f(x), the thrust line and the base normal forces for a ‘‘horizontal slope’’. It is demonstrated the equivalence between the different formulations under the ultimate condition of the system. It is also shown that if only that the ultimate state is considered, it is not important which forces are used in the stability formulation, either external boundary forces or internal forces. It is also presented that the slip-line solution using a classical bearing capacity problem is equivalent to the maximum extremum from the limit equilibrium analysis.

Furthermore, it is also demonstrated that the classical slope stability formulation is a lower bound to the true failure solution, as only a consistent set of internal forces are specified. For the true failure state, the full strength of the system has to be mobilized, and any set of specified consistent internal stresses will only be a lower bound of the true solution which is clearly illustrated in the present study.

(10) The classical bearing capacity and active lateral earth pressure problems are similar to each other, as they are controlled by the same yield and equilibrium equations. For a normal shallow foundation problem, it is proved in the present study that it can be viewed as a lateral earth pressure problem and vice versa. The surcharge (ultimate bearing capacity) behind an imaginary retaining wall which generate a net upward stresses outside the foundation (or equivalently the retaining wall) will be the ultimate limit state of the system. A bearing capacity problem can hence be viewed as a lateral earth pressure problem in this manner.

(11) Based on the minimum of the extremum from limit equilibrium method, it is also demonstrated that there are no practical differences between the slope stability problem and the lateral earth pressure and bearing capacity problems, provided that the extremum from the slope stability analysis is used in the comparisons. The three geotechnical problems are hence practically the same problem – the ultimate condition of the system where the maximum resistance of the system is fully mobilized. In this respect, the three geotechnical problems can be considered as equivalent under the ultimate condition. Just imagine oneself to be soil, the majority of the soil mass will be faced with the yield and movement, and they never know the present of retaining wall or foundation. The meaning of the wall or foundation will just be boundary condition to the soil particles, but other than that, the soil particles never know the existence of a wall or foundation. If we view from the standpoint of soil, lateral earth pressure, bearing capacity or slope stability problem are the same, as the soil particles are stressed to the state that a full failure mechanism is formed.

7.3 Recommendations and suggestions for the future work

Although the present works have studied the ultimate limit state in details, there are still many limitations and rooms for improvements, which can be suggested for the further works. Some of the more important recommendations are suggested in the following sections.

7.3.1 Three-dimensional analysis of bearing capacity problem for square and rectangular footings

Evaluation of the 3D bearing capacity of shallow foundations is usually assessed by introducing experimental and empirical shape factors into the ordinary 2D equations for the strip footings developed by researchers such as Meyerhof (1963), Terzaghi and Peck (1967), Hansen (1970), de Beer (1970), Vesic (973), and the others. These empirical shape factors are commonly based on the test results obtained from works of Golder (1941) and also some additional unpublished data. For the future study, three-dimensional analysis is worthy to be carried out to study the bearing capacity factors for square and rectangular footings by Finite Element Limit Analysis with automatic mesh adaptation, Finite Difference Method and Distinct Element Method.

Due to differences or even inconsistencies of the empirical shape factors, these shape factors need to be obtained from a realistic analysis. Therefore, three dimensional bearing capacity problem still require more experimental and theoretical research activities in the analysis.

The first three-dimensional collapse mechanism for punch indentation problems was presented by Shield and Drucker (1953) on a perfectly plastic and purely cohesive material which is clays in undrained conditions. Shield and Drucker (1953) presented a theoretical evaluation of 3D bearing capacity of rectangular foundations on homogeneous clay ($\varphi = 0$) by means of upper and lower bound solutions. Theoretical analyses of bearing capacity have also made use of Kötter's equation with a rigid perfectly plastic soil response assumption (Shield 1955, Cox et al. 1961). Nakase (1981) used an

ordinary limit equilibrium method and assumed cylindrical sliding surfaces for rectangular footings on normally consolidated clays, of which strength increases linearly with depth. Ugai (1985) introduced more rigorous solutions for rectangular foundations laid on NC clays by means of limit analysis, and also improved the admissible velocity field originally proposed by Shield and Drucker (1953), by including the effect of the footing base roughness. Narita and Yamaguchi (1992), presented a three dimensional analysis of bearing capacity of rectangular foundations by means of the method of slices, assuming that sliding surfaces are composed of a set of log-spirals with different initial radii in the direction of the longer axis of the footing base.

Michalowski (2001) proposed a 3D analysis of rectangular foundations based on limit analysis (upper-bound) approach, in which all the failure mechanism considered in the analysis consisted of four regions, each characterized by plane deformations. Then, Michalowski and Dawson (2002) compared the results of their proposed upper bound method with the numerical results of FLAC3D code. Also, Zhu and Michalowski (2005) calculated shape factors for square and rectangular footings based on the upper bound method they proposed, and compared them with finite element analysis results.

Lyamin et al. (2007) calculated rigorously the bearing capacity of strip, square, circular and rectangular foundations in sand, based on finite element limit analysis. Majidi et al. (2011) treated soil mass as discrete blocks connected with Winkler springs in three Dimension, to obtain bearing capacity of rectangular shallow foundations and the optimum shape of failure surface beneath the foundation, similar to the method which Shi (2001) presented for a rock block system called Discontinuous Deformation Analysis (DDA) in three Dimension. Takano et al. (2012) apply X-ray CT scanning techniques to nondestructively visualize and investigate the soil behavior and 3D bearing capacity mechanism for loaded shallow foundations.

The research plan in this topic is as follows:

(1) Distinct Element Analysis is carried out using PFC3D to get failure mechanism of bearing capacity problem on square footing in three-dimension. The regular packing soil particles in DEM are generated to obtain progressive failure of bearing capacity problem. Then the numerical results of DEM can be qualitatively compared with Michalowski (2001)'s 3D failure mechanism.

(2) 3D Finite Element Limit Analysis is applied to get bearing capacity factor N_γ for square and rectangular footings to use hand-made mesh adaptation to get precise mesh in original mesh generation. The Mohr-Coulomb yield criterion is used in three-dimensional study by FELA.

(3) Michalowski (2001) assumed log-spiral failure surface for N_c, N_q and N_γ cases of bearing capacity problems. The validity of the failure surface for N_γ case being log-spiral is not verified, which is experimented by many researchers. However, it is difficult to calculate the three-dimensional analysis and to generate 3D domain which requires too many variables. This work will be important for the better understanding of more realistic engineering problems.

7.3.2 Development of lower bound/extremum principle for three-dimensional analysis by global optimization method

The lower bound/extremum principle for three-dimensional analysis by global optimization method is never attempted by any researchers up to the present. Three-dimensional equilibrium differential equations and/or the yield criterion can be re-formulated to a discretized format. Under the new equilibrium equations, the internal forces will be the control variables while the yield criterion will become the constraints in the optimization analysis. A problem will then be classified as bearing capacity, lateral earth pressure or slope stability problem according to the boundary condition and geometry. The discretization will be in form of complete and semi discretization. For normal engineering problem, a semi discretization scheme will be adopted and less than 50 zones will be

formed in the analysis. The yield criterion will be checked at the sides of the relatively large domain. For the complete discretization which is more suitable for highly complicated problem, over thousands of sub-domains are formed, and the local yielding instead of the global yielding along a longer side will be checked.

The equilibrium equations will be re-written in discretized format and the internal forces between discretized zones will be the control variables while the yield criterion will become the constraints in the optimization analysis. This work will be the extension of the works by Cheng (2010a, 2011b), and the work is laid on the foundation of equivalent form of variational principle. Towards this, the author proposes a double looping method in the optimization analysis. In the first loop, a crude and approximate solution is evaluated by those stochastic methods which have been adopted by Cheng previously. As the yield criterion is only a constraint in the present method, local refinement of the solution domain will then proceed according to the initial results if the yield condition is approached. The outer loop of the analysis will start from the initial solution with a combination of gradient type method and heuristic method. The whole concept of the solution is : accuracy and time of solution have to be maintained at an acceptable limit. The classical finite element approach lower bound method is extremely time-consuming in the optimization analysis, and the number of control variables can exceed 100000 easily which will create the problem of multiple local minima. The zones in the present formulation will be much larger than the classical finite element approach to save the time in analysis, and the concept of zone is actually slice as used in the classical limit equilibrium method. After the completion of this work, the results will be compared with that from finite element analysis. The proposed method should yield a solution very close to that from the limit equilibrium strength reduction method, and the internal force distribution from the two different approaches will be assessed to demonstrate the equivalence between the equivalent discretized variational approach and the finite element approach (finite element is also based on the variational principle). This work will be particularly useful to in geotechnical engineering, as it provides an alternative to determine the

ultimate limit state for which finite element may sometimes come into difficulty (as experienced by the author in various works as given above).

REFERENCES

AbdelAziz Ahmed Ali senoon (2013), Passive earth pressure against retaining wall using log-spiral curve, Journal of Engineering Sciences, Assiut University, Vol. 41 No1.

Abramson L.W., Lee T.S., Sharma S. and Boyce G.M. (2002), Slope Stability and Stabilization Methods, 2nd edition, John Wiley, USA.

Atkinson J.H. (1981), Foundations and Slopes: An Introduction to Applications of Critical State Soil Mechanics, McGraw-Hill, Berkshire.

Baker R. and Garber M. (1978), Theoretical Analysis of the Stability of Slopes, Geotechnique, 28:395-341.

Baker R (1980), Determination of the critical slip surface in slope stability computations, International Journal of Numerical and Analytical Methods in Geomechanics, 4:333-359.

Baker R., (1981), Tensile strength, tension cracks, and stability of slopes, Soils and Foundation, Vol. 21, No. 2, pp. 1-17.

Baker R. (2003), Sufficient conditions for existence of physically significant solutions in limiting equilibrium slope stability analysis, International Journal of Solids and Structures, vol.40(13-14), 3717-3735.

Baker R. (2005), Variational slope stability analysis of materials with non-linear failure criterion, Electronic Journal of Geotechnical Engineering. Volume 10, Bundle A.

Bang S. (1985), Active earth pressure behind retaining walls. Journal of Geotechnical Engineering, 407-412.

Bhatia S.K. and Bakeer R.M. (1989), Use of the finite element method in modeling a static earth pressure problem. Int. J.Numer.Anal. Methods Geomech. 13, 207–213

Bolton M.D. and Lau C.K. (1993), Vertical bearing capacity factors for circular and strip footings on Mohr-Coulomb soil, Canadian Geotechnical Journal, 30(4):1024–1033.

Booker J.R., Zheng X. (2000), Application of the theory of classical plasticity to the analysis of the stress distribution in wedges of a perfectly frictional material, Modelling in Geomechanics, John Wiley, New York.

Bros B. (1972), The influence of model retaining wall displacements on active and passive earth pressure in sand. In: Proceedings of the 5th European Conference on Soil Mechanics, vol. 1, pp. 241–249

Buhan P. De and Garnier D. (1988), Three dimensional bearing capacity analysis of a foundation near a slope, Soils and Foundations, 38(3):153-163.

Calvetti F. (2008), Discrete modelling of granular materials and geotechnical problems, European Journal of Environmental and Civil Engineering, 12, 951-965.

Caquot A. and Kerisel J. (1953), Sue le terme de surface dans le calcul des foundations en milieu pulvelent, Proc. III Int. Conf. Mech. Found. Eng., Vol.1:336-337.

Caquot A. and Kerisel J. (1966), Traite de Mecanique des Sols. Paris: Gauthier-Villars.

Cascone E and Casablanca O. (2016), Static and seismic bearing capacity of shallow strip footings, Soil Dynamics and Earthquake Engineering, 84:204-223.

Cassidy M.J. and Houlsby G.T. (2002), Vertical bearing capacity factors for conical footings on sand, Geotechnique 52(9):687-692.

Caquot A. (1934), Equilibre des massifs a` frottement interne, Stabilite´ des terres pulve´rulents et cohe´rents, Gauthier-Villars, Paris.

Chen W.F. (1975), Limit analysis and soil plasticity, Amsterdam: Elsevier Scientific Publishing Company.

Chen W.F. and Liu X.L. (1990), Limit analysis in soil mechanics, New York: Elsevier

Chen Z.Y. and Morgenstern N.R. (1983), Extensions to generalized method of slices for stability analysis, Canadian Geotechnical Journal, 20(1), 104–109.

Chen Z.Y. (1998), On Pan's principles of rock and soil stability analysis, Journal of Tsinghua University (Sci &Tech), 38, 1–4 (in Chinese).

Chen Z.Y., Wang X.G., Chris Haberfield, Yin J.H. and Wang Y.J. (2001a), A three-dimensional slope stability analysis method using the upper bound theorem part I: theory and methods, International Journal of Rock Mechanics and Mining Sciences, Vol.38, No.3, 369-378.

Chen Z.Y., Wang Y.J., Wang J., Chris Haberfield and Yin J.H. (2001b), A three-dimensional slope stability analysis method using the upper bound theorem part II: numerical approaches, extensions and applications, International Journal of Rock Mechanics and Mining Sciences, Vol.38, No.3, 379-397.

Cheng Y. P., Nakata Y. and Bolton M. D. (2003), Distinct element simulation of crushable soil. Geotechnique, 53(7), 633–641.

Cheng Y.M. (2002), Slip Line Solution and Limit Analysis for Lateral Earth Pressure Problem, the Ninth Conference on Computing in Civil and Building Engineering, April 3-5, Taipei, Taiwan, p.311-314.

Cheng Y.M. (2003a), Locations of Critical Failure Surface and some Further Studies on Slope Stability Analysis, Computers and Geotechnics, 30: 255-267.

Cheng Y.M. (2003b), Seismic lateral earth pressure coefficients for c–φ soils by slip line method. Computers and Geotechnics, 30(8): 661-670.

Cheng Y.M. and Au S.K. (2005), Slip line solution of bearing capacity problems with inclined ground, Canadian Geotechnical Journal, vol.42, 1232-1241.

Cheng Y.M., Hu Y.Y. and Wei W.B. (2007a), General axisymmetric active earth pressure by method of characteristic-theory and numerical formulation, Journal of Geomechanics, ASCE, 7(1): 1-15.

Cheng Y M, Lansivaara T, Wei W B (2007b), Two-dimensional Slope Stability Analysis by Limit Equilibrium and Strength Reduction Methods, Computers and Geotechnics, vol.34, 137-150, 2007.

Cheng Y.M., Lansivaara T. and Siu J. (2008), Impact of Convergence on Slope Stability Analysis and Design, Computers and Geotechnics, 35(1), pp.105-115.

Cheng Y.M., Li L. and Chi S.C. (2008), Determination of critical slip surface using artificial fish swarms algorithm, Journal of Geotechnical and Geoenvironmental Engineering, ASCE, 134(2):244-251.

Cheng Y.M., Liu Z. N., Song W.D., Au S.K. (2009), Laboratory test and Particle Flow Simulation of Silos problem with nonhomogeneous materials, Journal of Geotechnical and Geoenvironmental Engineering, ASCE, 135, 1754-1761.

Cheng Y.M., Chau K.T., Xiao L.J. and Li N. (2010a), Flow pattern for silo with two layers of materials with single and double openings, Journal of Geotechnical and Geoenvironmental Engineering, ASCE, 136(9), 1278:1286.

Cheng Y.M., Zhao Z.H., Sun Y.J. (2010b), Evaluation of interslice force function and discussion on convergence in slope stability analysis by the lower bound method, Journal of Geotechnical and Geoenvironmental Engineering, ASCE, 136(8):1103-1113.

Cheng Y.M., Li L., Fang S.S. (2011a), Improved harmony search methods to replace variational principle in geotechnical problems, Journal of Mechanics, 27(1):107-119.

Cheng Y.M., Li D.Z., Li L., Sun Y.J., Baker R. and Yang Y. (2011b), Limit equilibrium method based on approximate lower bound method with variable factor of safety that can con-sider residual strength, Computers and Geotechnics, 38: 628-637.

Cheng Y.M., Lansivaara T., Baker R. and Li N. (2013a), The use of internal and external variables and extremum principle in limit equilibrium formulations with application to bearing capacity and slope stability problems, Soils and Foundation, 53(1), 130–143.

Cheng Y.M., Li D.Z., Li N., Lee Y.Y. and Au S.K. (2013b), Solution of some engineering partial differential equations governed by the minimal of a functional by global optimization method, Journal of Mechanics, 29(3), 493-506.

Cheng Y.M. and Lau C.K. (2014), Soil Slope stability analysis and stabilization – new methods and insights, 2nd edition, Spon Press.

Cheng Y.M., Li N. and Yang X.Q. (2015), Three Dimensional Slope Stability Problem with a Surcharge Load, Natural Hazards and Earth System Sciences, 15(10), 2227-2240.

Clayton C., Woods R., Bond A. and Milititsky J. (2013), Earth pressure and earth-retaining structures. London: CRC Press.

Clough G.W. and Duncan J.M. (1971), Finite element analysis of retaining wall behavior, J. Geotech. Eng. (ASCE) 97(12), 1657–1673

Craig R. (2004), CRAIG'S SOIL MECHANICS. London: Spon Press.

Conte E., Donato A., Troncone A. (2013), Progressive failure analysis of shallow foundations on soils with strain-softening behavior, Computers and Geotechnics, vol.54, 117-124.

Coulomb C.A. (1776), Essai sur une application des regles des maximis et minimis a quelques problemes de statique relatifs a l'architecture. Memoires de l'Academie Royale pres Divers Savants, vol. 7, pp. 343–387 (in French).

Cundall P.A. (1974), Rational Design of Tunnel Supports: A Computer Model for Rock Mass Behavior Using Interactive Graphics for the Input and Output of Geometrical Data.

Cundall P.A. and Strack O.D.L. (1979), A discrete model for granular assemblies, Geotechnique 29(1):47-65.

Das B. (2007), Principles of Foundation Engineering. Cengage Learning.

Davis R.O. and Selvadurai A.P.S. (2002), Plasticity and Geomechanics, Cambridge University Press.

De Jong G. and Josselin D. (1957), Graphical methodfor the determination of slip-line fields in soil mechanics. De Ingenieur, 69(29): 61-65.

Donald I.B. and Chen Z.Y. (1997), Slope stability analysis by the upper bound approach: fundamentals and methods. Canadian Geotechnical Journal, 34(6), 853-862.

Drescher A. and Detournay E. (1993), Limit load in translational failure mechanisms for associative and non-associative materials. Geotechnique, London, 43(3), 443–456.

Drucker D.C., Greenberg H.J. and Prager W. (1952), Extended limit design theorems for continuous media. Quarterly of Applied Mathematics, 9, 381-389.

Drucker D.C., and Prager W. (1952), Soil mechanics and plastic analysis or limit design. Quarterly of Applied Mathematics, 10, 157-165.

Drucker D.C. (1953), Limit analysis of two- and three-dimensional soil mechanics problems, Journal of the Mechanics and Physics of Solids, 1(14), 217-226.

Eberhardt and Erik (2003), Rock Slope Stability Analysis - Utilization of Advanced Numerical Techniques, Vancouver, Canada: Earth and Ocean Sciences, University of British Columbia.

Elchiti Imad, Saad George, Najjar Shadi and Nasreddine Nader (2017), Investigation of Active Soil Pressures on Retaining Walls Using Finite Element Analyses, Geotechnical Frontiers 2017 GSP 278, 159-169.

Fan K., Fredlund D.G. and Wilson G.W. (1986), An interslice force function for limit equilibrium slope stability analysis, Canadian Geotechnical Journal, 23(3), 287–296.

Fang Y.S. and Ishibashi I. (1986), Static earth pressure with various wall movements, J. Geotech. Eng (ASCE) 112(3), 317–333

Fang Y.S., Chen T.J. and Wu B.F. (1994), Passive earth pressure with various wall movements, J. Geotech. Eng. (ASCE) 120(8), 1307–1323.

Fang Y.S., Ho Y.C. and Chen T.J. (2002), Passive earth pressure with critical state concept, J. Geotech. Eng. (ASCE) 128(8), 651– 659.

Frydman S. and Burd H.J. (1997), Numerical studies of bearing-capacity factor N-gamma. Journal of Geotechnical and Geoenvironmental Engineering, 123(1): 20-29.

Gabrielia F., Cola S. and Calvetti F. (2009), Use of an up-scaled DEM model for analysing the behaviour of a shallow foundation on a model slope, Geomechanics and Geoengineering, 4 (2), 109–122.

Geotechnical Engineering Office (1990), Review of design methods for excavations. Hong Kong: GCO.

Graham, J., Andrew, M., Shields, D.H. (1988), Stress characteristics for shallow footing in cohesionless slopes. Canadian Geotechnical Journal 25 (2), 238–249.

Griffiths D.V. (1982), Computation of Bearing Capacity Factors Using Finite-Elements. Geotechnique, 32(3): 195-202.

Griffiths G.V., Fenton G.A. and Ziemann H.R. (2008), Reliability of Passive earth pressure, Georisk, 2(2), 113-121.

Gvozdev A.A. (1960), The determination of the value of the collapse load for statically indeterminate systems undergoing plastic deformation. International Journal of Mechanical Sciences, 1, 322.

Hamidi P., Akhlaghi T. and Bonab Hajialilou (2017), Active earth pressure in cohesive-frictional soils using FEM and optitmization, Int. J. Optim. Civil Eng., 7(2):257-267

Hansen J.B. (1961), A general formula for bearing capacity, Bull. Dan. Geotech. Inst ., 11: 38–46.

Hansen J.B. (1970), A revised and extended formula for bearing capacity, Danish Geotechnical Institute, Bulletin 28, Copenhagen.

Han D.D., Xie Z.Y., Zheng L.W. and Huang L (2016), The bearing capacity factor Nγ of strip footings on c–φ–γ soil using the method of characteristics, SpringerPlus (2016) 5:1482

Hazzard J.F., Maxwell S.C. and Young R.P., (1998), Micromechanical Modelling of Acoustic Emissions in Proceedings of ISRM/SPE Rock Mechanics is Petroleum Engineering, Eurock 98, Trondheim, Norway, pp 519-526, SPE 47320.

Hjiaj M., Lyamin A. V. and Sloan S. W. (2005), Numerical limit analysis solutions for the bearing capacity factor N-gamma, International Journal of Solids and Structures, 42(5-6), 1681-1704.

Hill R. (1950), The mathematical Theory of Plasticity. London: Oxford University Press.

Horner D. A., Peters J. and Carrillo A. R. (2001), Large scale discrete element modeling of vehicle-soil interaction, ASCE Journal of Engineering Mechanics, 127 (10), 1027–1032.

Itasca (1999), PFC2D/3D – Particle Flow Code in 2 Dimensions, Itasca Consulting Group Inc., Minneapolis.

Itasca (2000), UDEC – Universal Distinct Element Code (Version 3.1), Itasca Consulting Group Inc., Minneapolis.

Itasca (2004), Particle Flow Code in 2 Dimensions Version 3.1. (I.C.Group, Ed.) Minneapolis.

Itasca (2008). PFC3D 4.0 Particle Flow Code in Three Dimensions, Theory and Implementation Volume. Minneapolis, Minnesota.

Janbu N. (1957), Earth Pressures and Bearing Capacity Calculations by Generalized Procedure of Slices, Proceedings of the 4th International Conference Soil Foundation In Mechanical Engineering. Vol. 2, pp 207–212.

Janbu N. (1973), Slope stability computations, in: R.C. Hirschfield and S.J. Poulos (eds.), Embankment-Dam Engineering, pp. 47–86, John Wiley.

Jenck O., Dias D. and Kastner R. (2009), Discrete element modeling of a granular platform supported by piles in soft soil validation on a small scale model test and comparison to a numerical analysis in a continuum, Computers and Geotechnics, 36, 917–927.

Jiang M., He J., Wang J., Liu F. and Zhang W. (2014), Distinct simulation of earth pressure against a rigid retaining wall considering inter-particle rolling resistance in sandy backfill, Granular Matter, 16 (5), 797-814.

Kammoun Z., Pastor F., Smaoui H., and Pastor J. (2010), Large static problem in numerical limit analysis: A decomposition approach, International Journal for Numerical and Analytical Methods in Geomechanics, 34(18), 1960-1980.

Kerisel J. and Absi E. (1990), Active and Passive Earth Pressure tables, A.A. Ba1kema.

Kötter F. (1903), Die bestimmung des druckes an gekrummten gleitflachen, eine Aufgabe aus der Lehre vom eriddruck. Sizungsberichte der Akademie der Wissenschaften. City: Berlin, pp. 229-233.

Krabbenhoft K., Lyamin A. V., Hjiaj M., and Sloan S. W. (2005), A new discontinuous upper bound limit analysis formulation, International Journal for Numerical Methods in Engineering, 63(7), 1069-1088.

Kumar J. (2001), Seismic passive earth pressure coefficients for sands, Canadian Geotechnical Journal, 38, 876–81.

Kumar J. and Mohan Rao VBK. (2002), Seismic bearing capacity factors for spread foundations, Géotechnique, 52(2):79-88.

Kumar J. and Chitikela S. (2002), Seismic passive earth pressure coefficients using the method of characteristics, Canadian Geotechnical Journal, 39: 463-471.

Kumar J. (2003), N_γ for rough strip footing using the method of characteristics, Canadian Geotechnical Journal, 40(3):669–674.

Kumar J. and Khatri V. N. (2011), Bearing capacity factors of circular foundations for a general c-phi soil using lower bound finite elements limit analysis, International Journal for Numerical and Analytical Methods in Geomechanics, 35(3), 393-405.

Kusakabe O., Kimura T. and Yamaguchi U. (1981), Bearing capacity of slopes under strip loads on the top surfaces, Soils and Foundations, 21(4): 29-40.

Liang R.Y., Zhao J. and Vitton S.J. (1997), Determination of Interslice Forces in Slope Stability Analysis, Journal of Soils and Foundations, Japanese Geotechnical Society, Vol. 37, No. 1, pp. 65-72.

Li D.Z. (2014), Lower and upper bound limit analyses for stability problems in geotechnical engineering, PhD Thesis, Hong Kong Polytechnic University.

Li N. and Cheng Y.M. (2015), Laboratory and 3D-Distinct Element Analysis of Failure Mechanism of Slope under External Surcharge, Natural Hazards and Earth System Sciences, 15, 35-43, 2015

LimitState (2015), LimitState Geo Manual 3.2d, LimitState Ltd.

Liu F.Q., Wang J.H. and Zhang L.L. (2009a), Axi-symmetric active earth pressure obtained by the slip line method with a general tangential stress coefficient, Computers and Geotechnics, 36, No. 1–2, 352–358.

Liu F.Q., Wang J.H. and Zhang L.L. (2009b), Analytical solution of general axisymmetric active earth pressure, International Journal for Numerical and Analytical Methods in Geomechanics, 33, No. 4, 551–565.

Liu F.Q. (2014), Lateral earth pressures acting on circular retaining walls, International Journal of Geomechanics, 14, No. 3, 04014002.

Loukidis D. and Salgado R. (2013), Active earth thrust on walls supporting granular soils: effect of wall movement, Proceedings of the 18th International Conference on Soil Mechanics and Geotechnical Engineering, Paris, 2043-2046.

Lu M. and McDowell G.R. (2010), Discrete element modelling of railway ballast under monotonic and cyclic triaxial loading, Geotechnique, 60, 459-467.

Lyamin A.V. and Salgado R (2007), Two- and three-dimensional bearing capacity of footings in sand, Geotechnique 57(8), 647–662.

Majidi A. R., Mirghasemi A. A. and Arabshahi M. (2011), Three dimensional bearing capacity analysis of shallow foundations using discrete element method, International Journal of Civil Engineering, Vol. 9, No. 4.

Manna B., Rawat S., Zodinpuii R. Sharma K.G. (2014), Effect of Surcharge Load on Stability of Slopes - Testing and Analysis, EJGE, vol.19, 3397-3410.

Manoharan N. and Dasgupta S.P. (1995), Bearing capacity of surface footings by finite elements, Computers and Structures, 54 (4), pp. 563–586.

Martin C.M. (2004), User Guide for ABC – Analysis of Bearing Capacity (v1.0), Department of Engineering Science, University of Oxford.

Martin C.M. (2004), Discussion of "Calculations of bearing capacity factors N_γ using numerical limit analyses" by B. Ukritchon, A.J. Whittle and C. Klangvijit, Journal of Geotechnical and Geoenvironmental Engineering, ASCE, 130(10):1106-1107.

Martin CM (2005), Exact bearing capacity calculations using the method of characteristics, Proc. 11th Int. Conf. IACMAG, Turin, vol. 4: 441-450.

Matsuo M., Kenmochi S. and Yagi H. (1978), Experimental study on earth pressure of retaining wall by field test. Soils Found. 18(3), 27–41.

Matsuzawa H. and Hazarika H. (1996), Analyses of active earth pressure against rigid retaining walls subjected to different modes of movement. Soils Found. 36(3), 51–65.

Matteotti G. (1970), Some results of quay-wall model tests on earth pressure. Proc. Inst. Civ. Eng. Lond. 47, 184–204.

Maynar M. and Rodríguez L. (2005), Discrete Numerical Model for Analysis of Earth Pressure Balance Tunnel Excavation. Journal of Geotechnical and Geoenvironmental Engineering, 1234-1242.

Mei G., Chen Q., and Song L. (2009), Model for predicting displacement-dependent lateral earth pressure. Journal of Geotechnical Engineering, 969-975.

Meyerhof G.G. (1951), The ultimate bearing capacity of foundations, Geotechnique, 2: 301-332.

Meyerhof G.G. (1963), Some recent research on the bearing capacity of foundations, Canadian Geotechnical Journal,1(1): 16-26.

Michalowski R.L. (1989), 3-dimensional analysis of locally loaded slopes. Geotechnique, 39(1), 27-38.

Michalowski R.L. (1995), Slope stability analysis: A kinematical approach. Geotechnique, London, 45(2), 283–293.

Michalowski R.L. (1997), An estimate of the influence of soil weight on bearing capacity using limit analysis. Soils and Found., Tokyo,37(4), 57–64.

Michalowski R. L. (2001), Upper-bound load estimates on square and rectangular footings, Geotechnique, 51(9), 787-798.

Michalowski R.L. and Dawson E.M. (2002), Three dimensional analysis of limit loads on Mohr-Coulomb soil, Foundation of Civil and Environmental Engineering, no.1, 2002, 137-147.

Morgenstern N.R. and Price V.E. (1965), The analysis of stability of general slip surface, Geotechnique, 15(1), 79–93.

Morgenstern N.R. (1992), The Evaluation of Slope Stability – A 25 Year Perspective, Stability and Performance of Slopes and Embankments –II, Geotechnical Special Publication No. 31, ASCE.

Mwebesa J.M., Kalumba D. and Kulabako R. (2012), Simulating Bearing Capacity Failure of Surface Loading on Sand Using COMSOL, Second International Conference on Advances in Engineering and Technology, 409-415.

Novotortsev V.I. (1938), Application of the theroy of plasticity to problems of determining the bearing capacity of building foundation. Izv., VNIG, 22.

O'Sullivan C. (2011a), Particle‐Based Discrete Element Modeling: Geomechanics Perspective, International Journal of Geomechanics, 11, 449-464.

O'Sullivan C. (2011b), Particulate Discrete Element Modelling: A Geomechanics Perspectives, Spon Press.

Osman Emad (1990), Experimental, theoretical and finite element analysis of a reinforced earth retaining wall including compaction and construction process, PhD Thesis, University of Glasgow.

Ouria A. and Sepehr S. (2015), Active Earth Pressure on Retaining Wall Rotating About Top. Internaltional Journal of Geology, 1-5.

Ozawa Y. and Duncan J.M. (1976), Elasto-plastic finite element analyses of sand deformations, In: Proceedings of 2nd International Conference on Numerical Methods in Geomechanics, Blacksburg, USA, pp. 243–263.

Pathmanathan R. (2006), Numerical modelling of seismic behaviour of earth-retaining walls, Istituto Universitario di Studi Superiori.

Peng M. X. and Chen J. (2013), Slip-line solution to active earth pressure on retaining walls, Geotechnique, 63, No. 12, 1008–1019.

Prandtl L. (1920), Über die Härte plastischer Körper. Göttingen Nachr. Math. Phys. K1., 12, 74-85.

Potts D.M. and Fourie A.B. (1984) The behaviour of a propped retaining wall: results of a numerical experiment, Geotechnique, 34, 383–404.

Potts D.M. and Fourie A.B. (1985) The effect of wall stiffness on the behaviour of a propped retaining wall, Geotechnique, 35, 347–52.

Potts D.M. and Fourie A.B. (1986), A numerical study of the effects of wall deformation on earth pressure. Int. J. Numer. Anal. Methods Geomech. 10, 383–405.

Rankine W.J.M. (1857), On the stability of loose earth. Scotl. Philos. Trans. R. Soc. Lond. 147, 9–27.

Reissner H. (1924), Zum erddruckproblem, B. a. Burgers, (ed.) Proc. 1st Int. Congress on Applied Mech. City: Delft, pp. 295-311.

Salençon J. and Matar M. (1982), Capacité portante des fondations superficielles circulaires J. de Mécanique théorique et appliquée, Vol. 1, No. 2, pp 237-267.

Salman Firas, Al-Shakarchi Yousif, Husain Husain and Sabre Dunya (2010), Distribution of earth pressure behind retaining walls considering different approaches, International Journal of the Physical Sciences Vol. 5(9), pp. 1389-1400.

Sarma K. (1979), Stability analysis of embankments and slope. J. Geotech. Engrg. Div., ASCE, 105(12), 1511–1524.

Sarama S.K. and Iossifelis I.S. (1990), Seismic bearing capacity factors of shallow strip footings. Geotechnique, London, 40(2), 265–273.

Schofield A.N. (1961), The development of lateral force of sand against the vertical face of a rotating model foundation. In: Proceedings of the 5th InternationalConference on Soil Mechanics and Foundation Engineering, Paris, vol. 2, pp. 479–494.

Sherif M.M. (1977), Mackey, R.D.: Pressure on retaining wall with repeated loading. J. Geotech. Eng. (ASCE) 103(11), 1341–1345.

Shield R.T. (1954a), Plastic potential theory and the Prandtl bearing capacity solution. J. Appl. Mech., 21, 193–194.

Shield R.T. (1954b), Stress and velocity fields in soil mechanics. J. Math. Phys., 33(2), 144–156.

Shields D.H., Scott J.D., Bauer G.E., Deschenes J.H. and Barsvary A.K. (1977), Bearing capacity of foundations near slopes, Proceedings of the 9th International Conference on Soil Mechanics and Foundations Engineering, Tokyo, Vol. 2, pp.715–720.

Shukla S. K., Gupta S.K. and Sivakugan N. (2009), Active earth pressure on retaining wall for c-φ soil backfill under seismic loading condition, Journal of Geotechnical and Geoenvironmental Engineering ASCE, 135(5): 690–696.

Sieniutycz S. and Farkas H. (2005), Variational and Extremum Principles in Macroscopic Systems, Elsevier.

Sokolovskii V.V. (1965), Statics of granular media. New York: Pergamon.

Sokolovskii V.V. (1960), Statics of soil media. London: Butterworths Scientific.

Soubra A.H. (1999), Upper-bound solutions for bearing capacity of foundations.'' J. Geotech. and Geoenvir. Engrg., ASCE, 125(1), 59–68.

Spencer E. (1961), Perturbation method in plasticity-1 plane strain of nonhomogeneous plastic solids. Journal of the Mechanics and Physics of Solids, 9(4), 279-288.

Spencer E. (1967), A method of analysis of the stability of embankments assuming parallel inter-slice forces, Geotechnique, 17, 11–26.

Subra RAO K.S. and Choudhury D. (2005), Seismic passive earth pressures in soils, Journal of Geotechnical and Geoenvironmental Engineering, 131(1): 131–135.

Takano D., Otani J., Nakamura M., Mokwa R. (2012), X-ray CT imaging of 3-D bearing capacity mechanism for vertically loaded shallow foundations, Journal of Geotechnical Engineering, p.35-41.

Taylor D.W. (1948), Fundamentals of Soil Mechanics. New York: Wiley.

Terzaghi K. (1934a), Large retaining wall test I-pressure of dry sand. ENR 112(1), 136–140.

Terzaghi K. (1934b), Large retainingwall test II-pressure of saturated sand. ENR 112(22), 259–262, 316–318, 403–406, 503–508.

Terzaghi K. (1943), Theoretical soil mechanics. New York: Willey.

Terzaghi K., Peck R.B. and Mesri G. (1996), Soil Mechanics in Engineering Practice, 3rd edition, John Wiley & Sons, New York.

Thornton C. (1997), Coefficient of restitution for collinear collisions of elastic perfectly plastic spheres. Journal of Applied Mechanics, 64:383-386.

Ting J., Corkum B., Kauffman C. and Greco C. (1989), Discrete numerical model for soil mechanics. Journal of Geotechnical Engineering, 379-398.

Ukritchon B., Whittle A. J. and Klangvijit C. (2003), Calculation of bearing capacity factor Nr using numerical limit analysis, Journal of Geotechnical and Geoenviromental Engineering *ASCE*, 129(6), 468-474.

Vesic A.S. (1973), Analysis of ultimate loads of shallow foundations. J. Soil Mech. Found. Div., ASCE 99, No. SM1, 45–73.

Vo T. and Russell A.R. (2014), Slip line theory applied to a retaining wall–unsaturated soil interaction problem, Computers and Geotechnics, 55, No. 1, 416–428.

Vo T. and Russell A.R. (2016), Bearing capacity of strip footings on unsaturated soils by the slip line theory, Computers and Geotechnics, 74, No. 1, 122–131.

Wang Y.J., Yin J.H. and Chen Z.Y. (2001a), Calculation of bearing capacity of a strip footing using an upper bound method. International Journal for Numerical and Analytical Methods in Geomechanics, 25(8), 841-851.

Wang Y.J., Yin J.H and Lee C.F. (2001b), The Influence of a Non-Associated Flow Rule on the Calculation of the Factor of Safety of Soil Slopes, International Journal for Numerical and Analytical Methods in Geomechanics, Vol.25, pp.1351-1359.

Wang Y.J. and Yin J.H. (2002), Wedge stability analysis considering dilatancy of discontinuities, Rock Mechanics and Rock Engineering, Vol.35, No.2, 127-137.

Wang Y.J., Yin JH, Chen Z.Y. and Lee C.F. (2004), Analysis of wedge stability using different methods, Rock Mechanics and Rock Engineering, Vol.37, No.2, pp.127–150.

Weng M.C., Cheng C.C. and Chiou J.S. (2014), Exploring the Evolution of Lateral Earth Pressure Using the Distinct Element Methods, Journal of Mechanics, 30 (1), 77-86.

Yamamoto K. and Kusuda K. (2001), Failure mechanisms and bearing capacities of reinforced foundations, Geotextiles and Geomembranes, 19 (3), 127–162.

Yamamoto K., Lyamin A.V., Abbo A.J., Sloan S. W. and Hira M. (2009), Bearing capacity and failure mechanism of different types of foundations on sand, Soils and Foundations, 49(2), 305-314.

Yamamoto K. and Otani J. (2002), Bearing capacity and failure mechanism of reinforced foundations based on rigid-plastic finite element formulation, Geotextiles and Geomembranes, 20(6), 367-393.

Yin J.H., Wang Y.J. and Selvadurai A.P.S. (2001), The influence of a non-associative flow rule on the calculation of bearing capacity of a strip footing, Journal of Geotechnical and Geoenvironmental Engineering, ASCE, Vol.127, No.11, pp.985-989.

Yoo C.S. (2001), Laboratory investigation of bearing capacity behavior of strip footing on geogrid-reinforced sand slope, Geotextiles and Geomembranes, 19(5): 279-298.

Zhu H.P., Zhou Z.Y., Yang R.Y. and Yu A.B. (2007), Discrete particle simulation of particulate systems: Theoretical developments, Chemical Engineering Science, 62, 3378-3396.